SOME STUDIES ON CIRCULAR AND ANNULAR RING MICROSTRIP ANTENNA

A THESIS

SUBMITTED IN FULFILLMENT OF THE REQUIREMENTS

FOR

THE DEGREE OF

DOCTOR OF PHILOSOPHY

IN

PHYSICS

by

Madhurika Mahajan

JAYPEE UNIVERSITY OF
INFORMATION TECHNOLOGY

JAYPEE UNIVERSITY OF INFORMATION TECHNOLOGY
WAKNAGHAT
2008

JAYPEE UNIVERSITY OF INFORMATION TECHNOLOGY
(Established by H.P. State Legislative vide Act No. 14 of 2002)
Waknaghat, P.O. Dumehar Bani, Kandaghat, Distt. Solan – 173215 (H.P.) INDIA
Website : www.juit.ac.in
Phone No. (91) 07192-257999 (30 Lines)
Fax: (91) 01792 245362

Date: 10, July, 2008

CERTIFICATE

This is to certify that the thesis entitled, "**SOME STUDIES ON CIRCULAR AND ANNULAR RING MICROSTRIP ANTENNA**" which is being submitted by ***Ms. Madhurika Mahajan*** in fulfillment for the award of degree of **Doctor of Philosophy** in **Physics** by **Jaypee University of Information Technology**, is the record of candidate's own work carried out by her under my supervision. This work has not been submitted partially or wholly to any other University or Institute for the award of this or any other degree or diploma.

10/7/08

Sunil Kumar Khah
PhD
Associate Professor
Department of Physics

ACKNOWLEDGEMENTS

It is my privilege to take the opportunity to thanks all those who have helped me in the completion of this present research work.

I would like to express my most sincere gratitude to my supervisor, Dr. Sunil Kumar Khah, Associate Professor, Department of Physics, for his guidance, support and encouragement. I am indebted to him for his advice, constructive criticism and never ending patience at each step of my research work.

A special acknowledgement to Dr. Tapas Chakravarty (TCS, Embedded Systems Lab, Banglore) and Prof. Asok De. (Principal, Ambedakar College of Engineering, Delhi) for their guidance, concern, encouragement and help at all stages of my study.

I owe my thanks to Prof. (Dr.) S. C. Katyal, Head Department of Physics and other members Dr. P. B. Barman, Mr. Pankaj Sharma, Dr. Vineet Sharma and Mr. Dheeraj Sharma for providing me assistance, moral support, valuable suggestions and necessary facilities in the department during the course of my research work.

I also wish my gratitude to Dr. Y. Medury, Prof. (Dr.) D. S. Chauhan and Brig. (Retd.) Balbir Singh for their interest, encouragement and help during the course of my research tenure at JUIT. I would like to thank the authorities of Jaypee University of Information Technology, Waknaghat for providing the financial support. I would also like to acknowledge Mr. Shriram and Mr. Vipin Sharma, of LRC JUIT, for their help and cooperation.

Thanks are due for my friend Ishu for her support and encouragement during my research work. I also acknowledge Rakesh, Sangeeta and Ambika for their support.

Words failed to express my humble gratitude and profound regards to my dear parents, my husband and all family members for their affectionate encouragement and blessings to complete this research work.

I simply thank almighty for showering his blessings always to provide me enormous patience, inspiration, faith and strength to carry out this work.

(*Madhurika*)

Contents

List of Figures

List of Tables

Microstrip patch antennas are the most common form of printed antennas. A microstrip antenna (MSA) consists of a radiating patch on one side of dielectric substrate which has a ground plane on other side. The metallic patch is normally made of copper with a corrosion resistant metal such as gold, tin and nickel. Microstrip patch antennas have low profile configuration which can be easily made to host surface, capable of dual and triple frequency operations and they support both linear and circular polarization with single feed. Due to these advantages, these antennas are most suitable for aerospace and mobile applications. However, narrow bandwidth, lower gain, extraneous radiation from feed and junctions are their main disadvantages. To overcome these limitations, these antennas can be further loaded with stubs, shorting pins, diodes to obtain compactness, dual frequency operation, frequency agility and polarization control. Thus these antennas are finding increasing applications in the commercial sector of the industry especially in GPS (Global Positioning system), SDARS (Satellite Digital Audio Radio Services) and WLAN (Wireless Local Area Networks).

1.1 Origin

Microstrip geometries that radiate electromagnetic waves were originally contemplated in early fifties. The realization of a microstrip like antenna integrated with microstrip transmission line was developed in 1953 by Deschamps [1]. Gutton and Bassinot [2] patented a microstrip design in 1955. First practical antennas were fabricated after 20 years. Howell [3] and Munson [4] developed the first practical antenna. Since then an extensive research on microstrip antennas aimed to become most innovative topics in antenna theory and design. Thus these antennas are increasingly finding applications in wide range of modern microwave systems.

1.2 Methods of Analysis and Radiation Mechanism

There are various methods for analysis of microstrip antennas. The analysis can be broadly classified into two groups. Reduced analyses refer to microstrip antenna models that introduce one or more significant approximations to simplify the problem. These include (i) the transmission line model [5,6] which models the

transmission line section with lumped loads, (ii) the cavity model [5 - 7] which uses a magnetic wall boundary condition approximation for the periphery of the patch and (iii) the multiport network model [6] which generalizes the cavity model. The original transmission model was prepared by Munson [4]. This model represents the microstrip antenna by two slots of width W and height h, separated by a transmission line of length L. Most of the electric field resides in the substrate and parts of some line in the air. As a result, the transmission line cannot support pure TEM mode of transmission and dominant mode of propagation is quasi-TEM mode. The transmission model is basic of all the models and it gives good physical insight. However, it accuracy is limited so an improved transmission line model was given by [8]. This model can be applied only to rectangular and square patches. It is not possible to analyse proximity coupled and aperture coupled microstrip fed by this method. In GTLM (Generalized Transmission Line model) approach the transmission line sections which may be non uniform on either side of current source are converted into π network. This model has been described in detail [9,10] with different approaches. The patch shapes studied using this model include rectangular patch [9,10], circular patch [11], ring [12], annular and circular sectors [13]. Since all configurations such as proximity coupled, aperture coupled and stacked patches can not be analyzed with this model so the next model to overcome was the cavity model. Cavity model was advanced by Lo *et al.* [14]. The cavity model becomes a natural choice to analyse the patch antennas as it is the approximate model which leads to reactive input impedance and does not radiate any power. In cavity model, the region between the patch and the ground plane is modeled as a cavity bounded by magnetic wall along the periphery and by the electric wall from the top and bottom sides. When the microstrip patch is provided power, a charge distribution is seen on the upper and lower surfaces of the patch and at the bottom of the ground plane. The attractive mechanism is between the opposite charges on the bottom side of the patch and the ground plane, which helps in keeping the charge concentration intact at the bottom of the patch. The repulsive mechanism is between the like charges on the bottom surface of the patch which causes pushing of some charges from the bottom, to the top of the patch. As a result of this charge movement, current flow at the top and bottom surface of the patch. The cavity model assumes that the height to width ratio (*i.e.* height of

substrate and width of the patch) is very small and as a result of this the attractive mechanism dominates and causes most of the charge concentration and current to be below the patch surface. The cavity model has been applied to a number of patch shapes, including rectangular patches [15,16], circular patches [17-19], equilateral triangles [20], circular rings [21], annular and circular sectors. The multiport network model [MNM] is the extension of cavity model in which the impedance boundary conditions at the periphery is forced explicitly [6]. In this method the mutual coupling between various edges is taken into account. The fields in the interior and exterior region are modeled separately. The interior region is modeled as a multiport planar circuit, with ports located along the periphery. The fields in the exterior region, which includes the fringing fields, radiation fields and surface wave fields are represented by load admittances. The multiport impedance matrix of the patch is obtained from its 2 - *D* Green's function. These models were the first to be developed for microstrip antennas and have been extensively useful for practical designs, as well as providing a good intuitive explanation of the operation of microstrip antennas.

The second group of analysis technique namely numerical techniques that account for dielectric substrate in a rigorous manner are referred to as full wave solutions. These models assume that the substrate is infinite in extent in lateral dimensions and enforce the proper boundary conditions at the air – dielectric interface. Harrington [22] introduced the Method of Moment (MOM) technique, which is applied to electromagnetic problems. These methods are accurate and versatile as these include the surface wave, space wave radiation and mutual coupling into account.

However, these methods are numerically intensive, complex, time consuming and require careful programming in order to be computationally efficient. These techniques provide little of the physical insight required for antenna design. The first groups of techniques are simple to use and provide good physical insight. In cavity model, the analysis problem reduces to that of finding the edge voltage distribution for a given excitation and for a specified mode.

For a thin patch, this model offers accurate results suitable for most engineering applications. Hence, this model can form the basis of study of radiation mechanism of loaded circular disk and annular ring substrates.

1.3 Circular Disc and Stacked Circular Disc

The circular disc is characterized by a single parameter *i.e.* its radius *a*. Thus it is simplest geometry since other shapes require more than one parameter to describe them. The circular disc antenna has been studied extensively [23-29]. Circular disk antennas has been studied by various analytical methods *viz.* cavity model [25,27], the generalized transmission line model [9,11,12], mode matching with edge admittance [24,25] and Finite Difference Time Domain (FDTD) [29]. The cavity model is found to simple and useful in design of structure. As elaborated in the earlier section, in the cavity model the interior region of the patch is modeled as a cavity bounded by electric walls on the top and bottom and a magnetic wall all along the periphery. The following are the basic assumptions for thin substrates;

(i) The fields in the interior region do not vary with z (*i.e.* $\partial/\partial z = 0$) because substrate is very thin.

(ii) The electric field is z directed only and the magnetic field has only the transverse components in the region bounded by the patch and the ground plane *i.e.* the magnetic field essentially has only ρ and ϕ components.

(iii) The electric current in the patch has no component normal to the edge of the patch, which implies that the tangential component of magnetic field $\vec{H}$ along the edge is negligible.

Thus, the fields within the dielectric region of the microstrip cavity, corresponding to TM_{nmp} modes, can be determined by solving the wave equation in a cavity (Since field distribution along z-axis is constant, the index p is omitted in further references). For no excitation current, the wave equation for the electric field can be written as

$$(\nabla^2 + k^2)\vec{E} = 0$$

where $k = \dfrac{2\pi}{\lambda}$

After application of boundary conditions, the fields are derived. For each mode configuration, a radius can be found that results in a resonance corresponding to the zeroes of the derivative of the Bessel function. Thus, the cavity model is used to explain the circular disc antennas and other geometries. There has been a great

demand for wide - band antennas to be used in wireless communication applications so that a large amount of data can be transmitted in a short interval of time.

Bandwidth of microstrip antennas can be enhanced by different methods such as stacking, loading and using multilayered structures. For early versions of the direct feed stacked patch antenna only moderate bandwidth less than 15 % were achieved. The true potential of the direct fed stacked patch antenna could be realized in the late 1990's. An accurate analysis of probe fed stacked patch with rigorous full wave analysis based on spectral domain integral equation approach was devised. These formulations accurately model the discontinuity associated with the probe-patch interconnect. Stacking the antenna in multilayered configuration introduces additional resonance in the frequency resulting in the wide bandwidth and dual frequency operation. Stacked patches have been extensively studied [33-38] to obtain wide bandwidth and dual frequency operations. Tulinsteff *et al.* [33] presented the analysis of a probe - fed stacked circular microstrip antenna. The rigorous analysis based on dyadic Green's function formulation has been used. The mixed boundary value problem has been reduced to a set of coupled vector equations. 13 % (10 dB bandwidth) and dual frequency operation has been obtained. The central feeding scheme has been used to obtain two band responses in stacked microstrip square antenna [34]. The upper patch has been fed by coaxial probe extended through a hole in the centre of the ground plane and lower patch is fed from above forming a small loop from the centre to 50 Ω feed point on the upper patch. Good impedance matching of less than -10 dB has been obtained at two frequencies with no large pattern imbalance. Aperture coupled stacked microstrip patch antenna has also been studied [37,39]. A broadband circularly polarized stacked patch antenna element and its sub array, with high efficiencies at 10 GHz, has been presented by Chung *et al.* [42]. In addition to low boresight axial ratios, the subarray has measured bandwidth of about 25 %. Antenna efficiency is 89 % around center frequency for single element where as subarray has efficiency of 71 %.

The stacked microstrip ring antenna for dual frequency behavior and improved bandwidth has been studied [35,38]. The cavity model for single microstrip antennas has been extended with some modifications for stacked geometry to account

coupling between upper and lower cavities, fringe fields, dispersion effects and effective loss tangent of dielectric material.

1.4 Ring Resonator

Microstrip ring resonator was first proposed in 1969 for the measurement of phase velocity and dispersive characteristics of a microstrip line. In first 10 years most applications were concentrated on the measurements of characteristics of discontinuities of microstrip lines. Sophisticated field analysis was developed to give accurate modelling and prediction of ring resonator. In 1980, applications using ring circuits as antennas and frequency selective surfaces emerged. Microwave circuits using rings for filters, oscillators, mixers, baluns and couplers were also reported. Some unique properties and excellent performances had been demonstrated using ring circuits built in coplanar waveguide. The integration with various solid state devices was also realized to perform tuning, switching, amplification, oscillation and optoelectronic functions.

There are certain advantages of using ring antennas over other structures. The ring resonator would only support waves with integral multiple of the guided wavelength equal to the mean circumference. Ring microstrip antennas are alternatives to standard rectangular and circular disks. These antennas are geometrically and electrically an intermediate configuration between a printed loop and patch [43]. The ring antennas have smaller size as compared to circular patch when both are operated in lowest mode. The annular ring antenna can be combined with a second microstrip element. Thirdly, the separation of the modes can be controlled by the ratio of outer to inner radii. Finally, it has been found that by operating in one of the higher order broadside modes, *i.e.* TM_{12}, the impedance bandwidth is several times larger than is achievable in other patches. It has been shown that the structure is a good resonator (with very little radiation) for TM_{m1}mode (m odd) and a good radiator for TM_{m1} modes (m even).

The annular microstrip ring antenna has been studied extensively [44-52]. Various methods of analysis have been applied to the annular ring antenna including the cavity model [6,44-47], generalized transmission line model [12], analysis in the Fourier-hankel transform domain [49] and the method of matched asymptotic

expansion [50]. The field analysis "magnetic-wall model" for microstrip ring resonators was firstly introduced in 1971 by Wolff *et al.*[47]. In 1976, Ownes improved the magnetic-wall model [51]. Pinztos *et al.* [52] presented a rigorous solution in 1978 based on stationary principle. Wu *et al.* [53] obtained the mode chart for the fields in magnetic-wall model. Sharma *et al.* [54] carried out a numerical solution using the spectral domain method. Wolff *et al.* used perturbation analysis to design the open-end closed ring microstrip resonators [55]. So far, only the annular ring resonator has the field theory derivation for its frequency modes. For the square or the meander ring resonators, it is difficult to use the magnetic-wall model to obtain frequency modes of these ring resonators because of their complex boundary conditions. The field analysis based on electromagnetic theory is complicated and difficult to implement in a computer-aided-design (CAD) environment. Chang *et al.* [56] first proposed a straightforward but reasonably accurate transmission-line method that can include gap discontinuities and devices mounted along the ring. Gopalkrishnan *et al.* [57] further improved this method with a distributed transmission-line method that includes factors affecting resonances such as microstrip dispersion, the curvature of resonator and perturbation. The distributed transmission line method can accommodate many solid-state devices, notches, gaps and various discontinuities along the circumference of ring structure. The ring antenna has been rigorously analyzed using Galerkin's method [58,59]. It has been concluded that TM_{12} mode is the best mode for antenna applications. Another rigorous analysis of probe-fed ring antenna has been introduced by Kokotoff *et al.* [60]. Numerical method based on full-wave spectral-domain method of moment has been used to model the connection between probe feed and ring antenna.

Active antennas have received great attention because they offer savings in size, weight and cost over conventional designs. These advantages make them desirable for application in microwave systems such as wireless communications, collision warning radars, vehicle transceiver, self-mixing Doppler radar for speed measurement and microwave identification systems [61,62]. Ring resonator has also been proposed as a radiator for medical applications [63] and used to measure the dielectric constant of the substrate material [47].

1.5 Feeding Techniques

Microstrip patch antennas can be fed by a variety of methods. The feeding methods can be classified into two categories; contacting and noncontacting. In the contacting method, the RF power is fed directly to the connecting element such as microstrip line. In microstrip line feeding, coaxial probe are the contacting type techniques. In the other type, electromagnetic feed coupling is done to transfer power between the microstrip line and radiating patch. The aperture coupling and proximity coupling are of other type. In the microstrip line feeding, a conducting strip is connected directly to the edge of the microstrip patch. The conducting strip is smaller in width as compared to the patch and this type of feed has the advantage that the feed can be etched on the same substrate to provide a planar structure. This technique provides ease of fabrication, simplicity in modelling as well as impedance matching. If we use a thick dielectric substrate, surface waves and spurious wave radiations also increases, which hamper the bandwidth of the antenna. This feed radiation also leads to undesired cross-polarized radiation. The coaxial feed is very common technique used for feeding microstrip antenna. The inner conductor of the coaxial connector extends through the dielectric and is soldered to the radiating patch, while the outer conductor is connected to the ground plane. The main advantage of this type of feeding scheme is that feed can be placed at any desired location inside the patch in order to match with its input impedance. This method is easy to fabricate and has low spurious feed radiation. The disadvantage of this method is that it provides narrow bandwidth and it is difficult to model since a hole has to be drilled in the substrate. In aperture-coupled feed, the ground plane separates the radiating patch and the microstrip feed line. The coupling aperture is centered under the patch, leading to lower cross-polarization due to symmetry of the configuration. The amount of coupling from the feed line to the patch is determined by the shape, size and location of aperture. Since the ground plane separates the patch and the feed line, spurious radiation is minimized. The major disadvantage of this feed technique is that it is difficult to fabricate due to multiple layers. Electromagnetic coupling scheme is also called as proximity coupled feed. Two dielectric substrates are used such that feed line is in between the two substrates and the radiating patch is on the top of upper substrate. The main advantage of this feed technique is that it eliminates spurious feed

radiation and provides very high bandwidth (as high as 13 %) due to overall thickness of the microstrip patch antenna. The major disadvantage of this feeding is that it is difficult to fabricate because two dielectric layers need proper alignment. Coupling between the patch and the microstrip line is capacitive in nature. Pozar *et al.* [64] proposed an alternative method of obtaining enhanced bandwidth from a microstrip antenna, using a microstrip feed line proximity-coupled to a patch antenna printed on a superstrate above the feedline. A small tuning stub is also required so that an enhanced bandwidth of 13 % is obtained. Oltman *et al.* [65] gave different electromagnetic coupling (EMC) microstrip dipole configurations, which employ varying amount of electric and magnetic coupling to radiate with varying degree of efficiency. Transmission line model was used to explain the coupling mechanism from the circuit viewpoint, while a moment method solution has been used to provide insight from field viewpoint. These two methods were used as approximations to the actual situations, however they provided the valuable information on the physics involved with this type of radiator. Theoretical viewpoint of EMC microstrip dipole and arrays has been presented and has been used with good success. Rectangular shorted patch antenna has been designed with proximity coupling to obtain wideband performance and size reduction [66]. The patch size is reduced to 25% to full size patch with over 30% matching bandwidth. 16 elements array has also analyzed with different feeding arrangements indicating an improvement in the array performance. The achieved gain in this case is 15%.

A remarkable amount of work needs to be done on electromagnetic coupled microstrip patch antennas as this is the best method of feeding microstrip antennas.

1.6 Short Loaded Antenna

Antennas which are used in wireless local area networks (WLANs) needs operation at two or more discrete bands and an arbitrary separation of bands. It is not possible to achieve these objectives from the basic microstrip antennas having regular shapes. Hence to obtain these applications we can suitably load the regular microstrip structures. Loading of microstrip antennas is used to obtain circular polarization, frequency tuning, broadbanding, impedance matching, radiation pattern control *etc.* Loading can take various forms such as stub loading, slots, shorting posts, parasitic

couplings, substrate loading, superstrate cover, resistors, capacitors and diodes. A good overview of loaded microstrip structures has been given by Garg *et al.* [66]. A microstrip antenna can be easily made to resonate at many frequencies corresponding to a TM_{np} mode. If the patch is loaded (*e.g.* with strategically placed shorts), the field and current distributions for various modes will be disturbed and therefore their characteristics will change. This change will depend on the amount of load and the mode under consideration. Loading can lead to polarization diversity [67], frequency agility [67,68] and radiation pattern control [69-71]. Shorting pins can be used to load the microstrip antenna. Shorting pins will tend to give compactness, tunability and improve frequency operations. Microstrip antennas of different shapes loaded with shorting pins [72-75] has been extensively studied. Depending upon the applications, a shorting pin may be located at the edge or at the centerline of the patch. The analysis of post loaded microstrip antenna has been carried out using the transmission line model [67,76], cavity model [77,78], multiport network model [79], integral equation approach [80] and FDTD technique [81,82]. Wong *et al.* [83] presented a triangular antenna loaded with shorting pin which can significantly reduce the size of antenna at a given frequency. The antenna without shorting pin resonates at 1.9 GHz where as after loading the frequency of antenna is much lower than 1.9 GHz. Dual-frequency has been obtained from H - shaped microstrip antenna loaded with a shorting pin [84]. This antenna in comparison to a conventional rectangular patch antenna can achieve both significant reduction of antenna size and a dual-frequency operation with a single feed. Finite difference time domain (FDTD) method is used for theoretical analysis. It has been seen that various frequency ratios (1.91 - 4.23) are obtained by varying the design parameters of this antenna. Dual frequency microstrip antenna with a single feed using a shorting pin has been presented by Shan *et al.* [85]. The design has been first applied to a rectangular microstrip antenna. By short-circuiting the antenna at proper positions the first two frequencies with same polarization plane can be excited with good matching conditions. The first (f_1) and second (f_2) frequencies are respectively in the range 950-722 MHz and 1900-2310 MHz which indicates the frequency ratio tunable in the range 2.0~3.2. The design is then applied to an equilateral triangle which shows a tunable frequency ratio of about 2.5~4.9. The two resonant frequencies strongly depend on the position of shorting pins.

Circular microstrip antenna with off-centered posts has been proposed by De [86]. In this, treatment has been developed for single or multiple posts when the posts are symmetrically located *i.e.* equi-spaced along the circumference of circle concentric with the patch radiator. The resonance is dependent on radial distance of posts from the centre, the angular location and the radius of posts. The dual band antenna can be designed with flexible band separation. In case of asymmetric loading the angular dependence vanishes and (1,1) is the dominant mode. An analytical theory for the eigenfrequencies and eigenmodes of shorting post loaded microstrip antennas has been presented [87]. It is shown that the zero mode of the unloaded MSA plays a central role for reducing the lowest operating frequency of the loaded microstrip patch antennas. The lowest values for the resonant frequency have been obtained when positioning the shorting post at the edge of the patch. In general, the resonant frequencies obtainable from a loaded circular patch are larger than those of a rectangular patch of equal cross section. It is also seen that the sensitivity of the resonance frequency against variations of the shorting-post position of the circular patch is stronger than in the rectangular patch.

Recently an approximate analysis of short circuited ring patch antenna has been presented in [88]. The analysis is based on cavity model and different parameters of antennas such as the resonant frequency, fields, radiation pattern, and input impedance of a short-circuited ring working at TM_{01} mode are calculated. In a recent work [89], neural networks have been used for the first time in short circuited ring patch antenna working at TM_{01} mode. The dependence between the fundamental antenna parameters such as internal radius, external radius, permittivity of the substrate has been studied. Finally a neural network has been proposed for the analysis of these antennas and this tool is useful as it provides advantages in computation time with negligible error in real terms.

In the light of the above discussions, significant amount of work can be done for a loaded annular ring microstrip antenna. Also an accurate model of such antenna is necessary to predict the various performances. As mentioned earlier, the full-wave methods are rigorous and computationally resource intensive. An elegant alternative method giving insight to the problem is therefore worth searching. Theoretical modelling for symmetric and asymmetric loaded annular patch is not reported in

literature and is therefore attempted in this present work. This analysis may lead to a practical design where the shorting posts are replaced by switching diodes positioned symmetrically about the feed. A pair of switching diode can be electronically switched on/off based on the operating frequency desired.

1.7 Fabricated Antenna and Experimental set up

In the Present work an analytical numerical model is developed for the circular disc and ring resonators. This analysis is further extended to stacked circular disc antenna and shorting posts in ring resonators. Proximity coupled antenna is also analytically modeled. The validation of the analytical model is carried out by comparison with the standard software simulator (IE3D^{TM}) results. Representative results were experimentally validated with the existing facilities. The return loss measurements were tested using Vector Network analyzer model no 8714ET.

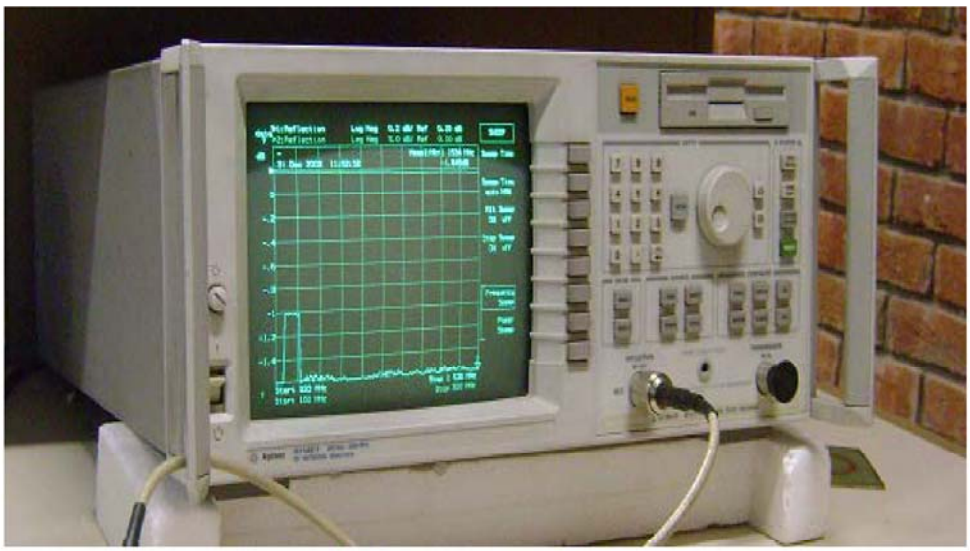

Photograph of RF Network Analyzer (8714 ET) used for measurements

The Block diagram of the test setup is given in the figure1.1. The calibration of the Network analyzer is first done by using open, short, 50ohm with terminator. After the

The basic specifications of the analyzer are:

Type	Vector
Integral Signal Source	Yes
Integral Test Set	T-R Parameter
Frequency Range	300 kHz -3GHz
Source Frequency Resolution and Accuracy	1 Hz and 0.0005%
Minimum Output Power	0.001 Watts
Maximum Output Power	19.9526 mW
Output Accuracy	1 dB
Output Impedance	50 Ohm
No. of Receiver Channels	2
Receiver Minimum Frequency	300 kHz
Receiver Maximum Frequency	3 GHz
Minimum Dynamic Range	100 dB
Maximum Dynamic Range	100 dB
Maximum Input Decibel	20 dBm
Input Connector Type	Type-N(f)

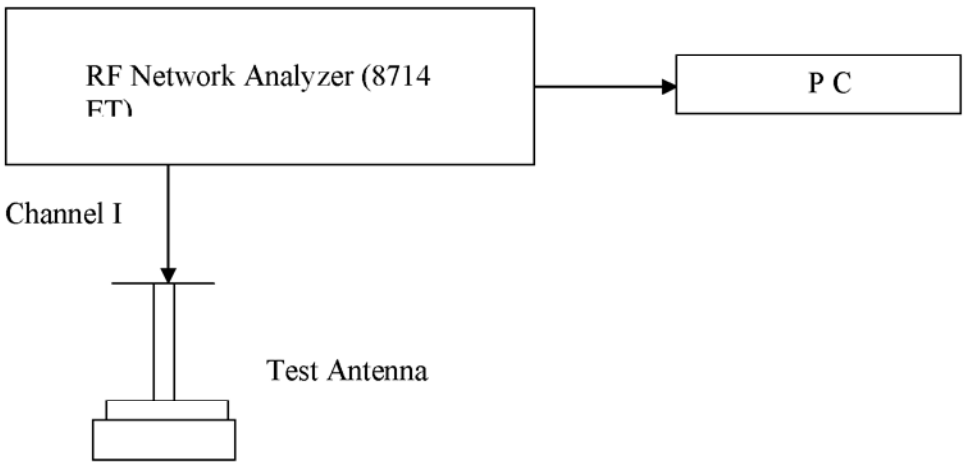

Figure 1.1 Block Diagram for measurement of Reflection Coefficient

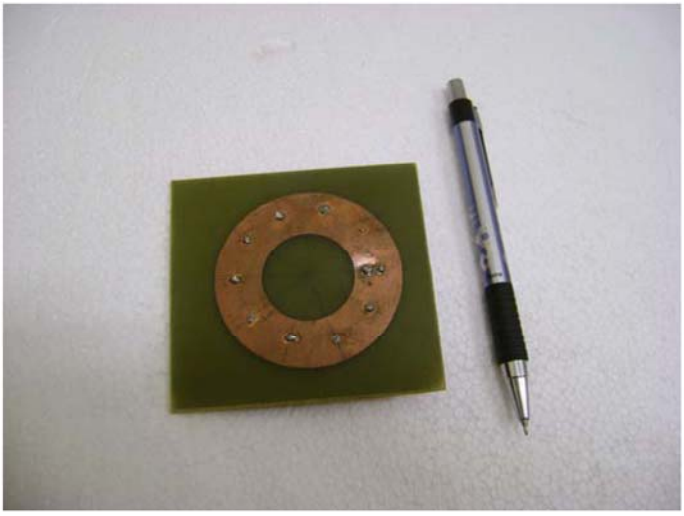

Photograph of Symmetrically loaded Annular Ring Antenna with posts

calibration is completed then the test antenna is connected to the network analyzer and the measurement is done by selecting the frequency range of the interest.

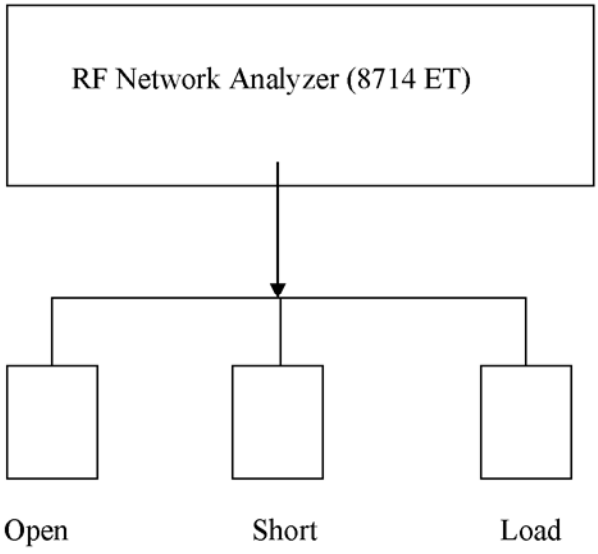

Figure 1.2 Calibration Set up

1.7 Outline of Thesis

Pursuing the introductory chapter the rest of thesis is organized as follows;

Chapter II presents the evaluation of input impedance of circular patch by using cavity model. Various parameters such as wall admittance and radiation parameters are evaluated. The fields in the regions inside the circle are evaluated from the solution of the appropriate scalar Helmholtz equation for the TM modes. Evaluation of the constants using the boundary conditions leads to a transcendental equation. The resonant frequencies for different modes are determined from the equation of resonant frequency of circular patch antenna. In the proposed model, the impedance expression of end correction network suggested by Zheng *et al.*[90] has been utilized. The theory is further extended to find out the input impedance of stacked circular disc. The upper patch is considered as uncoupled cavity with an air gap. For the upper patch the effective dielectric constant is given by [91]. The main and fringing capacitances are used for the calculation of effective dielectric constant. Radiation parameters are calculated by magnetic current density approach.

Chapter III presents the method of evaluation of input impedance of annular ring antenna fed with coaxial line feeding. The cavity model along with circuit theory is used to find out input impedance. The fields inside the cavity appearing in the expression for self reaction are expressed as a superposition of normal cavity modes. The amplitude coefficients appearing in the series are determined in terms of wall admittance and the conductor losses. The dielectric loss is taken into account by assuming that permittivity is complex. Computed results are compared with the presented experimental results of Garg *et al.* [49] and simulated results obtained from moment-method based solver IE3D [92]. The analysis is further extended to calculate the resonant frequency of asymmetrically loaded annular ring antennas.

In chapter IV, the eigen frequencies of symmetrically loaded annular microstrip antenna are evaluated. The shorting is done with the help of posts. The impedance per unit length for small cylindrical circular current distributions is given as [93]. A circular disk antenna with off-centred shorting posts proposed by De [86] is used. The resonant frequency of the loaded patch is computed and the results are compared with measurements. It is predicted that TM_{01} is the dominant mode of these antennas. This configuration results in a compact antenna, which is electronically

tunable over a wide range of frequencies. The input impedance of loaded microstrip antenna is presented. The analysis is same as described in chapter III. The computed results are compared to the simulated results; the simulation is done on IE3D software based on method of moment. The radiation parameters are also calculated and plotted. The results show that loading of antenna with the help of shorting pins will help to enhance the bandwidth and as the size of antenna is also reduced. These types of antennas have key role in communication.

In chapter V, the evaluation of input impedance of annular ring antenna fed by electromagnetic coupling. A microstrip line of length 'l' and width 'w' is used to feed the antenna. The method is based on cavity model in conjunction with circuit theory. It is shown that the proposed structure can act as a compact antenna with proper impedance matching.

The last chapter is the summary of work carried out.

References

1. Deschamps, G. A., "Microstrip microwave antennas," 3rd USAF Symposium on Antennas, 1953
2. Gutton, H. and G. Bassinot, "Flat Aerial for ultra high frequencies," French patent no. 70313, 1955
3. Howell, J. Q., "Microstrip antennas," IEEE AP-S Int. Symp. Digest, 1972, pp. 177 - 180
4. Munson, R. E., "Conformal microstrip antennas and microstrip phased arrays," IEEE Trans. Antennas Propag., vol AP-22, 1974, pp. 74 - 78
5. Carver, K.R. and J. Mink, "Microstrip antenna technology," IEEE Trans. Antennas Propag., vol. AP-29, 1981, pp. 2 - 24
6. James, J., R and P. S. Hall, "Handbook of microstrip antennas," Peter Prengrinus, London, UK, 1989
7. Richards, W.F., Lo Y.T. and D.Harisson, "An improved theory of microstrip antennas and applications," IEEE Trans. Antennas Propag., vol. AP-29, 1981, pp. 38 - 46
8. Pues, H. and A. Capelle, "Accurate transmission line model for the rectangular microstrip antenna," IEE Proc, vol. 129, Pt H, 1984, pp. 334 - 340
9. Bhattcharya, A. K., "Generalised transmission model of microstrip patch antenna and some applications," Ph.D. Thesis, IIT Kharagpur, India, 1985
10. Bhattcharya, A. K., Shafai, L. and R. Garg, "Microstrip antenna –a generalized transmission line," Progress in Electromagnetics Research PIER, vol. 4, 1991, pp. 45 - 84
11. Bhattacharyya, A. K. and R. Garg, "Generalised transmission line model for microstrip patches," IEE Proc., vol. 132, Pt. H., 1985, pp.93 - 98
12. Das, A. and S.K. Das, "Input impedance of a probe excited circular microstrip ring antenna," IEE Proc. H., 1985, pp. 384 - 390
13. Bhattacharyya, A. K. and R. Garg, "Analysis of annular sectors and circular sectors microstrip patch antennas," Electromagnetics, vol. 6, no. 3, 1986, pp. 229 - 242
14. Lo, Y.T., "Theory and experiments on microstrip antennas," IEEE Trans. Antennas Propag., vol AP-27, 1979, pp. 137 - 145

15. Richards, W.F., "An improved theory for microstrip antennas and applications," IEEE Trans. Antennas Propag., vol. AP-27, 1979, pp. 137 - 149
16. Thouroude, D., "CAD-Oriented cavity model for rectangular patches," Electron. Letts., vol. 26, 1990, pp. 842 – 844
17. Lo, Y.T. and W.F. Richards, "Perturbation approach to design of circularly polarized microstrip antennas," Electron. Letts., 1981, pp. 383 - 385
18. Long, S.A., "Impedance of circular disc printed –circuit antenna," Electron. Letts., vol. 14, 1978, pp. 684 - 686
19. Dahele, J.S. and K.F. Lee, "Effect of substrate thickness on the performance of circular disc antenna," IEEE Trans. Antennas Propag., vol. AP-31, 1983, pp. 358-360
20. Lee, K.F., Luk, K. M. and J. S. Dahele, "Characteristics of the equilateral triangular patch antenna," IEEE Trans. Antennas Propag, vol. AP-36, 1988, pp. 1510 - 1518
21. Richards, W. F., "A theoretical and experimental investigations of annular ring," IEEE Trans. Antennas Propag., vol. AP-32, 1984, pp. 864 - 866
22. Harrington, R.F., "Time Harmonic Electromagnetic Fields," McGraw-Hill, N.Y., 1961
23. Watkins, J., "Circular resonant structures in microstrip," Electron. Letts., vol. 5, 1969, pp. 524 - 525
24. Shen, L. C., "Resonant frequency of a circular disc printed circuit antenna," IEEE Trans. Antennas Propag., vol. AP-25, 1977, pp. 595 - 596
25. Yano, S. and A, Ishimaru, "A theoretical study of the input impedance of a circular microstrip disk antenna," IEEE Trans. Antennas Propag., vol. AP-29, 1981, pp. 77 - 83
26. Derneryd, A. G., "Analysis of the microstrip disk antenna element," IEEE Trans. Antennas Propag., vol. AP-27, vol. AP-27, 1979, pp. 660 - 664
27. Araki, K. and T. Itoh, "Hankel transform domain analysis of open circular microstrip radiating surfaces," IEEE Trans. Antennas Propag., vol. AP-29, 1981, pp. 84 - 89

28. Lo, Y, T., Solomon, D. and W.F. Richards, "Theory and experiments on microstrip antennas," IEEE Trans. Antennas Propag., vol. AP-27, 1979, pp. 137 - 145
29. Turner, G.M. and C.G.Christodoulu, "Finite difference time domain analysis of circular microstrip antenna," IEEE AP-S Int. Symp. Digest, 1996, pp. 1292 - 1295
30. Kotokoff, D.M., Abrele, J.T. and R.B. Waterhouse, "Rigorous analysis of probe fed printed annular rings," IEEE Trans. on Antennas Propag., vol. AP-47, 1999, pp. 384 - 388
31. Long, S.A. and D.M. Walton, "A dual-frequency stacked circular disc antenna," IEEE Trans. on Antennas Propag., vol. AP-27, 1979, pp. 270 - 273
32. Aberle, J.T., Pozar, D. M. and J. Manges, "Phased arrays of probe-fed stacked microstrip patches," IEEE Trans. on Antennas Propag., vol. AP-42, 1994, pp. 920 - 927
33. Tulintseff, A., Ali, N. and Jin, A. Kong, "Input impedance of a probe- fed stacked circular microstrip antenna," IEEE Trans. on Antennas Propag., vol.AP-39,1991, pp. 381 - 390
34. Keerti, S. and Y. Samii, "Design and analysis of a novel probe – feeding method for stacked microstrip patch antenna," IEEE, 2003, pp. 425 - 428
35. Fan, Z. and K. F. Lee, "Hankel transform domain analysis of a dual frequency stacked circular disk and annular ring microstrip antennas," IEEE Trans. Antennas Propag., vol. 39, 1991, pp. 867 – 870
36. Shen, Z. and R.H. Macpbie, "Waveguide model analysis of single and stacked probe-fed microstrip antenna with circular geometries," IEEE Antennas Propag., Symposium, vol. 2, 1998, pp. 598 - 601
37. Nishiyama, E. and M. Aikawa., "Wide band and high gain microstrip antenna with thick parasitic patch substrate," IEEE Antennas Propag., Society International Symposium, vol. 1, 2004, pp. 273 - 276
38. Tagle, J.,G. and C. G. Christodoulou., "Extended cavity model analysis of stacked microstrip ring antenna,' IEEE Trans Antennas Propag., vol. 45, No-11, 1997, pp. 1628 - 1637

39. Nishiyama, E., Aikawa, M. and Egashira, "FDTD analysis of stacked microstrip antenna with high gain," Progress in Electromagnetics Research, PIER, vol. 33, 2001, pp. 29 - 43
40. Wang, J., Fralich, R., Wu, C. and J. Litva., "Multifunctional aperture coupled stack patch antenna," Electron. Letts., vol. 26, 1990, pp. 2067 - 2068
41. Hu, Y., Wang, H. and D. G. Fang., "A novel wide band aperture- coupled circularly polarized stacked patch antenna," CEEM, 2006, pp. 904 – 907
42. Chung, K. L. and Mohanan, A. S., "A circularly polarized stacked electro-magnetically coupled patch antenna," IEEE Trans. on Antennas and Propag., vol. 52, no. 5, 2004, pp. 1365 -1370
43. Shafai, L., "Characteristics of printed ring loop antennas," ANTEM' 96, pp. 379 - 382
44. Bahl, I. J. and P. Bhartia., "Microstrip antennas", Artech House, Deldham, MA, 1980
45. James, J. R., Hall, P.S. and C. Wood, "Microstrip antennas: Theory and design," Peter Perengrinus, London, UK, 1981
46. Mink, J.W., "Circular ring microstrip antenna elements," IEEE AP-S Int. Symp. Digest, 1980, pp. 605 - 608
47. Wolff, I. and N. Knoppik, "Microstrip ring resonator and dispersion measurement on microstrip lines," Electron. Letts., vol. 7, 1971, pp. 779 - 781
48. Bhattacharyya, A. K. and R. Garg, "Analysis of annular ring microstrip antenna using cavity model," Arch. Elek. Ubbertragung, vol. 39, 1985, pp. 185 - 189
49. Bhattacharyya, A. K. and R. Garg, "Input impedance of annular ring microstrip antenna using circuit theory approach," IEEE Trans. Antennas Propag., vol. AP 33, 1985, pp. 369 - 374
50. Bafrooei, P. M. and L. Shafai, "Characteristics of single and double-layer microstrip square ring antenna," IEEE Trans. Antennas Propag., vol.47 no. 10, 1999, pp. 1633 - 1639
51. Ownes, R. P., "Curvature effect in microstrip ring resonators," Electron. Letts., vol. 12, no. 14, 1976, pp. 356 - 357

52. Pintzos, S. G. and R. Pregla, "A simple method for computing the resonant frequencies of microstrip ring resonators," IEEE Trans. Microwave Theory Tech, vol. MTT-26, 1978, pp. 809 - 813
53. Wu, Y.S. and F.J. Rosenbaum, "Mode chart for microstrip ring resonators," IEEE Trans. Microwave Theory Tech, vol. MTT-21, 1973, pp. 487 - 489
54. Sharma, A.K. and B. Bhat, "Spectral domain analysis of microstrip ring resonators," Arch. Elek. Ubertragung, vol. 33 1979, pp. 130 - 132
55. Wolff, I. and V. K. Tripathi, "The microstrip open ring resonator," IEEE Trans. Microwave Theory Tech, vol. MTT-32, 1984, pp. 102 - 106.
56. Chang, K., Martin, T. S. and F. Wang, "On the study of microstrip ring and varactor tuned ring circuits," IEEE trans. Microwave Theory Tech, vol. MTT-35, 1987, pp. 1288 - 1295
57. Gopalkrishnan, G.K. and K. Chang, "Band pass characteristics of split-modes in asymmetric ring resonators," Electron. Lett., vol. 26, no. 12, 1990, pp. 774 - 775
58. Ali, S. M., Chew, W. C. and J.A. Kong., "Vector Hankel transform analysis of annular ring microstrip antenna," IEEE Trans- Antennas Propag., vol. AP 30, 1982, pp. 637 - 644
59. Chew, W. C., "A broad band annular ring microstrip antenna," IEEE Trans-Antennas Propag., vol. AP 30, 1982, pp. 918 - 922
60. Kokotoff, D.M., Abrele, J. T. and R. B. Waterhouse, "Rigorous analysis of probe-fed annular ring antenna," IEEE Trans. on Antennas Propag., vol. 47, 1999, pp. 384 - 388
61. Navarro, J.A. and K. Chang., "Integrated active antennas and spatial power combining," Wiley, New York, 1996
62. Hagerty, J.A. and Z. Popovic., "A 10 GHz active annular ring antenna," IEEE AP-S Int. Symp. Dig., vol. 2, 2002, pp. 284 - 287
63. Bahl, I. J., Stuchly, S. and M. A. Stuchly., "A new microstrip radiator for medical applications," IEEE Trans on Microwave Theory and Tech. vol. MT-28, 1980, pp. 1464 - 1468
64. Pozar, D.M. and B. Kaufman, "Increasing the bandwidth of microstrip antenna by proximity coupling," Electronic Lett., vol. 23, 1987, pp. 368 - 369

65. Oltman, H. and D. A. Huebner, "Electromagnetic coupled microstrip Dipoles," IEEE Trans. on Antennas Propag., vol. 29, pp. 151 - 156
66. Kishk, A., Lee, K., Mok, W.C. and K. Luk., "A wide-band small size microtrip antenna proximity coupled to a hook shaped probe," IEEE Trans. Antennas Propag., vol. AP-52,no.1,2004, pp. 59 - 65
67. Garg, R., Bhartia, P., Bahl, I. and A. Ittipiboon, "Microstrip antenna design handbook," Artech House, Norwood, MA 2000
68. Schaubert, D. H., Farrar, F.G., Sindoris, A. and S. T. Hayes, "Microstrip antennas with frequency agility and polarization diversity," IEEE Trans. Antennas Propag., vol. AP-29,1981, pp. 118 - 123
69. Bhartia, P. and I. J. Bahl, "Frequency agile microstrip antennas," Microwave Journal, Oct.1982, pp. 67 - 70
70. Daryoush, A. S., Bontzos, K. and P.R. Hercsfeld, "Optically tuned patch antenna for phased array applications," IEEE AP-S Int. Symp. Digest, 1986, pp. 361 - 364
71. Guo, Y. J., Paez, A., Sadeghzadeh, R.A. and S.K. Barton, "A circular patch antenna for radio LANs," IEEE Trans. Antennas Propag., vol. AP-45, 1997, pp. 177 - 178
72. Zhou, G., "Shorting-Pin loaded annular ring microstrip antenna," IEEE AP-S Int. Symp. Digest, 1998, pp. 900 - 903
73. Zhu, Q. and C. Chang., "Analysis of microstrip antennas loaded with shorting pin," IEEE, 2005, pp. 138 - 141
74. Singh. A. and M. Mehram., "Shorted rectangular microstrip antenna for dual band operation," IEEE, 2006, pp. 2661 - 2664
75. Z. Guangping., "Shorted-pin loaded annular ring microstrip antenna," IEEE, 1998, pp. 900 - 903
76. George. J., Vasudevan, K., Mohanan, P. and K. G. Nair., "Dual frequency miniature microstrip antenna," Electron. Letts., vol. 34, 1998, pp. 1168 - 1170
77. Sengupta, D. L., "Resonant frequency of a tunable rectangular patch antenna," Electon. Letts., vol. 20, 1984, pp. 614 - 615
78. Wong, K. and W. S. Chen, "Compact microstrip antenna with dual-frequency operation," Electon. Letts, vol. 33, 1997, pp. 646 - 647

79. Richards, W. F. and Y. T. Lo, "Theoretical and experimental investigations of a microstrip radiator with multiple lumped linear loads," Electromagnetics, no. 3, 1983, pp. 371 - 387

80. Srinivasan, V., Kapur, R. and G. Kumar, "MNM for compact dual frequency rectangular microstrip antenna," Proc. APSYM-98, Cochin, India, 1998, pp. 88 - 91

81. Waterhouse, R.B., "Small microstrip patch antenna," Electron. Letts., vol. 31, 1995, pp. 604 - 605

82. Liu, Z.D. and P.S. Hall, "Dual-band antenna for handheld portable telephones," Electon. Letts., vol. 32, 1996, pp. 609 - 610

83. Rowell, C. R. and R. D. Murch, "A capacitively loaded PIFA for compact mobile telephone handsets," IEEE Trans. Antennas and Propag., vol. AP-45, 1997, pp. 837 - 842

84. Wong, K. and P. Shang- Cheng, "Compact triangular microstrip antenna," Electron. Letts., vol. 33, no. 6, 1997, pp. 433 - 434

85. Gao, S., Li, L. W. and A. Sambell, "FDTD analysis of a dual-Frequency microstrip patch antenna" Progress In Electromagnetics Research, PIER, vol. 54, 2005, pp. 155 - 178

86. Shan, P. and K. Wong, "Design of dual-frequency microstrip antennas using a shorting pin loading," IEEE, 1998, pp. 312 - 315

87. De, A., "Studies on rectangular and circular patch radiators," Ph.D Thesis, Indian Institute of Technology, Kharagpur, 1985

88. Porath, R., "Theory of miniaturized shorting-post microstrip antenna," IEEE Trans Antennas Propag., Vol 48, no.1, January 2000, pp. 41 - 47

88. Posadas, V., Vargas, D., Iglesias, E., Roy, J. and M. Pascual, "Approximate analysis of short circuited ring patch antenna working at TM_{01}mode", IEEE Trans. Antennas and Propag. AP-54, no.6, 2006, pp. 1875 - 1879

89. Teruel, O. and E. Iglesias, "Design of short circuited ring patch antennas working at TM_{01}mode based on neural networks," IEEE Antennas and Wireless Propag., Letters, vol.5, 2006, pp. 349 – 352

90.Zheng, J.X. and D. C. Chang, "End-Correction Network of a coaxial probe for microstrip patch antennas", IEEE Trans. Antennas Propag., 1991, AP-39, no.1, pp. 115 – 118

91.Guha D., "Resonant frequency of circular microstrip antenna with or without air gaps," IEEE Trans. Antennas Propag., AP-49(1), Jan. 2001, pp. 55-59

92. Zeland Software Inc, IE3d Software Release 7.0, Fremont, California, USA, December 1999

93. Schelkunoff, S.A. and H. T. Friis, "Antennas: Theory and practice," John Wiley and Sons, Inc., New York, 1952

2.1 Introduction

Bandwidth enhancement of microstrip patch antennas is the most researched field in the history of microstrip patch technology. There are various methods to enhance the bandwidth of microstrip patch antennas. Stacking the antenna in multilayered configuration is one of these methods. It introduces additional resonance in the frequency resulting in the wide bandwidth and dual frequency operation. Several techniques have been appearing in the last years to improve the bandwidth and to have dual frequency operations in the microstrip antennas by stacking the microstrip antenna. Different methods have been employed to analyze the stacked microstrip antenna like Method of Moments [1], Hankel transform domain analysis [2], Coupled cavity methods [3], Wave guide mode analysis [4], FDTD [5,6] *etc.* Stacked patch solution also presents many degrees of freedom like feeding point location, gap between patches, dielectric constant *etc.* To enhance the bandwidth Tsao [7] and Garidol [8] used the technique of stacked patches in which a parasitic element has been placed over a lower patch. Pozar *et al.* [9] presented an aperture coupled stacked microstrip patch antenna in which the bandwidth has been enhanced upto one octave. A dual frequency antenna can be designed by stacking two slightly different sized circular discs, though a proper choice of the two discs diameters and their spacings and two separate resonances can be found and adjusted [10,11]. A two layered stacked antenna in which radiating element has been excited via electromagnetically feeding element closer to ground plane with a bandwidth of about 9 - 15% for VSWR 2:1[12] has been presented. Several methods for obtaining larger bandwidth for stacked antennas have been carried out using special feeding techniques, variations of the size of two patches [13] or different dielectric layers [14,15].

A numerical model of the stacked circular disc microstrip antenna is developed. The outline of the method of evaluation of input impedance has been presented by De [16]. The expressions for the amplitudes of the excited fields in the resonant cavity are derived by taking the effect of wall admittance, dielectric loss and conductor loss into account. The expression for electric field appearing in the formulation of input impedance is given as superposition of perturbed eigen-modes in the circular patch. The number of higher order modes used for computation is suitably

truncated. Truncation however does not introduce any error in the computation of real value of input impedance. The radiation pattern for the loaded patch is evaluated by considering the magnetic current density at the electrical equivalent edge of the circular patch. Since the height of the substrate is very small and the current density is uniform along the z direction, we can approximate this by a filamentary magnetic current. The detail analysis and the development of the model is first given by developing equations of the circular disc antenna and then extending it to the stacked elements in the proceeding sections

2.2 General Formulation for Input Impedance

Consider a circular disk antenna with a radius r_1 and thickness h, excited by a line current $I_0(z')$ on the feed pin. The feed pin has diameter d_f and is located at (r_0, ϕ_0) and the current density on the pin is given as $\vec{J}(r)$. The input impedance of the antenna seen by a coaxial probe is given by [17]

$$Z_{in} = -\frac{1}{I_0^2}\int_{S_0} \vec{E}^* . \vec{J}^* \, dS \tag{2.1}$$

where the surface integral is over the feed pin surface S_0.This expression for Z_{in} has been derived and is given as

$$Z_{in} = -\frac{1}{I_0^2}\sum_n \sum_p \frac{(j\omega + A)p_n^2}{(j\omega - C)(j\omega + A) + \omega_{np}^2} \tag{2.2}$$

where ω_{np} corresponds to the resonance of eigen-mode corresponding to TM_{np} mode. The parameters A and C are given as

$$A = Z_s \int_{s_e} \left|H_i^2\right| dS \tag{2.3}$$

$$C = -Y_W \int_{s_m} \left|E_i^2\right| dS \tag{2.4}$$

where s_e corresponds to top & bottom surfaces and s_m corresponds to side walls. Z_s and Y_W are the surface impedance of the conductor and wall admittance on the side walls respectively. In equation (2.2), p_n is given as

$$p_n = \int_{S_0} E_i . J^* dS$$

Since the current in the feed pin and fields in the patch radiator are uniform along *z*-axis, the above expression reduces to the form

$$p_n = \frac{I_0 h}{2\pi} \int_0^{2\pi} E_i . d\beta \tag{2.5}$$

2.2.1 Impedance Expression for a Circular Disc Antenna

The circular disc antenna can be easily modified to produce a large range of impedance values, radiation pattern and frequencies of operation. The cavity model is applicable to thin substrates because the variation of field along the substrate thickness is assumed to be negligible. The impedance of circular disc is analyzed on cavity model [18] where it is assumed that the substrate is electrically thin ($h << \lambda_0$). The electric field within the substrate has only *z*-component and is non variant in *z*-direction. The magnetic field has essentially *x* and *y* components. For source free resonator the wave equation can be written in cylindrical co-ordinates as

$$\frac{1\partial}{r\partial r}(r\frac{\partial \psi}{\partial r}) + \frac{1}{r^2}\frac{\partial^2 \psi}{\partial \phi^2} + k^2 \psi = 0$$

The geometry of the circular patch is shown in figure 2.1**.** The circular radiator is excited by coaxial probe of diameter d_f. The equation (2.2) is used for evaluation of input impedance. The use of the equation requires evaluation of normal mode fields. The normal mode fields are evaluated by assuming $Y_W = 0$. While formulating the basic theory concerning the computation of input impedance around a given resonant frequency f_{np} corresponding to the excited TM_{np} mode, it is important to differentiate the notations for wave propagation constant. These are given below

$$k = \omega\sqrt{\mu_0 \varepsilon_0 \varepsilon_{eff}}$$

For measurement frequency $f = f_{np} \pm \Delta f$

$$k_{np} = \omega_{np}\sqrt{\mu_0 \varepsilon_0 \varepsilon_{eff}}$$

$$k_0 = \omega\sqrt{\mu_0 \varepsilon_0}$$

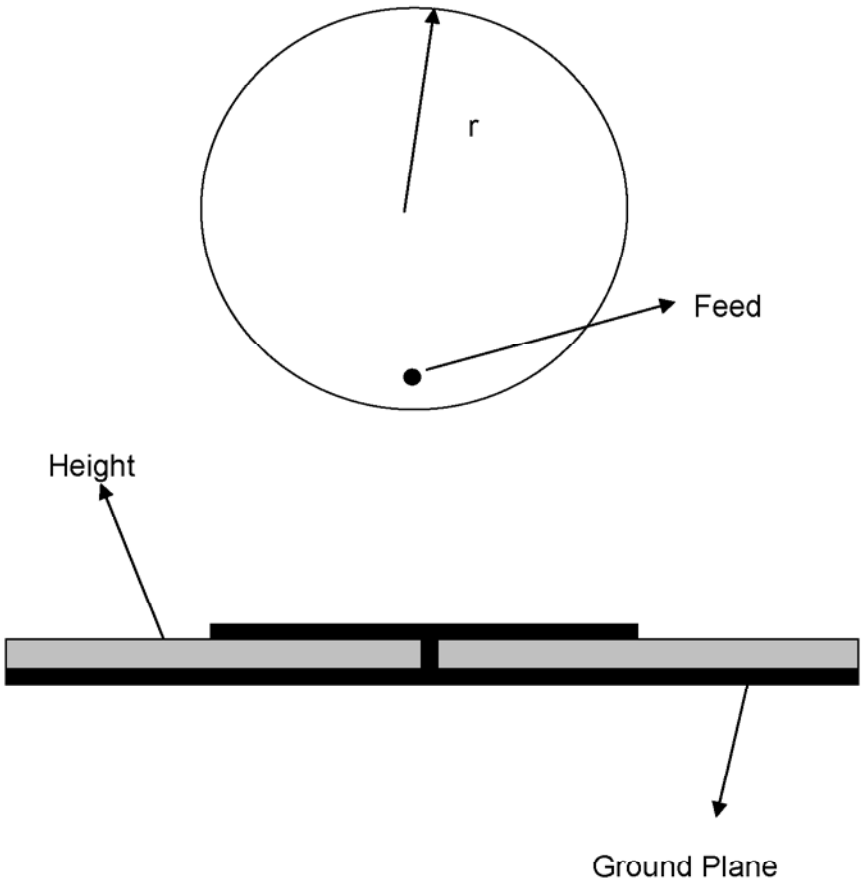

Figure 2.1 Geometry of a circular patch antenna

For thin microstrip antenna $(h/\lambda_g < 0.02)$, $\varepsilon_{eff} \cong \varepsilon_r$

In region I, the expressions for electric field and magnetic field are given as

$$E_z = -j\omega_{np}\mu C_n^1 F_n^{(1)}(k_{np}.r)\cos(n\phi) \tag{2.6}$$

$$H_r = -(\frac{n}{r})C_n^1 F_n^{(1)}(k_{np}.r)\sin(n\phi) \tag{2.7}$$

and

$$H_\phi = -k_{np}C_n^1 F_n^{(1)}(k_{np}.r)\cos(n\phi) \tag{2.8}$$

where

$C_n^{(1)}$ is a constant.

$$F_n^{(1)}(k_{np}r) = J_n(k_{np}.r) \tag{2.9}$$

where J_n is the first order Bessel function

$$F_n^{(1)'}(k_{np}r) = J_n^{'}(k_{np}.r) \tag{2.10}$$

where $J_n^{'}$ is the derivative of first order Bessel function

Application of boundary conditions

$H_\phi(a) = 0$

$J_n^{'}(k_{np}a) = 0$

Application of the boundary condition gives the resonant frequency.

For evaluating the constant $C_n^{(1)}$ the normalization condition [19] is used.

$$\int_V \varepsilon|E|^2 dV = 1$$

For the entire volume the normalization condition for the problem under consideration assumes the form

$$\int_0^h \int_0^{2\pi} \{\int_0^a \varepsilon|E_z|^2\} r dr = 1 \tag{2.11}$$

This result in

$$C_n^{(1)} = \frac{1}{k}\sqrt{\frac{1}{\pi h \mu I_1}} \tag{2.12}$$

where

$$I_1 = \int_0^a J_n^2(k.r) r dr$$

The different parameters appearing in equation (2.2) for input impedance for the problem under consideration assumes the following form

$$A = Z_s \int_0^{2\pi} \int_0^a \{ \left| H_\phi \right|^2 + \left| H_r \right|^2 \} r dr \tag{2.13}$$

where surface resistance Z_s is given as

$$Z_s = \{ \frac{\pi f \mu}{\sigma} \}^{\frac{1}{2}}$$

and

$$C = -Y_w \int_0^h \int_0^{2\pi} \left| E_z \right|^2 r d\phi dz \qquad (at\ r = a) \tag{2.14}$$

From this

$$A = Z_s \pi C_n^{(1)} \left[k^2 I_3 + n^2 I_4 \right] \tag{2.15}$$

where

$$I_3 = \int_0^a J_n^{2\prime}(k.r) r dr$$

$$I_4 = \int_0^a \frac{J_n^2(k.r)}{r^2} r dr$$

The expression of A corresponds to the copper loss in the microstrip.

Consider a loaded microstrip patch radiator excited by a coaxial line feeding a probe located at $(r_0, \phi_0, 0)$. Using the transformation [20]

$$r = r_0 + \frac{d_f}{2} \cos\beta$$

and expanding the Bessel function in Taylor series, the function $F_n^{(1)}(k.r)$ is obtained as

$$F_n^{(1)}(k.r) = J_n(k.r_0) + \frac{k d_f}{2} J_n^{'}(k.r_0) \cos(\beta) \tag{2.16}$$

where the higher order terms of the Taylor series expansion are neglected.

Using the transformation

$$\phi = \frac{d_f}{2r_0}\sin\beta$$

and expanding cos*(nϕ)* & sin*(nϕ)* in series of Bessel function it is found

$$\cos(n\phi) = J_0(\frac{nd_f}{2r_0}) + 2\sum_{q=1}^{\infty} J_{2q-1}(\frac{nd_f}{2r_0})\cos(2q\beta) \tag{2.17}$$

$$\sin(n\phi) = 2\sum_{q=1}^{\infty} J_{2q-1}(\frac{nd_f}{2r_0})\sin[(2q-1)\beta] \tag{2.18}$$

Substituting in equation (2.5) and carrying out the integration

$$p_n = -j\omega\mu h I_0 C_n^{(1)} J_n(k.r_0) J_0(\frac{nd_f}{2r_0}) \tag{2.19}$$

Substituting equation (2.19) in eq. (2.2), we get

$$Z_{in} = \mu^2 h^2 \sum_n \sum_p \frac{(j\omega + A) C_n^{(1)^2} \omega^2 \left[J_n(k.r_0) J_0\left(\frac{nd_f}{2r_0}\right)\right]^2}{(j\omega - C)(j\omega + A) + \omega_{np}^2} \tag{2.20}$$

From equation (2.20) we can evaluate the impedance of circular patch antenna.

2.2.2 Formulation of Computation of Radiation Pattern

The fields radiated by circular patch can be found by using Equivalence principle where the circumferential wall of the cavity is replaced by equivalent magnetic current density. The magnetic current density evaluated at the electrical equivalent edge r_e of the circular patch can be written as

$$\overrightarrow{M_s} = -2\hat{n} \times E_z\big|_{\rho'=r_e} \tag{2.21}$$

Since the height of the substrate is very small and the current density given by equation (2.21) is uniform along the z-direction, we can approximate (2.21) by a filamentary magnetic current

$$I_m = h\overrightarrow{M_s} = \hat{a}_\phi 2h(-j\omega\mu) C_n^{(1)} F_n^{(1)}(k.r_e)\cos(n\phi) \tag{2.22}$$

In the far-field the total $\vec{E}$ fields can be written as [21]

$$E_r = 0 \tag{2.23}$$

$$E_\theta \cong -jk_0 \frac{e^{-jk_0 r}}{4\pi r} L_\phi \tag{2.24}$$

$$E_\phi \cong +jk_0 \frac{e^{-jk_0 r}}{4\pi r} L_\theta \tag{2.25}$$

where

$$L_\phi = \iint_S M_\phi \cos(\phi - \phi') e^{+jk_0 r' \cos\Psi} ds' \tag{2.26}$$

$$L_\theta = \iint_S M_\phi \cos\theta \sin(\phi - \phi') e^{+jk_0 r' \cos\Psi} ds' \tag{2.27}$$

In equations (2.26) and (2.27)

$r' \cos\Psi = \rho' \sin\theta \cos(\phi - \phi')$

$ds' = \rho' d\rho' d\phi'$

Using the following two relations

$$\int_0^{2\pi} \cos(\phi' - \phi) e^{jm\phi'} e^{jk\rho' \sin\theta \cos(\phi' - \phi)} d\phi' = \pi j^m e^{jm\phi} \{ j[J_{m+1}(k\rho' \sin\theta) + J_{m-1}(k\rho' \sin\theta)] \}$$

and

$$\int_0^{2\pi} \sin(\phi' - \phi) e^{jm\phi'} e^{jk\rho' \sin\theta \cos(\phi' - \phi)} d\phi' = \pi j^m e^{jm\phi} [J_{m+1}(k\rho' \sin\theta) + J_{m-1}(k\rho' \sin\theta)]$$

we obtain for TM_{11} mode

$$E_\theta = -\frac{e^{-jk_0 r}}{r} \left(\frac{h}{\pi}\right) \left(\frac{\omega\mu_0}{\sqrt{\varepsilon_r}}\right) C_n^{(1)} [J_0(k_0 r_e \sin\theta) - J_2(k_0 r_e \sin\theta)] \{\cos\phi\} \tag{2.28}$$

and

$$E_\phi = +\frac{e^{-jk_0 r}}{r} \left(\frac{h}{\pi}\right) \left(\frac{\omega\mu_0}{\sqrt{\varepsilon_r}}\right) C_n^{(1)} \cos\theta [J_0(k_0 r_e \sin\theta) + J_2(k_0 r_e \sin\theta)] \sin\phi \tag{2.29}$$

2.2.3 Radiated Power

The power radiated by a circular patch is estimated as

$$P_r = \frac{1}{2\pi} \int_0^{2\pi} \int_0^{\frac{\pi}{2}} \left(\left|E_\theta^{\,2}\right| + \left|E_\phi^{\,2}\right|\right) r^2 \sin\theta d\theta d\phi \tag{2.30}$$

For TM_{11} mode expression (2.30) can be written as

$$P_r = \frac{2\pi}{\eta_0}\left(\frac{E_0}{k_0 r_e}\right)^2 [(k_0 r_e)^2 I_5 + I_6] \tag{2.31}$$

where

$\eta_0 = 120\pi$

$$E_0 = \frac{h}{\pi}\left(\frac{\omega\ \mu_0}{\sqrt{\varepsilon_r}}\right) C_n^{(1)} \tag{2.32}$$

$$I_5 = \int_0^{\frac{\pi}{2}} \left[J_1'(k_0 r_e \sin\theta)\right]^2 \sin\theta\, d\theta \tag{2.33}$$

$$I_6 = \int_0^{\frac{\pi}{2}} \left[J_1(k_0 r_e \sin\theta)\right]^2 \frac{\cos^2\theta}{\sin\theta} d\theta \tag{2.34}$$

2.2.4 Evaluation of Wall Admittance

In order to determine the input impedance of the circular patch, it is necessary to take into account the reactive power due to the electric and magnetic stored energy in the fringe of the disk and the real power due to radiation. These reactive and active powers are given by equivalent boundary admittance at the disk edge. The boundary admittance Y_W is given by [18];

$$Y_W = g_n + jb_n \tag{2.35}$$

where

$$g_n = \frac{P_T}{\frac{1}{2}\int_{S_m} |E_z|^2 ds|_{\rho=r_e}} \tag{2.36}$$

and

$$b_n = \frac{-P_i}{\frac{1}{2}\int_{S_m} |E_z|^2 ds|_{\rho=r_e}} \tag{2.37}$$

where P_i is the reactive power and P_T is the total power given by

$P_T = P_r + P_c + P_d$

where P_r is the radiated power, P_c is the copper loss and P_d is dielectric loss. P_c is same as A given by equation (2.13) and the dielectric loss is given as

$$P_d = \frac{1}{2} h\omega\varepsilon_r\varepsilon_0 \tan\delta\pi(\omega\mu)^2 C_n^{(1)2}[I_1]$$

where $C_n^{(1)}$ is given by equation (2.12).

Thus

$$g_n = \frac{h}{\eta_0 r_e}[(k_0 r_e)^2 I_5 + I_6].\frac{1}{eff_{np}} \tag{2.38}$$

where eff_{np} is the efficiency of the antenna when TM_{11} mode is excited and is given as

$$eff_{np} = \frac{P_r}{P_T} \tag{2.39}$$

Estimation of the reactive power, is made by computing the fields at the edge of the disk

Substituting, values of P_i in equation (2.37) we get the expression for b_n

$$b_n = \frac{1}{\eta_0}\frac{\varepsilon_0\varepsilon_r\omega\pi r_1^2}{h}[\{1 + \frac{2h}{\pi r_1\varepsilon_r}(\ln(\frac{\pi r_1}{2h}) + 1.7726)\}^{1/2} - 1] \tag{2.40}$$

Using equations (2.38) and (2.40), we can compute Y_W.

From expression (2.40), it is evident that wall susceptance accounts for the fringing fields which increases the physical radius to an effective radius r_e. It is important to note that while computing the input impedance around resonance, the resonant frequency ω_{np} is to be given as input value. This ω_{np} already accounts for the fringing field using r_e as the effective radius of the patch. Therefore, to avoid multiple corrections due to fringing fields b_n is taken to be zero. In general, since the substrate height is small compared to the wavelength, it can be assumed that the fringing field is extended up to a distance from the edges so a magnetic wall can be set at that region. The effective radius can be calculated as follows;

$$\Delta C_{LCP} = \ln(\frac{a}{2h}) + 1.41\varepsilon_r + 1.7726 + \frac{h}{a}(0.286\varepsilon_r + 1.65) \tag{2.41}$$

$$r_e = a\sqrt{1+\frac{2h}{\pi a \varepsilon_r}\Delta C_{LCP}} \tag{2.42}$$

The electric and magnetic energies stored inside the lower cavity becomes

$$W_e = \frac{P_d}{2\omega \tan\delta} \tag{2.43}$$

and

$$W_h = \frac{1}{4}\mu_0 h \frac{P_c}{R_s} \tag{2.44}$$

2.2.5 Application of End-Correction Network of a Coaxial Probe

The theory developed in the previous sections for a circular microstrip antenna assumes the use of a coaxial probe. For validating this theory through experimental verification, it is necessary to properly model the coaxial probe. A survey of analytical models used for evaluating the input impedance of probe-fed microstrip antenna is given in [22]. For purpose of computing input impedance, the end-correction network suggested by Zheng *et al.* [23] is used. Zheng suggests that TEM aperture field approximation can provide an accurate result of input admittance and there is no need to introduce a specific correction network for most applications. Constant current probe model is valid only when both $k_1 d << 1$ and $a'/d << 1$ are satisfied (where d is the substrate height and a is the radius of the centre conductor of the coaxial probe). An end-correction network consisting of a series inductor and a shunt capacitance should be used for higher accuracy. Using this correction network the input impedance for the probe-fed microstrip antenna is given as

$$Y_{TEM} \approx \frac{1}{[R_p + j\omega(L_p + L_0)]} + j\omega C_0 \tag{2.45}$$

where

$$\begin{aligned} C = {} & \varepsilon_0 \varepsilon_r [6d \ln^2(b'/a')]^{-1} \{3\pi[b'^2 - a'^2 - 2b^2 \ln(b'/a')] \\ & + 4\pi h^2 \ln(b'/a') - 12h^3(\pi^2 b')^{-1} X_0\} \end{aligned} \tag{2.46}$$

where

$$X_0 = \xi(3) - \sum_{n=1}^{\infty} n^{-3} \exp[-2n\pi(b'-a')/h]$$

$$L_0 = -\mu_0 h k_1^2 [4\pi \ln(b'/a')]^{-1} . [(b'^2 + a'^2)\ln(b'/a') - b'^2 + a'^2][\ln(k_1 a'/2) + \gamma] \quad (2.47)$$

ξ is the Riemann zeta function and $\xi(3) = 1.202$ b and b is the radius of the outer conductor of the probe. The $R_p + j\omega L_p$ in equation (2.45) is the same input impedance derived from the constant current probe approximation. The end-correction network formed by C_0 and L_0 can be used even when the input impedance Z_p associated with the infinite parallel plates is replaced with that of a finite size patch when the probe is not located very close to the edge. The expression for input impedance resembles the form of a parallel *RLC* circuit, although in this case each element can be considered as frequency dependant. Based on the analogy with a parallel resonant circuit the input impedance for a probe free circular patch can also be re-written as

$$Z_{in} = \frac{1}{\frac{2P_T}{|V|^2} + j\frac{4\omega}{|V|^2}W_e - j\frac{4\omega}{|V|^2}W_h} \quad (2.48)$$

where

$V = -dE_{av}$

and

$$E_{av} = \frac{1}{2d}\int_0^{2\pi} E_z^2(r_1, \phi) d\phi$$

2.3 Theory of Stacked Circular Patch

The cavity model developed for a single circular patch can now be extended for a stacked geometry. In this case the stacked antenna has to be considered as two coupled cavities. It is necessary to accurately predict the upper and lower cavity resonant frequency; next the electric fields generated inside the upper and lower cavities are added together using the correct effective values of the dielectric constant. The Green's function is obtained for the lower circular patch and the upper circular patch. The main difference lies in the effective dielectric constants and the patch dimensions. The resulting total electric field inside the cavities can be calculated by adding together the contributions of the field in the superstrate and in the substrate.

This assumption can be supported by the fact that the cavity model assumes no z variations of the electric field. The assumption gets invalidated if the height of the superstrate is large as compared to wavelength. The lower cavity can be considered to be loaded by a dielectric material ignoring the upper patch. This is valid as the fields are concentrated between the lower patch and the ground. The superstrate on the other hand will alter the effective dielectric constant. However, in the present case there is a substantial air-gap between the substrate and the superstrate. For this case exact computation of effective dielectric constant is not necessary since height of air-gap >> d. If the air-gap is reduced, it will be necessary to replace ε_r by $\varepsilon_{r,eff} = p.\varepsilon_r$ where p is an empirical correction factor less than one. The upper patch can be considered in isolation as uncoupled cavity with an air gap. For such cases the expression for effective dielectric constant is given as [24]

$$\varepsilon_{re} = \frac{\varepsilon_r(1+h/d)}{(1+\varepsilon_r h/d)} \tag{2.49}$$

where h is the air-gap and d is the superstrate height. The resonant frequency is obtained from the relation

$$f_{np} = \frac{\chi_{np}.300}{2\pi b_{eff}\sqrt{\varepsilon_{ef}}} \tag{2.50}$$

where

$$\varepsilon_{ef} = \frac{4\varepsilon_{re}\varepsilon_{r,dyn}}{(\sqrt{\varepsilon_{re}}+\sqrt{\varepsilon_{r,dyn}})^2} \tag{2.51}$$

where

$$\varepsilon_{r,dyn} = \frac{C_{dyn}(\varepsilon=\varepsilon_0\varepsilon_{re})}{C_{dyn}(\varepsilon=\varepsilon_0)} \tag{2.52}$$

where C_{dyn} is the dynamic capacitance defined as

$$C_{dyn} = C_{0,dyn} + C_{\varepsilon,dyn} \text{ (main and fringing capacitances)} \tag{2.53}$$

The dynamic capacitances are related to static capacitances as

$$C_{0,dyn} = 0.3525 C_{0,stat} \tag{2.54}$$

$$C_{0,dyn} = 0.5\, C_{\varepsilon,dyn} \tag{2.55}$$

The static capacitances are evaluated as follows.

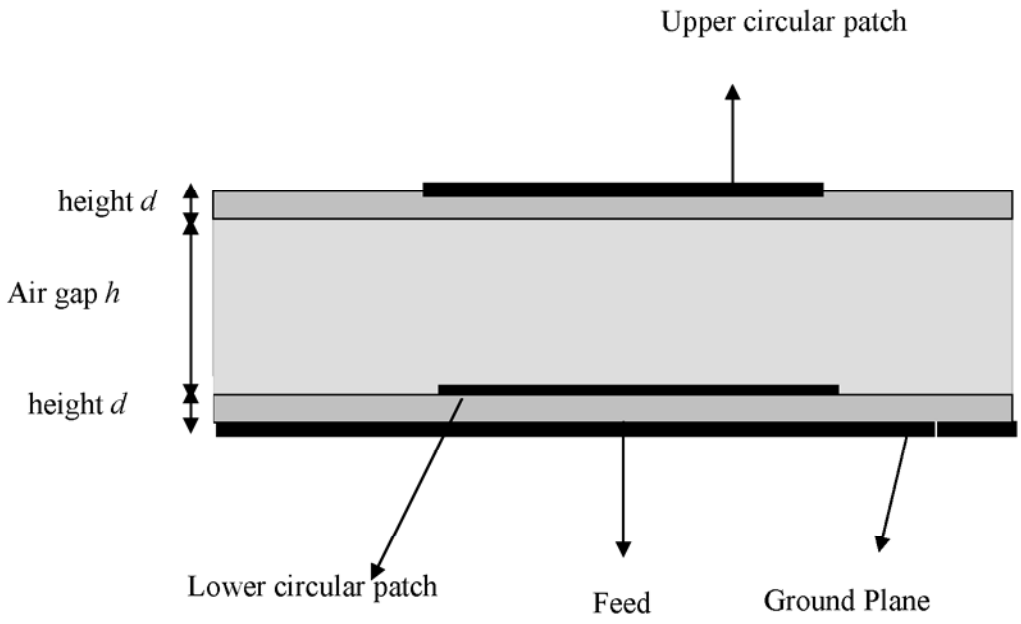

Figure 2.2 Geometry of a stacked circular patch antenna.

$$C_{0,stat} = \frac{(\varepsilon_0 \varepsilon_{re} \pi b^2)}{h_T} \tag{2.56}$$

where,

$h_T = d + h + d$ = total height over the ground plane

$$C_{\varepsilon,stat} = C_{0,stat} . q \tag{2.57}$$

$q = \mathrm{u} + \mathrm{v} + \mathrm{uv}$

$$u = \frac{1+\varepsilon_{re}}{\varepsilon_{re}} \frac{4}{\pi b / h_T}$$

$$v = \frac{2}{3t}\left(\frac{\ln(p)}{8 + \pi b / h_T}\right) + \left(\frac{1}{t} - 1\right) / g$$

$\mathrm{t} = 0.37 + 0.63\varepsilon_{\mathrm{re}}$

$$p = \frac{1 + 0.8(b/h_T)^2 + (0.31 b/h_T)^4}{1 + 0.9 b / h_T}$$

$$g = 4 + 2.6 b/h_T + 2.9 h_T / b$$

The effective radius of the microstrip disk is

$$\mathrm{b_{eff}} = \mathrm{b}\sqrt{1 + m.q} \tag{2.58}$$

The upper patch has to be analyzed like an uncovered microstrip patch. However lower patch does not provide sufficient ground plane and this fact will introduce errors. The effects of coupling between the substrate and the superstrate will change the effective dimensions of the upper ring and thus will increase the resonant frequency as compared to the case without substrate. It is necessary to accurately account for the interaction between fringing fields in the lower and the upper patch by changing the effective radii of the upper patch. Once the effective dielectric constant is obtained for the upper patch, the effective dimension b_{eff} is obtained. In equation (2.58), m is an empirical correction factor. Next, the input impedance for the probe free upper patch is obtained using equation (2.48) with suitable changes in the various parameters. Thus each cavity is studied separately as though they are uncoupled. The coupling is done through adding the individual impedances. Though the resonance of the cavities is studied in capacitive mode, the radiated fields are strongly coupled.

Therefore in the formulation mentioned above, P_r remains a single expression taking into account both the uncoupled fields.

$$P_r = \frac{2\pi}{\eta_0}\left(\frac{E_0}{k_0 r_e}\right)^2 [(k_0 r_e)^2 I_5 + I_6] \tag{2.59}$$

where I_5 and I_6 are defined in equation (2.33) and (2.34) respectively.

2.4 Results and Discussion

The stacked antenna approach is used for the design of broadband antennas. The stacked antenna consists of a circular patch of a radius a on the lower substrate of dielectric thickness d and dielectric constant ε_r. Another circular patch of radius b is placed on top of the lower patch on identical dielectric with an air gap h between these two cavities. For numerical calculation and simulation of the antenna input parameters taken are a = 22.65 mm, d = 0.787 mm, h = 9 mm and the ratio of patch sizes b/a = 1, 1.05 and 1.1. Figures 2.3 and 2.4 show the real and imaginary parts of input impedance with frequency of a circular patch antenna respectively. A very good agreement has been observed in the resonant frequency as well as magnitudes of impedances. The problem of stacked patch is considered as two uncoupled impedances coupled through capacitive coupling. Now the upper circular patch is placed and the problem is solved both numerically and compared with simulated results.

Figures 2.5 and 2.6 show the real and imaginary part of input impedances respectively for b = 1 a when feedpoint location (r_0) is at 12 mm along the radial direction. In case of b = 1.1a, there is a disagreement to the extent of 4 - 5% in resonant frequency. This is due to the fact that lower circular patch which is acting as ground plane for upper circular patch is not fully covering upper circular patch. Also cavity model exhibits error when height of substrate is thick as in this case. Figures 2.7 and 2.8 show the real and imaginary part of input impedance respectively when b = 1.1 a and feed point location r_0 = 20 mm. Figures 2.9 and 2.10 show the real and imaginary part of input impedance respectively for b = 1.1 a for r_0 = 12 mm. Figures 2.11 and 2.12 show results for b = 1.05 a for r_0 = 20 mm. It has been observed that for b/a = 1.1 there is fairly mismatch as it amounts to the fact that the lower patch is

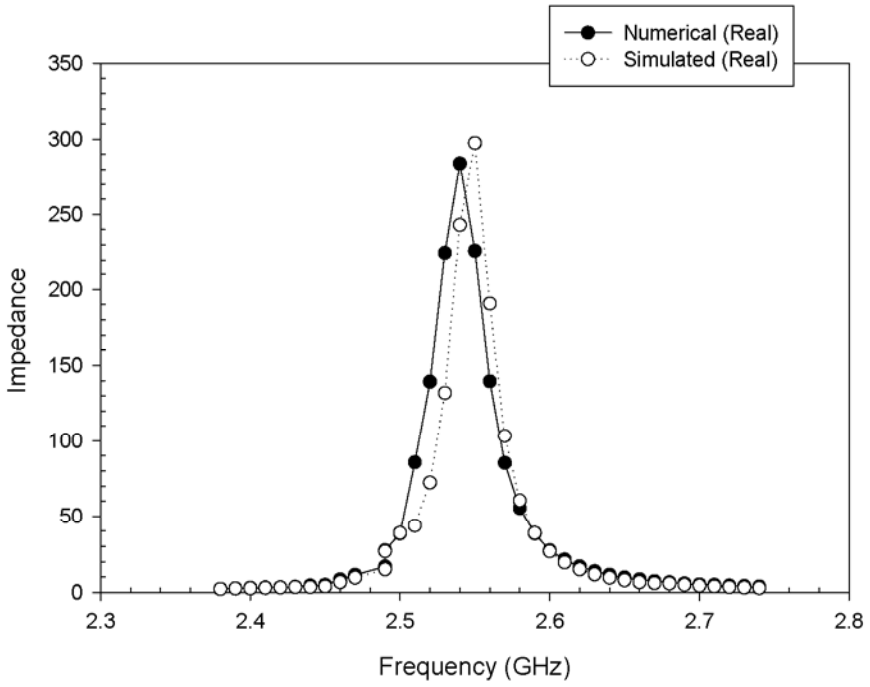

Figure 2.3 Variation of Impedance (Real) with Frequency for single patch $r_0 = 20$ mm.

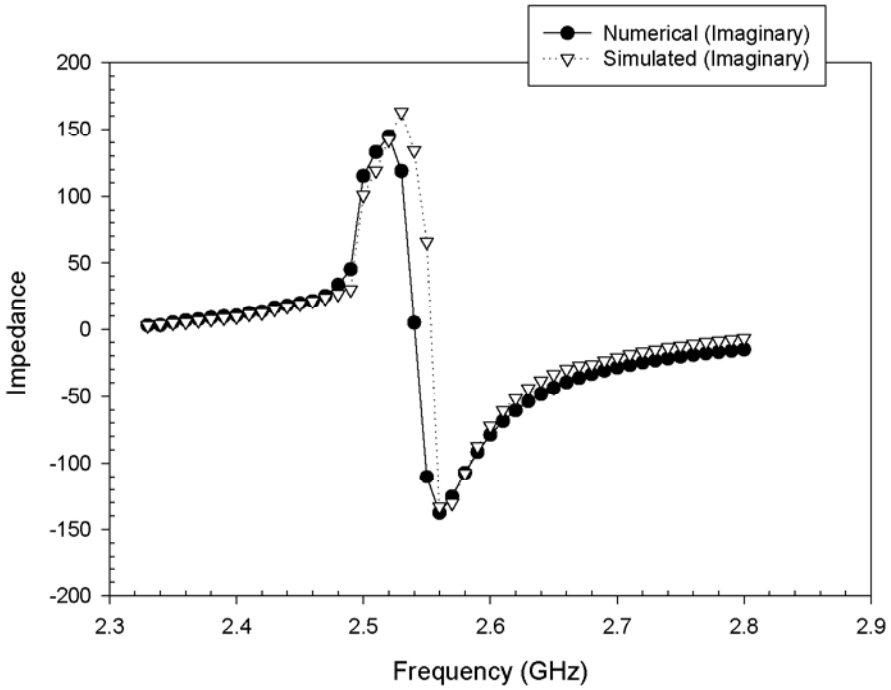

Figure 2.4 Variation of Impedance (Imaginary) with Frequency for single patch $r_0 = 20$ mm.

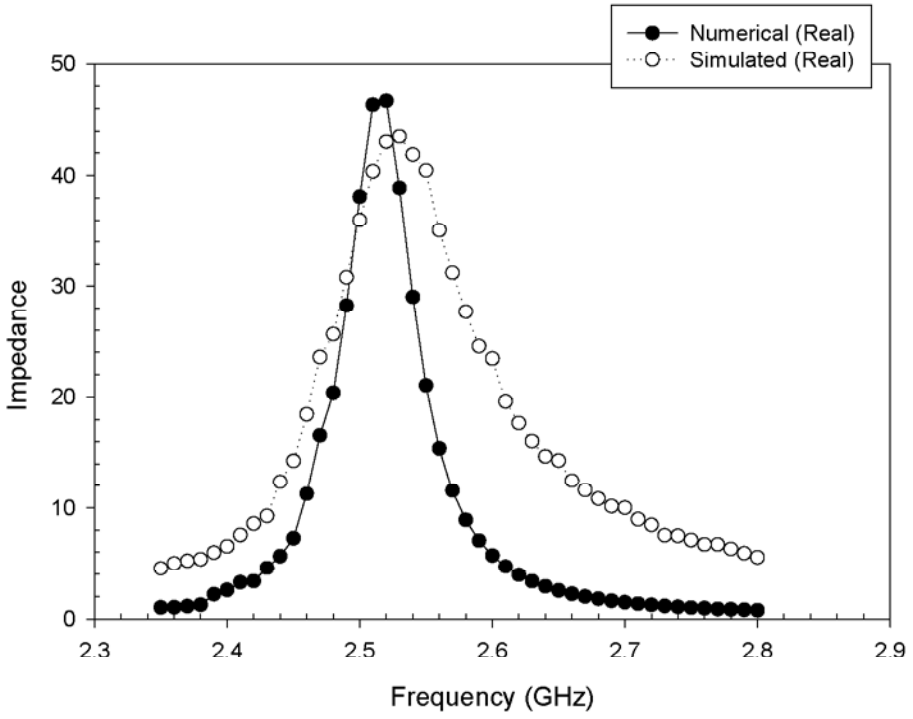

Figure 2.5 Variation of Impedance (Real) with Frequency for the ratio of patch sizes $b/a = 1$ and $r_0 = 12$ mm.

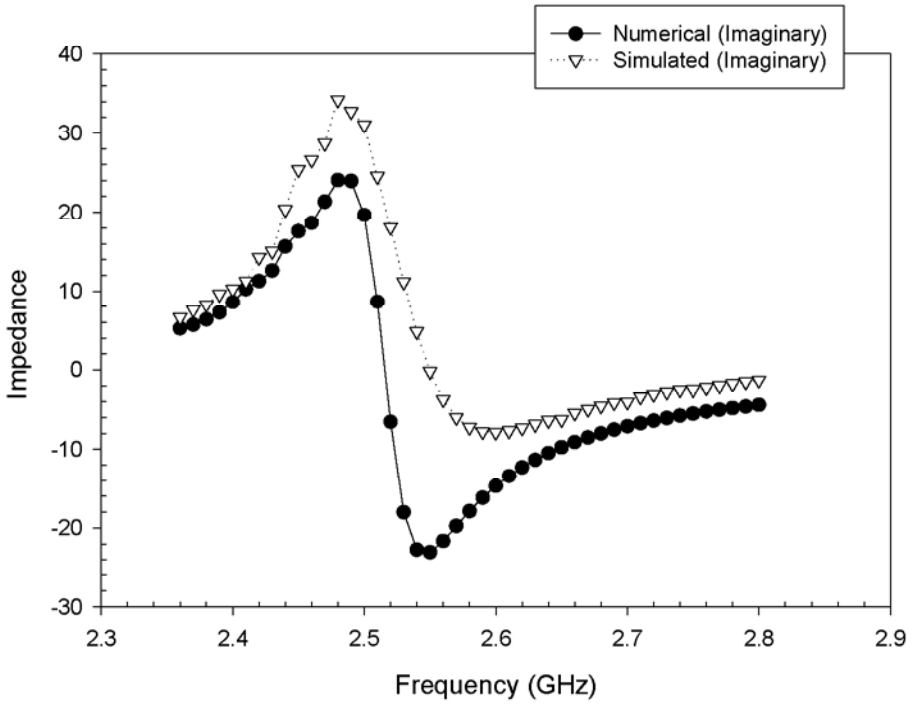

Figure 2.6 Variation of Impedance (Imaginary) with Frequency for the ratio of patch sizes $b/a = 1$ and $r_0 = 12$ mm.

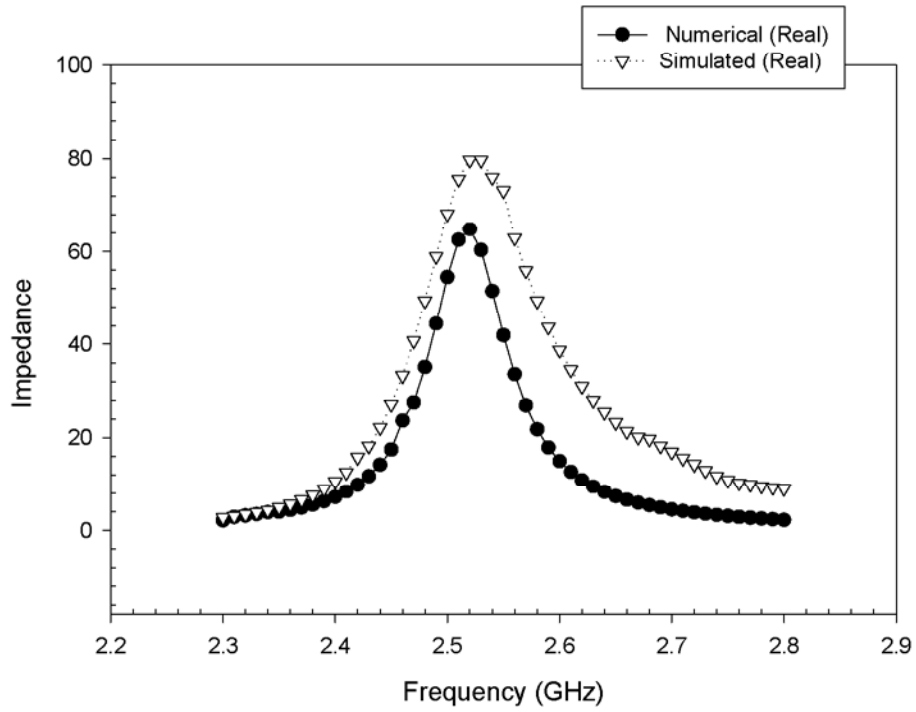

Figure 2.7 Variation of Impedance (Real) with Frequency for the ratio of patch sizes $b/a = 1.1$ and $r_0 = 20$ mm.

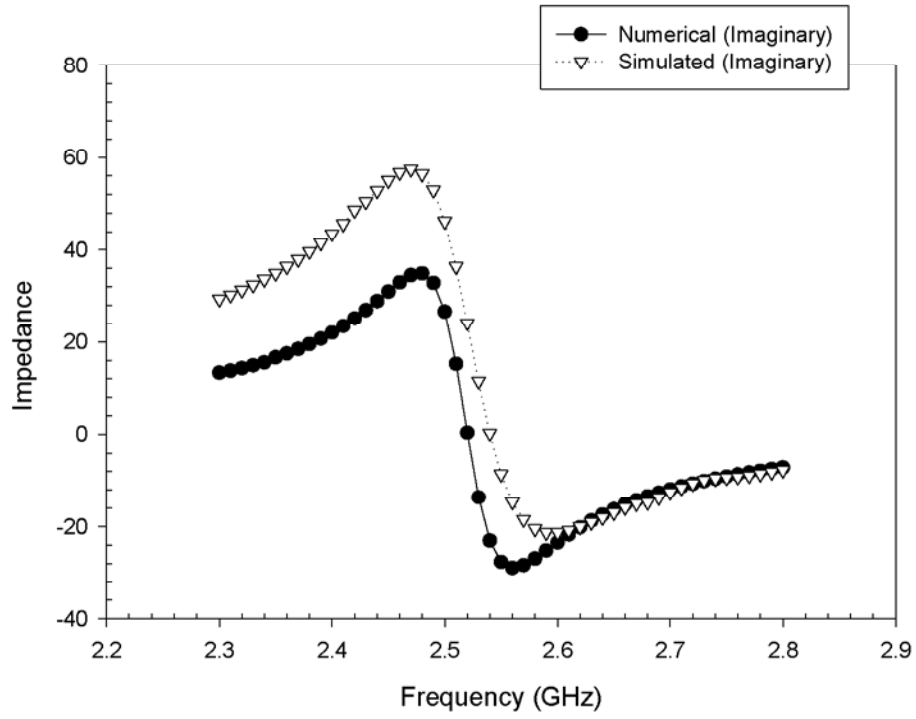

Figure 2.8 Variation of Impedance (Imaginary)] with Frequency for the ratio of patch sizes $b/a = 1.1$ and $r_0 = 20$ mm.

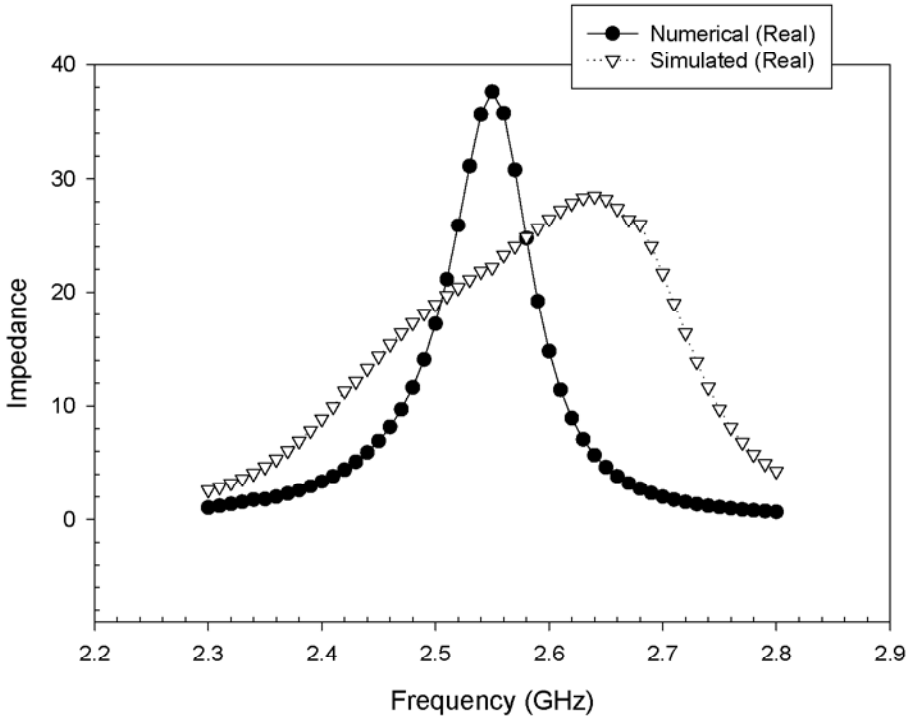

Figure 2.9 Variation of Impedance (Real) with Frequency for the ratio of patch sizes $b/a = 1.1$ and $r_0 = 12$ mm.

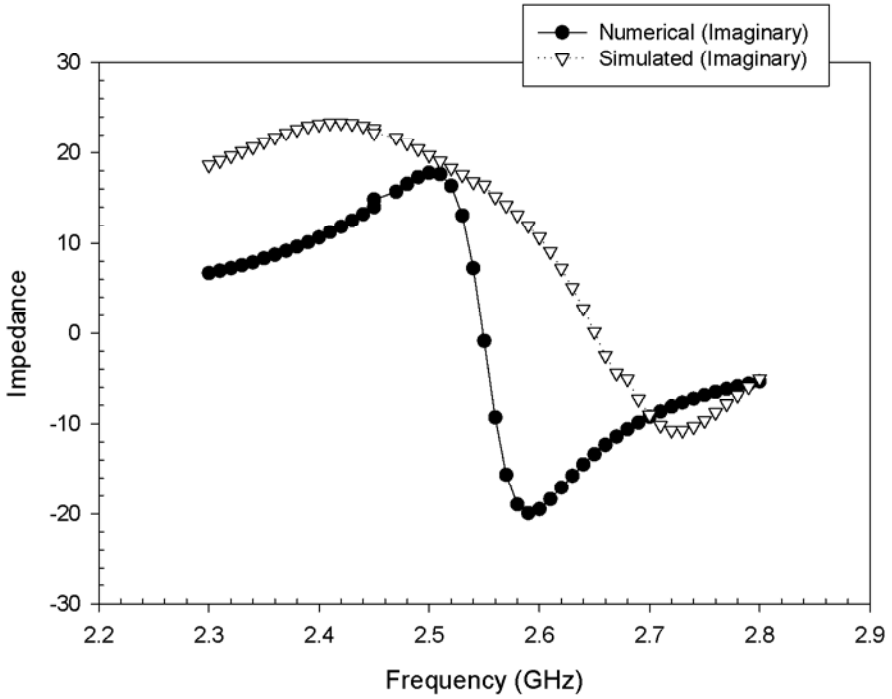

Figure 2.10 Variation of Impedance (Imaginary) with Frequency for the ratio of patch sizes $b/a = 1.1$ and $r_0 = 12$ mm.

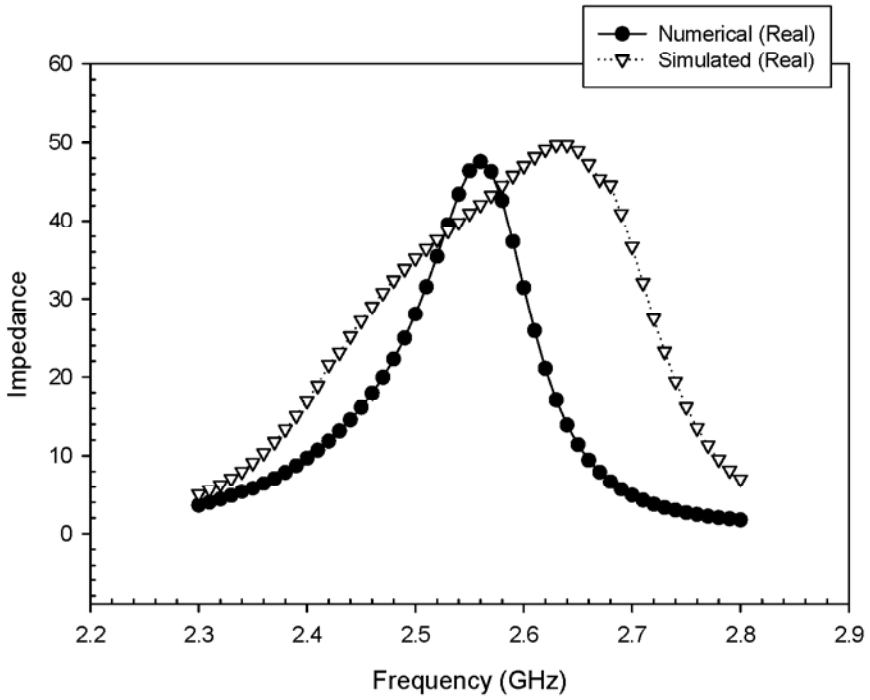

Figure 2.11 Variation of Impedance (Real) with Frequency for the ratio of patch sizes $b/a = 1.05$ and $r_0 = 20$ mm.

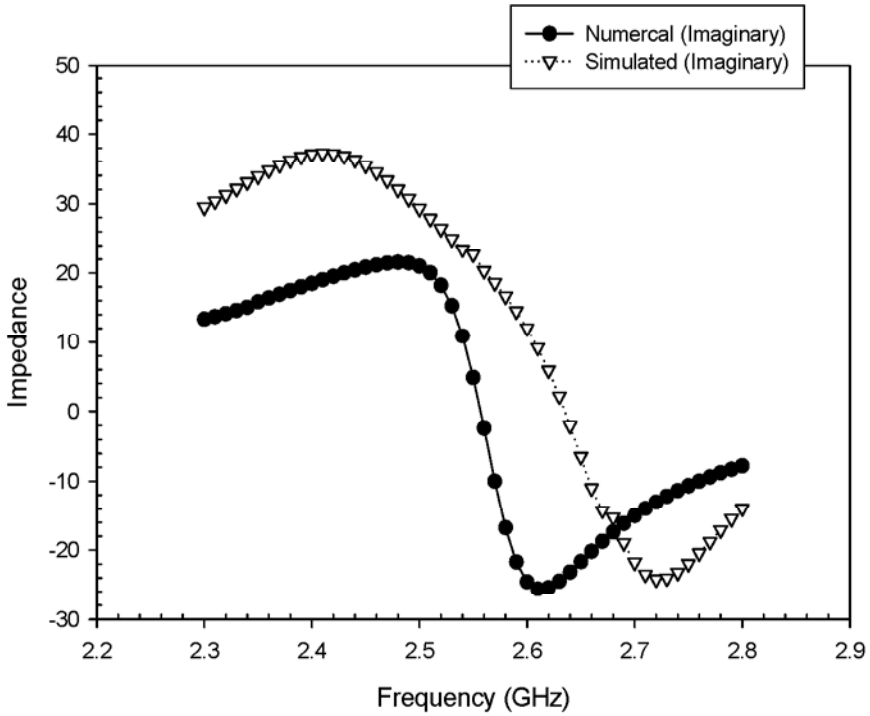

Figure 2.12 Variation of Impedance (Imaginary) with Frequency for the ratio of patch sizes $b/a = 1.05$ and $r_0 = 20$ mm.

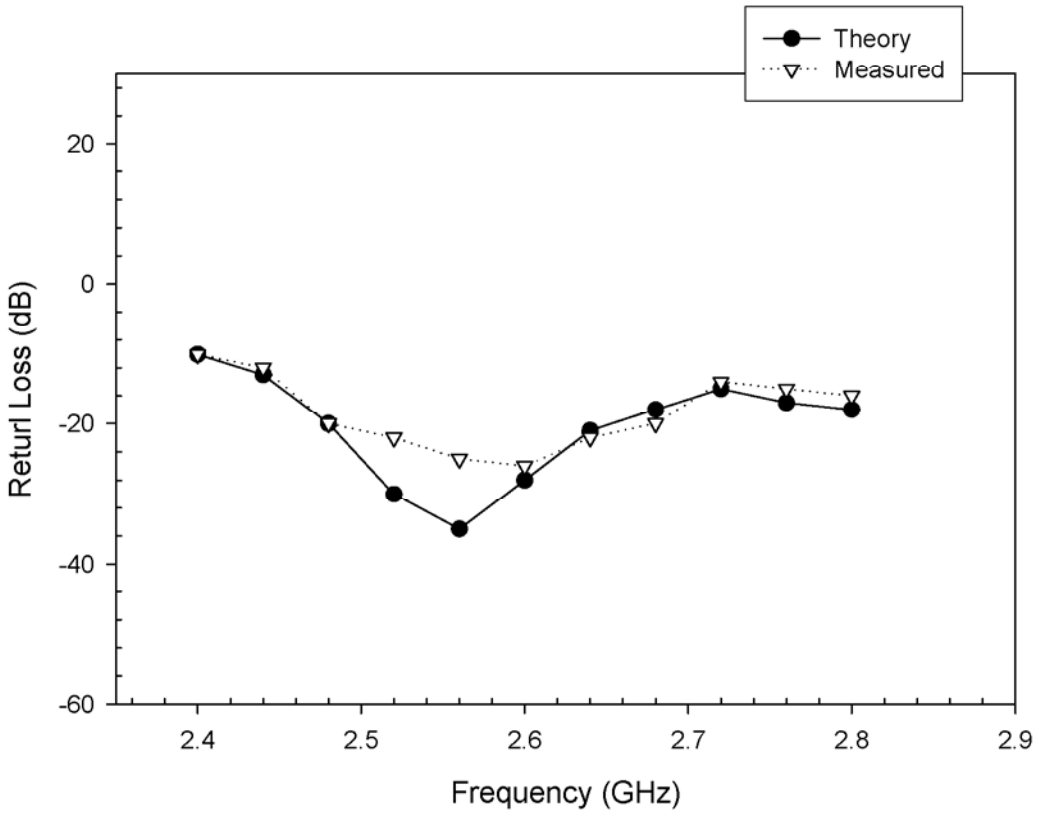

Figure 2.13 Theoretical and measured return loss for a single element stacked antenna.

Table 2.1 Comparison of gain of stacked patch and single patch antenna.

Antenna Type	Frequency in GHz	Gain in dB
Single Patch (Radial feed at 12 mm)	2.56	5.23
Stacked Patch (Radial Feed at 12 mm and $b/a = 1$)	2.51	7.72
	2.55	8.26
	2.62	8.11

Table 2.2 Numerical and Simulated values of radiation efficiency of stacked antenna with radial feed using equation (2.39) ($r_0 = 12$ mm and ratio of patch size $b/a = 1$).

Antenna	Frequency in GHz	Radiation Efficiency in Percentage	
		Numerical	Simulated
Stacked	2.51	97.75	94.20
	2.55	97.80	94.25
	2.62	97.42	94.16

assumed to be ground plane for the upper patch. This model is valid for $\frac{b}{a} \leq 1$ and for $\frac{b}{a} < 1$, this model is not applicable. Now edge fed stacked antenna is fabricated for dimensions; a = 22.65 mm, h = 9 mm, d = 0.787 mm and b = 1.05 a and is tested. With these values the resultant structure exhibits input impedance of 50 Ω (characteristic impedance of feed line). While in the absence of stacked element the input impedance is nearly 270 Ω. The band width in this case is found 200 MHz around the central frequency of 2.6 GHz. The theory is applied to single patch with dimensions a = 22.65 mm, and r_0 = 12 mm and to the stacked elements of dimensions a = 22.65 mm, r_0 =12 mm and $b = a$. For this case, the band size observed is 2.51 GHz - 2.62 GHz around central frequency of 2.55 GHz. In case of patch antenna it is at 2.56 GHz. Comparison of gain of single patch and stacked antenna is calculated numerically and is given in table 2.1. It is evident from the table 2.1 that gain is considerably high in case of stacked elements even at the edges of the band width. Numerical and simulated values of the radiation efficiency are reported in Table 2.2 which is calculated numerically using equation (2.39). These values are in good agreement.

2.5 Conclusion

An analytical technique to find out the impedance of stacked circular microstrip antenna around fundamental resonance for a probe fed case is presented. The result for an edge-fed case shows that 10 % bandwidth is achievable. It has been observed that with the stacking of elements input impedance is considerably reduced to the feed line impedance (50 Ω) or near it. Gain is considerably high in case of stacked elements and radiation efficiency is more than 94 % for different cases. The feed point locations at different radial positions also predict not only the enhancement of bandwidth but the improvement of radiation characteristics A major application for such antenna is the ease with which a circular polarized array can be designed with large bandwidth. For some applications it is required to have two closely spaced resonances for transmission and reception mode with circular polarization. The same approach can be applied to other geometries to design broadband antenna.

References

1. Tulintseff, A. N. and R. M. Sorbello, "Current and radiation fields of electromagnetically coupled microstrip antennas," IEEE AP-S, vol. 2, 1987, pp. 928 - 931
2. Fan, Z. and K. F. Lee, "Hankel transform domain analysis of a dual frequency stacked circular disk and annular ring microstrip antennas," IEEE Trans. Antennas Propag., vol. 39, 1991, pp. 867 - 870
3. Cock, R. T. and C. G. Christodoulou, "Design of a two-layer capacitively coupled, microstrip patch antenna element for broadband applications," IEEE Antennas Propag. Soc. Int. Symp. Dig., vol. 2, 1987, pp. 936 - 939
4. Shen, Z. and R. H. Macpbie, "Waveguide model analysis of single and stacked probe-fed microstrip antenna with circular geometries," IEEE Antennas Propag Symposium, vol. 2, 1998, pp. 598 - 601
5. Nishiyama, E. and M. Aikawa, "Wide band and high gain microstrip antenna with thick parasitic patch substrate," IEEE Antennas Propag Society International Symposium, vol.1, 2004, pp.273 - 276
6. Nishiyama, E. and Aikawa, M., Egashira, "FDTD analysis of stacked microstrip antenna with high gain," Progress in Electromagnetics Research., PIER, vol.33, 2001, pp. 29-43,
7. Tsao, C. H., Hwang, Y. M., Killburg, F.and F. Dietrich, "Aperture coupled patch antenna with wide bandwidth and dual polarization capabilities," IEEE Antennas Propag. Soc. Symp. Dig., New York, June 1998, pp. 936-939
8. Garidol, F. E. and J. F. Zurcher, "Broadband patch antennas- A SSFIP update," IEEE Antennas Propag. Soc. Symp. Dig., Baltimore, July 1996, pp. 936-939
9. Targonski, S. D., Waterhouse, R. and D. M., Pozar, "Design of wide-band aperture–stacked patch microstrip antenna," IEEE Trans. Antennas Propag., vol. 46, no.9, 1998, pp.1245 -1251
10. Sanford, G. G., "Multiple resonance radio frequency microstrip antenna structures," U.S. Patent 4070676, Jan. 1978

11. Long, A. S. and D. M. Walton, " A dual-frequency circular-disc antenna," IEEE Trans. Antennas Propag., vol. 27, no.2, 1979, pp. 270 - 273
12. Sabban, A., "A new broadband stacked two-layer microstrip antenna," IEEE, 1983, pp. 63-66
13. Iglesias, E. and C. Pascaul, "A simple model for the design of broadband and dual-band stacked patches," 8th Cost 260, Rennes (France) Oct., 2000
14. Waterhouse, R., "Stacked patches using high and low dielectric constant material combinations," IEEE Trans. Antennas Propag., vol. 47, 1999, pp.1761-1771
15. Gracia, Q. and C. Pascaul, "Broadband stacked annular ring," ICAP 95, Eindoven
16. De, A., "Studies on rectangular and circular patch radiators," PhD Thesis, Indian Institute of Technology, Kharagpur, 1985
17. Collin, R. E. and F. J. Zucker, "Antenna theory Part-I," McGraw-Hill, 1969
18. Bahl, I. J. and P. Bhartia, "Microstrip antennas", Artech House, Deldham, MA, 1980
19. Harrington, R. F. "Time Harmonic Electromagnetic Fields," McGraw-Hill, N.Y., 1961
20. Yano, S. and A. Ishimaru, "A theoretical study of input impedance of a circular microstrip disk antenna," IEEE Trans. Antennas Propag., vol. 29, no. 1, 1981, pp.77 - 83
21. Balanis, C. A., "Antenna Theory: Analysis and Design," 2nd ed., John Wiley, New York, 1997, Chap. 14
22. Damiano, J. P. and A. Papiernik., "Survey of analytical and numerical models for probe fed microstrip antennas," IEE Proc.-Microwave Antennas Propag., vol. 141, no. 1, 1994, pp 15-21
23. Zheng, J. X. and D. C. Chang, "End-Correction Network of a coaxial probe for microstrip patch antennas", IEEE Trans. Antennas Propag., AP-39, no. 1, 1991, pp 115-118
24. Guha, D., "Resonant frequency of circular microstrip antenna with or without air gaps," IEEE Trans. Antennas Propag., AP- 49 no. 1, 2001, pp. 55-59

3.1 Introduction

There are several interesting features associated with annular ring patch. Annular ring patch antennas have a smaller size as compared to square or circular patch antenna for same frequency. Ring resonators have an advantage of being free of open ended effects and negligible curvature effects. The ring geometry introduces additional parameters to the antenna that can be used to control its impedance, resonance frequency and bandwidth. It was observed that the TM_{12} mode is the best mode for antenna applications, where as TM_{11} mode is the best for ring resonators [1]. Correct estimation of resonant frequency and input impedance of annular ring antennas is therefore a crucial design parameter. The annular ring antenna has been used in different applications, such as measurement of dielectric constant [2], phase velocity dispersion [3,4], discontinuities [5,6], medical applications [7] *etc.*

We have presented an analytical methodology for the estimation of input impedance, bandwidth and radiation pattern of a ring antenna with coaxial line feeding. The mathematical formulation for calculating the input impedance obtained done using cavity model. In an earlier reference [8] input impedance of ring antenna is calculated using circuit theory, in this paper an error is seen while evaluating the imaginary part of impedance. So the cavity model and circuit theory is used to correct the same. The same reference only evaluates the TM_{12} mode of the ring antenna, so a mathematical formulation is given to calculate other higher modes of ring antenna. Various losses are also considered while obtaining the mathematical model.

Further, there has been considerable interest in the development of dual frequency microstrip antennas. Among the several methods of obtaining the dual frequency characteristics, one typical method used is shorting posts. For a given patch geometry, the different resonance modes are related in fixed ratios. If two modes with similar radiation pattern and polarization have to be found then inserting shorting pins at suitable locations can alter their resonant frequency ratio and dual frequency design is possible with single patch [9]. Various different geometries such as triangular and square patch antennas have been used to study dual frequency operation and to enhance the bandwidth [10-12]. The analysis is further extended to find resonant frequency of loaded annular ring antenna with shorting posts. The posts are located asymmetrically *i.e.* not on the same line of axis joining the centre of the patch with the

feed probe on the annular ring. The results show that the resonant frequency depends on the radius of shorting post and it is interesting to note that for these cases angular dependence vanishes means that the posts can be located anywhere regardless of the angle.

3.2 Theory of Annular Ring Antenna

Annular ring antennas are geometrically and electrically an intermediate step between printed loops and patches. The annular ring antenna is constructed on a substrate of thickness h and relative dielectric constant ε_r. The inside radius is a, the outside radius is b. The geometry is shown in figure 3.1. The ring is excited by a line current $I_0(z')$ on the feed pin. The feed pin has diameter d_f and is located at (r_0, ϕ_0) and the current density on the pin is given by $\vec{J}(r)$.

$$p_n = \frac{I_0 h}{2\pi} \int_0^{2\pi} E_i . d\beta \tag{3.1}$$

The feed is assumed to support only a z-directed current with no variation in z direction. This current will produce transverse magnetic (TM) to z-fields. The normal mode fields are evaluated by assuming

$Y_W = 0$

Application of boundary conditions

$H_\phi(a) = 0$

$H_\phi(b) = 0$

gives the transcendental equation

$$J_n'(kb_e)N_n'(ka_e) - J_n'(ka_e)N_n'(kb_e) = 0 \tag{3.2}$$

Where J_n' is the derivative of first order Bessel function and N_n' is the derivative of first order Neumann function. a_e and b_e are the effective inner and outer radius [1] respectively

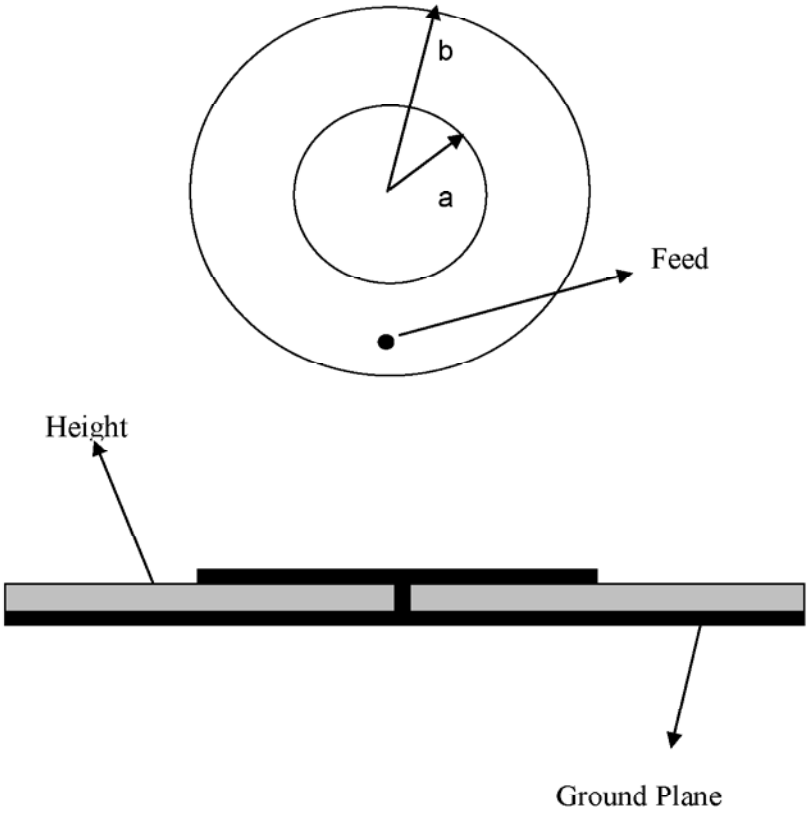

Figure 3.1 Geometry of an annular ring antenna.

$$a_e = a\sqrt{1-\frac{2h}{\pi a \varepsilon_r}\Delta C} \tag{3.3}$$

and

$$b_e = b\sqrt{1+\frac{2h}{\pi a \varepsilon_r}\Delta C} \tag{3.4}$$

$$\Delta C = \ln(\frac{a}{2h}) + 1.41\varepsilon_r + 1.7726 + \frac{h}{a}(0.286\varepsilon_r + 1.65)$$

The expressions for electric and magnetic field are given as

$$E_r = -j\omega_{np}\mu\{C_1 J_n(k_{np}r) + C_2 N_n(k_{np}r)\}\cos n\phi \tag{3.5}$$

$$H_r = -(\frac{n}{r})\{C_1 J_n(k_{np}r) + C_2 N_n(k_{np}r)\}\sin n\phi \tag{3.6}$$

and

$$H_\phi = -k_{np}\{C_1 J'_n(k_{np}r) + C_2 N'_n(k_{np}r)\}\cos n\phi \tag{3.7}$$

On the application of boundary conditions

$H_\phi = 0$ at $r = b$ redefines the electric and magnetic field equations as

$$E_z = -j\omega_{np}\mu C_n^{(1)} F_n^{(1)}(k_{np}r)\cos n\phi \tag{3.8}$$

$$H_r = -(\frac{n}{r})C_n^{(1)} F_n^{(1)}(k_{np}r)\sin n\phi \tag{3.9}$$

and

$$H_\phi = -k_{np} C_n^{(1)} F_n'^{(1)}(k_{np}r)\cos n\phi \tag{3.10}$$

where

$C_n^{(1)}$ is a constant

$$F_n^{(1)}(kr) = J_n(k_{np}r)N'_n(k_{np}b_e) - J'_n(k_{np}b_e)N_n(k_{np}r) \tag{3.11}$$

and

$$F_n'^{(1)}(k_{np}r) = J'_n(k_{np}r)N'_n(k_{np}b_e) - J'_n(k_{np}b_e)N'_n(k_{np}r) \tag{3.12}$$

In order to evaluate the constant $C_n^{(1)}$, the normalization condition [13] is used.

$$\int_V \varepsilon |E|^2 dV = 1$$

For the entire volume the normalization condition for input impedance of annular ring antenna under consideration assumes the form

$$\int_0^h \int_0^{2\pi} \int_a^b \varepsilon \left| E_z \right|^2 r dr = 1$$

Hence by evaluating the above equation the constant $C_n^{(1)}$ is obtained as

$$C_n^{(1)} = \frac{1}{k} \cdot \sqrt{\frac{1}{\pi h \mu I_1}} \tag{3.13}$$

where

$$I_1 = \int \left(J_n(k.r) N_n'(k.b_e) - N_n(k.r) J_n'(k.b_e) \right)^2 r dr$$

Similarly when effective radius a_e is considered then

$$I_2 = \int \left(J_n(k.r) N_n'(k.a_e) - N_n(k.r) J_n'(k.a_e) \right)^2 r dr$$

The impedance is calculated by using the formulation described in chapter II in section (2.1).

$$Z_{in} = -\frac{1}{I_0^2} \sum_n \sum_p \frac{(j\omega + A) p_n^2}{(j\omega - C)(j\omega + A) + \omega_{np}^2} \tag{3.14}$$

The different parameters appearing in expression for input impedance for the problem under consideration assumes the following form. The expression of A corresponds to the copper loss in the microstrip

$$A = Z_s \int_0^{2\pi} \int_a^b \left\{ \left| H_\phi \right|^2 + \left| H_r \right|^2 \right\} r dr \tag{3.15}$$

where surface resistance Z_s is given as

$$Z_s = \left\{ \frac{\pi f \mu}{\sigma} \right\}^{\frac{1}{2}}$$

and

$$C = -Y_w \int_0^h \int_0^{2\pi} \left| E_z \right|^2 r d\phi dz \qquad (\text{at } r = b_e) \tag{3.16}$$

From this

$$A = Z_s \pi C_n^{(1)2} [k^2 I_3 + n^2 I_4] \tag{3.17}$$

where

$$I_3 = \int_a^b \left(J_n'(k\cdot r)N_n'(k\cdot b_e) - J_n'(k\cdot b_e)N_n'(k\cdot r)\right)^2 r dr$$

$$I_4 = \int_a^b \frac{\left(J_n(k\cdot r)N_n'(k\cdot b_e) - J_n'(k\cdot b_e)N_n(k\cdot r)\right)^2}{r^2} r dr$$

Consider a loaded microstrip patch radiator excited by a coaxial line feeding a probe located at $(r_0, \phi_0, 0)$

Using the transformation [14,15]

$$r = r_0 + \frac{d_f}{2}\cos\beta$$

and expanding the Bessel function in Taylor series, the function $F_n^{(1)}(k.r)$ is obtained as

$$F_n^{(1)}(k.r) = J_n(k.r_0) + \frac{k.d_f}{2} J_n'(k.r_0)\cos\beta) \tag{3.18}$$

where the higher order terms of Taylor series expansion are neglected

$$p_n = -j\omega\mu h I_0 C_n^{(1)}\left[J_n(k.r_0)N_n'(k.b) - J_n'(k.b)N_n(k.r_0)J_0\left(\frac{nd_f}{2r_0}\right)\right] \tag{3.19}$$

Substituting eq. (3.19) in eq. (3.14), we get

$$Z_{in} = \mu^2 h^2 \sum_n \sum_p \frac{(j\omega + A)C_n^{(1)2}\omega^2\left[J_n(k.r_0)Y_n'(k.b_e) - J_n'(k.b_e)N_n(k.r_0))J_0\left(\frac{nd_f}{2r_0}\right)\right]^2}{(j\omega - C)(j\omega + A) + \omega_{np}^2} \tag{3.20}$$

To formulate theory for input impedance of annular ring microstrip antenna, we assume the use of a coaxial probe. In the present study, to compute the input impedance the end correction network suggested by Zheng *et al.* [16] is used.

$$Y_{TEM} = \frac{1}{[R_p + j\omega(L_p + L_0)]} + j\omega C_0 \tag{3.21}$$

The expression for input impedance resembles the form of a parallel RLC circuit, although in this case each element can be considered as frequency dependant. Using this correction network the input impedance of the ring antenna is given as

$$Z(ring) = Z_{in} + \frac{1}{Y_{TEM}}$$

3.2.1 Radiated Power

The total radiated power of the annular ring antenna is given by following set of equations [17]

$P_T = P_r + P_c + P_d$ where P_T is the radiated power, P_c and P_d are the copper loss and dielectric loss respectively. P_c is same as A derived in the previous section.

$$P_r = \frac{2\pi}{\eta}\left(\frac{E_0}{kb_e}\right)^2 \left((kb_e)^2 I1 + I2(1-\delta)n\right) \tag{3.22}$$

where $E_0 = \left(\frac{h}{\pi}\right)\left(\frac{\omega\mu_0}{\sqrt{\varepsilon_r}}\right)C_n^1$

$$P_d = \frac{1}{2}h\omega\varepsilon_r\varepsilon_0 \tan\delta\pi(\omega\mu)^2 C_n^{(1)2}(I_1) \tag{3.23}$$

where $E_0 = \left(\frac{h}{\pi}\right)\left(\frac{\omega\mu_0}{\sqrt{\varepsilon_r}}\right)C_n^1$ (3.24)

The efficiency of the antenna is given by

$$Eff = \frac{P_r}{P_r + P_d + A} \tag{3.25}$$

3.2.2 Wall Admittance

To determine impedance, it is necessary to take into account the reactive power due to electric and magnetic energy stored in the fringe of the ring. The reactive and active powers are given by equivalent boundary admittance Y_W. The total wall admittance can be expressed in terms of self and mutual inductance. The *s* subscript is used to donate self admittance and *m* subscript is used to donate mutual admittance. The mutual admittance is [12, 18]

$$Y_m(a,b) = \frac{jabh}{2\pi^2\omega\mu}\int_0^{2\pi} \cos\phi \left[\int_0^{2\pi} \cos\alpha\left(\frac{e^{-jk_0r}}{r^3}\right)\times \left\{\begin{array}{l} 2\cos(\phi-\alpha)(1+jk_0r) \\ +\dfrac{(b\cos(\phi-\alpha)-\alpha)(b\cos(\phi-\alpha)-\alpha))}{r^2}(k_0^2r^2-3jk_0r-3)\end{array}\right\} d\alpha\right] \tag{3.26}$$

The boundary admittance Y_W is given by [19]

$$Y_W = g_s^n + jb_n \tag{3.27}$$

where

$$g_s^n(b) = \frac{2.h}{(1+\delta_n)\eta_0}[(1+\delta_n)(k_0^2 b_e)I_4 + n^2(1-\delta_n)I_5] \tag{3.28}$$

where $\eta_0 = \sqrt{\frac{\mu_0}{\varepsilon_0}}$, $\quad \delta_n = 1, for n = 0$
$\quad = 0, for n > 0$

$$I_5 = \int_0^{\frac{\pi}{2}} [J_n^{'}(k_0 b_e \sin\theta)]^2 \sin\theta d\theta \tag{3.29}$$

$$I_6 = \int_0^{\frac{\pi}{2}} \frac{\cos^2\theta}{\sin\theta} J_n^2(k_0 b_e \sin\theta) d\theta \tag{3.30}$$

A similar expression can be obtained for $g_s^n(a)$ by replacing b by a in above equations.

The wall susceptance is given by equation

$$b_s^n = \frac{\varepsilon_0 \varepsilon_r \omega \pi}{\eta_0 h}(b^2 - b_e^2) \tag{3.31}$$

$$a_s^n = \frac{\varepsilon_0 \varepsilon_r \omega \pi}{\eta_0 h}(a^2 - a_e^2) \tag{3.32}$$

The active load admittance can be expressed as [20]

$$Y_n^t(b) = Y_W - Y_m(a,b) + \frac{E_z(a) - E_z(b)}{E_z(b)} \times Y_m(a,b) \tag{3.33}$$

Similarly for radiating aperture at a, we get

$$Y_n^t(a) = Y_W - Y_m(a,b) + \frac{E_z(a) - E_z(b)}{E_z(a)} \times Y_m(a,b) \tag{3.34}$$

Hence the total admittance for the ring can be evaluated as

$$Y_W(total) = Y_n^t(b) + Y_n^t(a) + Y_m(a,b) \tag{3.35}$$

The efficiency of the antenna is given by equation (3.24)

$$\eta = \frac{P_r}{P_r + P_d + A} \tag{3.36}$$

Hence the total reactive and active powers are given as equivalent boundary admittance at the ring edge.

$$Y_W^{'}(total) = Y_W(total) \times \frac{1}{\eta}$$

3.2.3 Formulation of Computation of Radiation Pattern

The radiation fields of annular ring antenna can be obtained either from magnetic current approach or electric current distribution on the surface of the ring. As described in chapter II the radiated field patterns are derived by equivalent magnetic current formulation. The radiation fields due to magnetic ring source at $\rho = a$ are obtained [17]

$$E_\theta^a = j^n \frac{e^{-jkr}}{r} akhE_z(a) J_n^{'}(ka\sin(\theta))\cos n\phi \tag{3.37}$$

$$E_\iota^a = -\eta j^n \frac{e^{-jkr}}{r} akhE_z(a)(\frac{J_n(ka\sin\theta)}{ka\sin\theta})\sin n\phi\cos\theta \tag{3.38}$$

The radiation fields due to magnetic ring source at $\rho = b$ are obtained by replacing a by b in above equations where for TM_{np} mode gives

$$E_{zn}(a) = E\,[J_n(k_{nm}a_e)Y_n^{'}(k_{nm}a) - J_n^{'}(k_{nm}a_e)Y_n(k_{nm}a)]$$

$$= \frac{2E_0}{\pi k_{nm}a}$$

Using wronskian for Bessel function.

Similarly

$$E_{zn}(a) = E\,[J_n(k_{nm}b_e)Y_n^{'}(k_{nm}a_e) - J_n^{'}(k_{nm}a_e)Y_n(k_{nm}b_e)]$$

$$= \frac{2E_0}{\pi k_{nm}a}\frac{a}{b}\frac{J_n^{'}(k_{nm}a)}{J_n^{'}(k_{nm}b)} \tag{3.39}$$

The effect of ground plane is included in the derivation of equation (3.38 - 3.39) but it is assumed that magnetic current is constant along radial direction. The radiation pattern of ring antenna are then written as

$$E_\theta^a = j^n \frac{e^{-jkr}}{r} kh[aE_{zn}(a)J_n^{'}(ka\sin\theta) - bE_{zn}J_n^{'}(kb\sin\theta)]\cos n\phi \tag{3.40}$$

$$E_\theta^a = -\eta j\frac{e^{-jkr}}{r} kh\left[aE_{zn}(a)\frac{J_n(ka\sin\theta)}{ka\sin\theta} - bE_{zn}\frac{J_n(kb\sin\theta)}{kb\sin\theta}\right]\sin n\phi\cos\theta \tag{3.41}$$

Substituting the values for $E_{zn}(a)$ and $E_{zn}(b)$ the radiated field equations can be written as

$$E_\theta = j^n \frac{2E_0}{\pi k_{nm}} \frac{e^{-jkr}}{r} kh \left[J_n'(ka\sin\theta) - \frac{J_n'(k_{nm}a)}{J_n'(k_{nm}b)} J_n'(kb\sin\theta) \right] \cos n\phi \tag{3.42}$$

$$E\phi = -nj \frac{2E_0}{\pi k_{nm}} \frac{e^{-jkr}}{r} kh \left[\frac{J_n(ka\sin\theta)}{ka\sin\theta} - \frac{J_n'(k_{nm}a)}{J_n'(k_{nm}b)} \frac{J_n(kb\sin\theta)}{kb\sin\theta} \right] \sin n\phi \cos\theta \tag{3.43}$$

3.2.4 Quality Factor

The quality factor Q is a measure of frequency selectivity of a resonant antiresonant circuit, and is defined as [21]

$$Q = 2\pi \frac{\text{maximum energy stored}}{\text{energy dissipated per cycle}} = \frac{\omega \text{W}}{\text{P}} \tag{3.44}$$

where W is the maximum stored energy and P is the average power loss.

At resonant frequency, the electric and magnetic energies are equal and in time quadrature. When the electric energy is maximum, the magnetic energy is zero and vice- versa. The total energy stored is obtained by integrating the energy density over the volume of resonator.

$$W_e = \int_v \frac{\varepsilon}{2} |E|^2 dv = \int_v \frac{\mu}{2} |H|^2 dv = W \tag{3.45}$$

where $|E|$ *and* $|H|$ are the peak values of field intensity.

The average power loss in the resonator can be evaluated by integrating the power density is given by

$$P = \frac{R_s}{2} \int_s |H_t|^2 da$$

where H_t is the peak value of tangential magnetic intensity and R_s is the surface resistance of the resonator. The equation (3.44) is used to find out quality factor for ring antenna numerically.

3.2.5 Return Loss and Bandwidth

Return loss is simply the magnitude of logarithmic form of reflection coefficient. The relationship for return loss is given by [22]

$$RL = -20\log|\Gamma| \tag{3.46}$$

We know that

$$\Gamma = \frac{Z_{in} - Z_0}{Z_{in} + Z_0} \tag{3.47}$$

where $|\Gamma|$ is magnitude of reflection coefficient and RL is return loss measured in dB. The input impedance of the ring antenna which is found by using equation (3.20)is used to find out reflection coefficient where value of Z_0 = 50 ohms. Thus we can find out the value of return loss for the probe f ring antenna. Bandwidth is the range of frequencies within which the performance of antenna with respect to some characteristics, confirms to a specific standard.

3.2.6 Results and Discussion

For calculating the input impedance of annular ring antenna the following parameters are used; $\varepsilon_r = 2.2$, h = 1.59 mm, a = 30mm, b = 60mm, and feed point location are r_0 = 31 mm and 35 mm. Figure 3.2 shows the impedance of ring antenna for first dominant mode when feed is located at r_0= 35mm. The resonant frequency is 0.734 GHz. The numerical and simulated results are in good agreement. This shows the accuracy of predicted model. The error percentage is 1.3 % which is marginal. It is observed that the numerically calculated results of real part of impedance are in close agreement with simulated one. Figure 3.3 shows the second dominant mode of the ring antenna at the resonant frequency of 1.44 GHz when r_0 = 35 mm. The maximum percentage error is 2 % in numerical and simulated values. The input impedance of annular ring antenna for TM_{12} mode is compared with [7]. Figures 3.4 and 3.5 show the comparison of real and imaginary part of impedance for both numerical and simulation respectively. The numerical and simulated results are in complete agreement but there is disagreement with [7] and this is possibly due to method of feeding. Figure 3.6 shows the variation of resonant resistance with radial location of feed. This shows that the resonant resistance goes on increasing as the feed point is moved towards the periphery of ring. This plot also helps to find out the exact location of feed point. Figures 3.7 and 3.8 show the variation of return loss and radiation pattern with frequency for second dominant mode respectively.

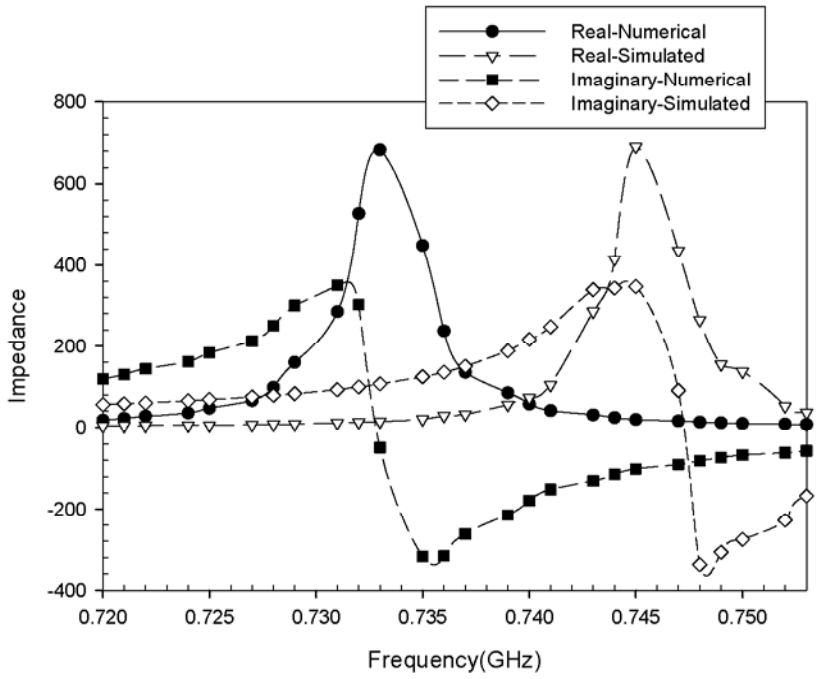

Figure 3.2 Variation of Impedance with Frequency for first dominant mode ($\varepsilon_r = 2.2$, $h = 1.59$ mm, $a = 30$ mm, $b = 60$ mm and feed location $r_0 = 35$ mm).

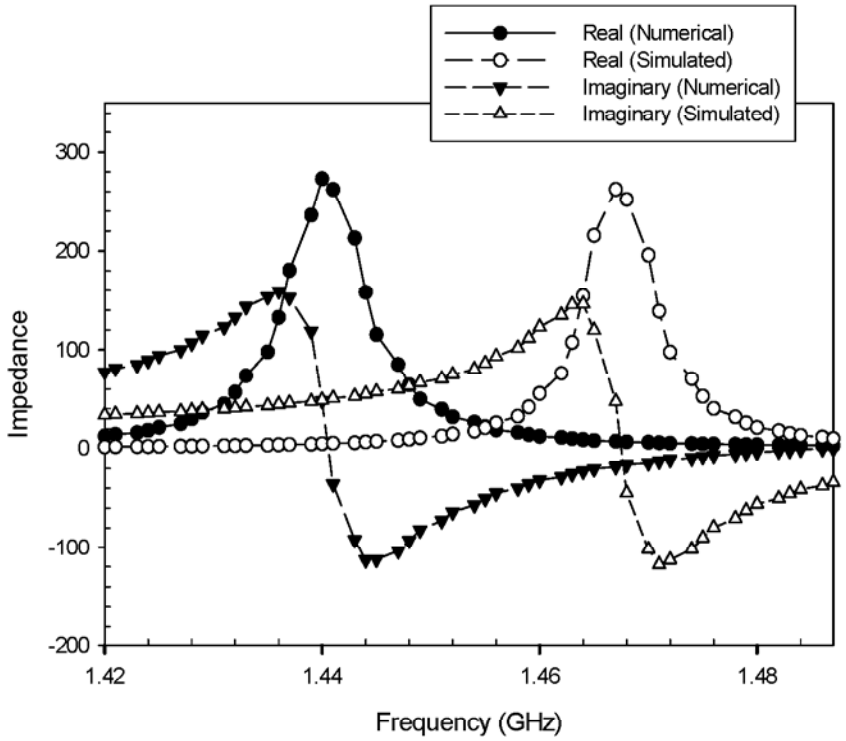

Figure 3.3 Variation of Impedance with Frequency for second dominant mode ($\varepsilon_r = 2.2$, $h = 1.59$ mm, $a = 30$ mm, $b = 60$ mm and feed location $r_0 = 35$ mm).

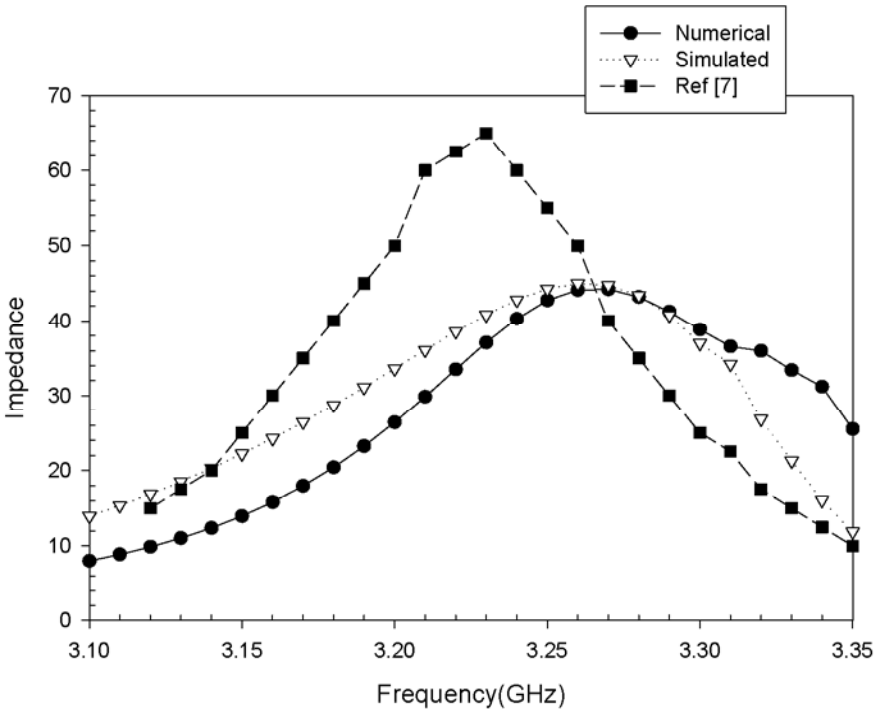

Figure 3.4 Variation of Impedance (Real) with Frequency for TM_{12} mode ($\varepsilon_r = 2.2$, $h = 1.59$ mm, $a = 30$ mm, $b = 60$ mm and feed point location $r_0 = 35$ mm).

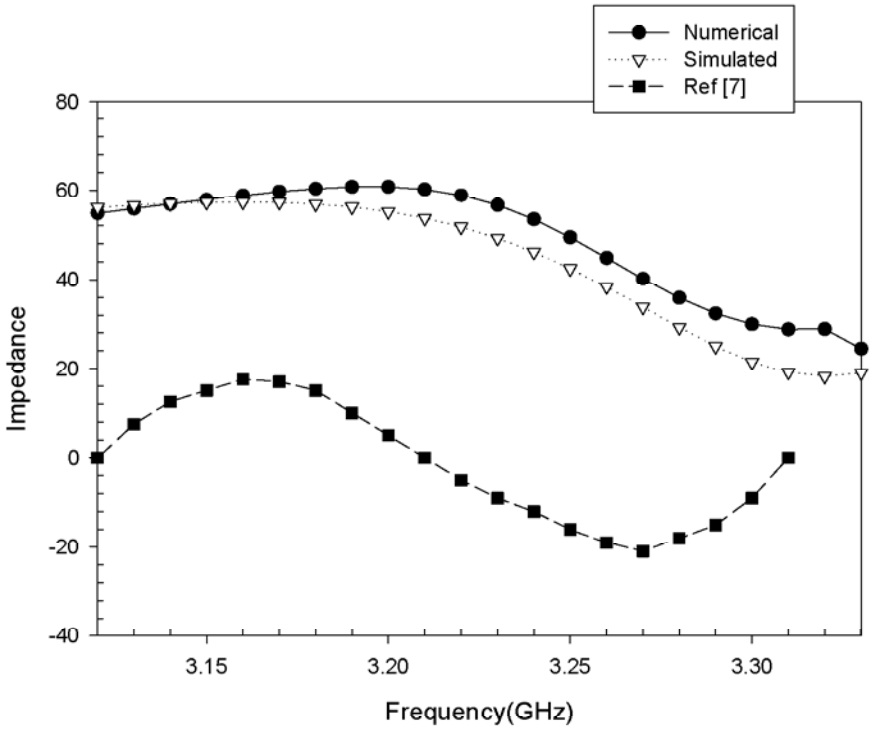

Figure 3.5 Variation of Impedance (Imaginary) with Frequency for TM_{12} mode ($\varepsilon_r = 2.2$, $h = 1.59$ mm, $a = 30$ mm, $b = 60$ mm and feed point location $r_0 = 35$ mm).

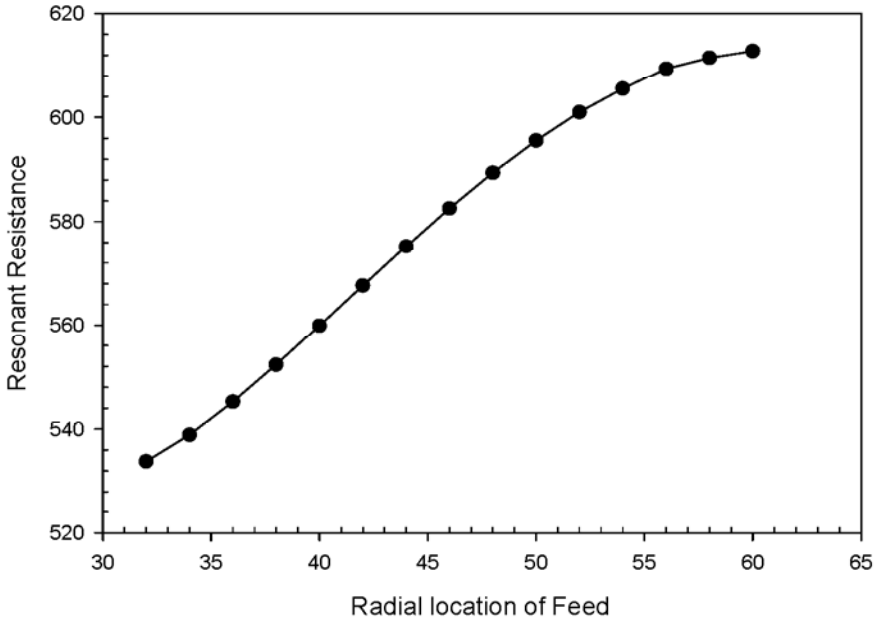

Figure 3.6 Variation of Resonant Resistance with Radial location of Feed ($\varepsilon_r = 2.2$, $h = 1.59$ mm, $a = 30$ mm, $b = 60$ mm and $r_0 = 35$ mm).

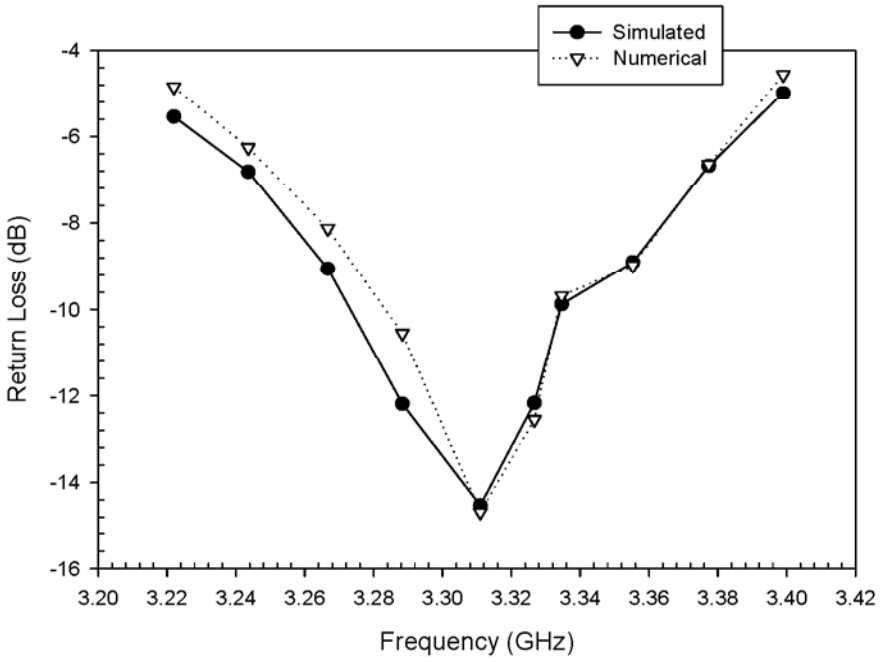

Figure 3.7 Variation of Return Loss with Frequency for TM_{12} mode ($\varepsilon_r = 2.2$, $h = 1.59$ mm, $a = 30$ mm, $b = 60$ mm and $r_0 = 35$ mm).

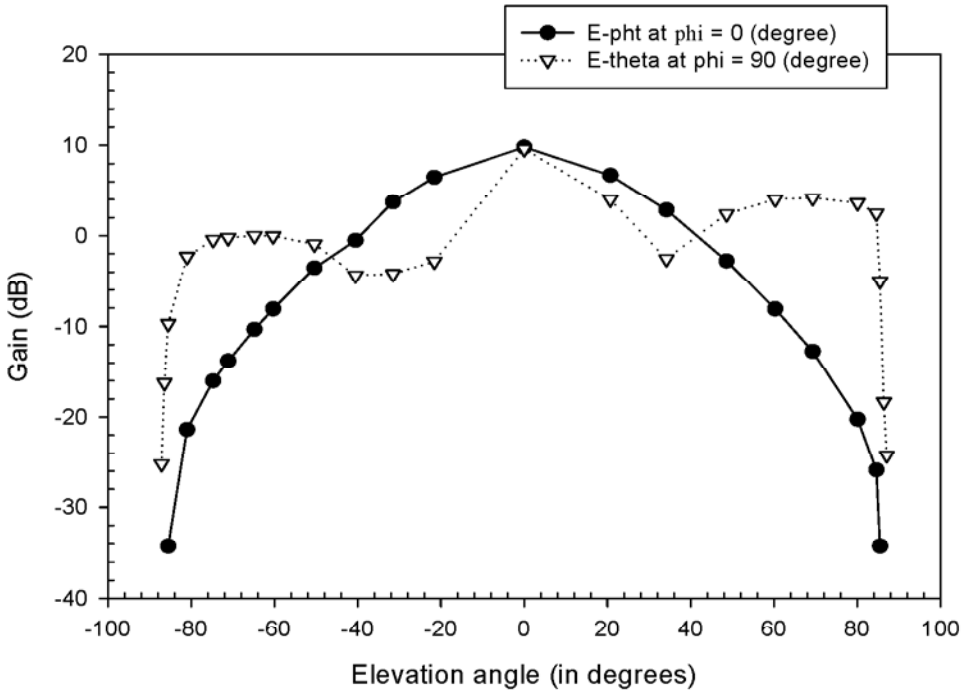

Figure 3.8 Radiation Pattern (Simulated) for probe feed annular ring antenna for TM_{12} mode (a = 30 mm, b = 60 mm, h = 1.59 mm, ε_r = 2.2 and r_0 = 35 mm).

The numerical and simulated results are in complete agreement. 10 dB bandwidth for TM_{12} mode is also calculated for the annular ring antenna, which is about 15 %. The Q factor for first dominant mode is also calculated numerically and its value is 229.8 at resonant frequency of 0.734 GHz. The factor goes on decreasing for higher order modes such as for $n = 2$, Q factor is 23.65 at 1.44 GHz.

3.3 Asymmetric Loaded Annular Ring Antenna

Investigations have been carried out [23-25] to study the effect on resonant frequency of a circular microstrip patch radiator when loaded with single or double posts. It had been demonstrated that the normal mode frequencies of a circular patch can be tuned when loaded with a passive conducting post. Loading can be asymmetric or symmetric. Thus the effect of loading of annular microstrip antenna due to asymmetric loading is studied in the present section. The analysis is presented for multiple shorting posts.

3.3.1 Impedance Expression for Shunt Post in Annular Microstrip Patch

Vertical shunt posts in microstrip transmission lines are currently found in relatively few microwave circuit applications and are, in general, poorly characterized. However, accurate model for such posts are necessary for predicting the resonance behaviour of post loaded annular microstrip antenna. The field disturbances produced by a short are very complex in nature and cannot be described simply as a perturbation effect. However, the effect on input impedance in certain cases can be described by a shunt inductor. Therefore, it is necessary to obtain a fairly accurate expression for inductive impedance of shunt posts in order to validate the model of loaded circular microstrip antenna. In another work on post loaded circular patch [23], the post has been considered as a small cylindrical current distribution.
The impedance per unit length for such small circular current distributions is given as [26]

$$Z_0 = \frac{j\omega_{np}\mu}{2\pi}\ln\left(\frac{\lambda_{np}}{2\pi\Delta}\right) \tag{3.47}$$

where Δ is the post radius.

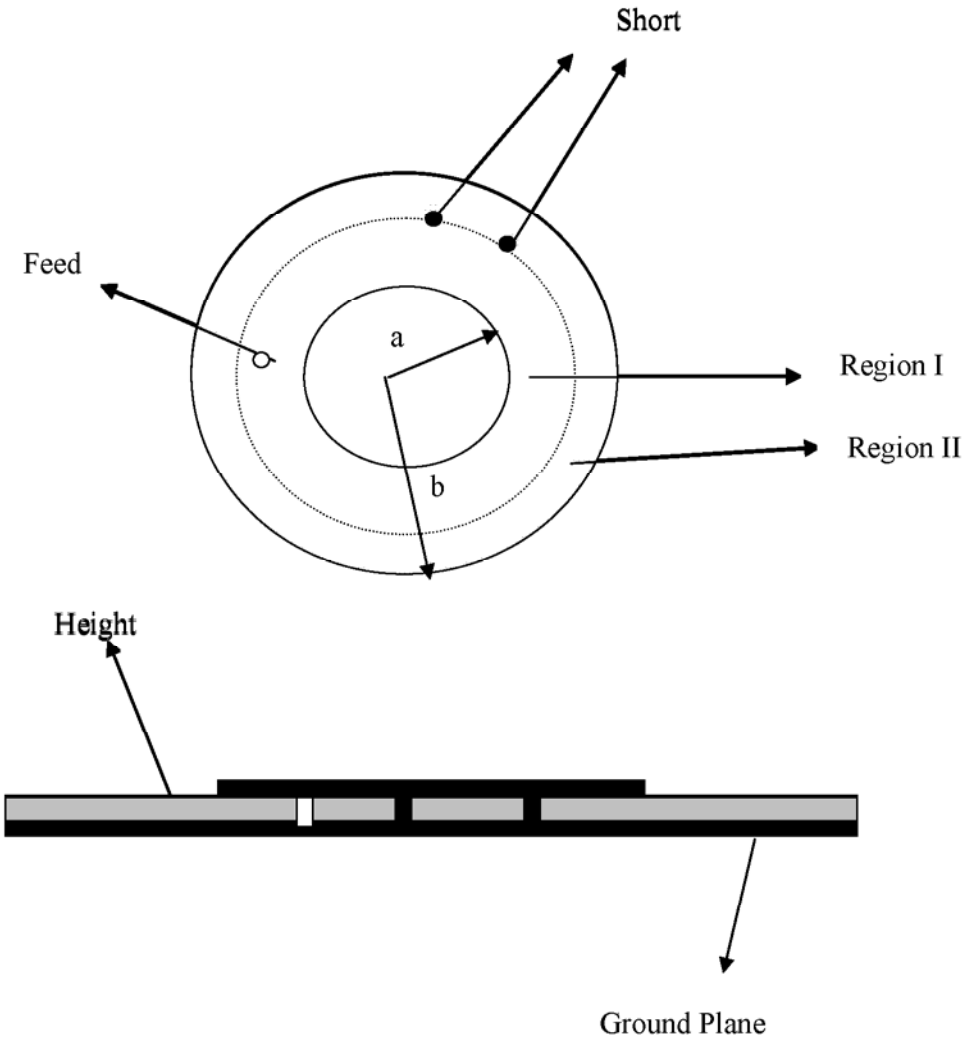

Figure 3.9 Geometry of asymmetrically loaded annular ring antenna.

The impedance per unit length for such a cylinder of uniform z-directed currents is also derived in [27] and is given as

$$Z_0 = \frac{\eta k}{4} J_0(k\Delta) H_0^{(2)}(k\Delta) \tag{3.48}$$

These expressions have been used to obtain eigen frequencies for loaded circular patch [23,28]. It is seen that these expressions though reasonably accurate for TM_{11} and higher order modes, they are wholly inadequate to justify the monotonic decrease in resonant frequency for dominant (0,1) mode. These models also break down when the post is located at the periphery of the patch. Full-wave techniques are capable of analyzing all situations where attachment modes are used at the patch-post junctions. However, these are rigorous solutions and are not useful for deriving closed-form expressions for loaded patch.

The expression derived by Sengupta [25] assumes an axially oriented metallic post in an infinite radial waveguide ($\rho = \infty$) which sustains only E-type radial modes. Use of this expression in conjunction with the theory developed in [26] reveals that this particular model is accurate for all modes of loaded disk resonator when the post is not very close to the edge of the patch. Possible solution to this is suggested in [27]. In this the shunt posts are characterized using planar waveguide model where sidewalls are replaced with fictitious "perfect magnetic conductor". The presence of magnetic walls makes it necessary to consider the reflected field components which are generated by the infinite array of imaged multipoles located at the points.

In the proposed model of loaded annular patch, the impedance expression derived in [25] has been utilized. However, to compensate for the edge effects, an empirically generated correction factor has also been incorporated. It is shown in the following sections that such combination leads to a very accurate model of post loaded circular patch. The impedance per unit length for a shunt post is given as

$$Z_0 = \frac{\eta k}{4}[1 - J_0^{\,2}(kr_2) + j\{\frac{2}{\pi}\ln(\frac{2}{\gamma k\Delta}) + J_0(kr_2)N_0(kr_2)\}.CF] \tag{3.49}$$

where r_2 is the radial distance of the post from the centre of the patch, CF is the correction factor and is given as

$$CF = \frac{\sin(\frac{\pi}{2\varepsilon_n})\{\left|J_0(\frac{P}{4V})\right|\}^{2P}}{J_0(\alpha t_d)^{\frac{D}{2}-0.7} J_0(t_d)^2 J_0(\frac{c-a_e}{a_e})^2} \tag{3.50}$$

where $t_d = \frac{c-b_e}{b_e}$ where b_e is the effective radius of the ring due to fringing fields.

D = 4 for P ≤ 4

Else D = P

$$V = (\frac{R_P}{Q_P}\beta_n + \alpha_n R_P)$$

where

$\alpha_n = 0$ for $n = 0$ else 1

$\beta_n = 1$ for $n = 0$ else 0

Q_i and R_i values are obtained from table 3.1.

$\varepsilon_n = 1$ for $n = 0$ & $\varepsilon_n = 2$ for $n \neq 0$

The real part of equation (3.49) accounts for the power loss in the higher order modes excited by the post and the imaginary part represents the external inductance of the post. For computation of eigen modes, only imaginary part is used.

3.3.2 *Analysis of Resonant Frequency of Annular Ring Antenna Loaded with Multiple Posts Located Asymmetrically*

The analysis is based on cavity model where it is assumed that the substrate is electrically thin $h << \lambda_0$. The basic ring geometry with shorting posts is shown in figure 3.9. The annular ring of inner radius a and outer radius b is loaded with P number of passive conducting posts of radius Δ on the circumference of a concentric circle of radius c where $a < c <$ b. The ring is assumed to be converted into two rings which lie side by side and each ring is assumed to be a single region converting the ring into two regions I and II. The pins are located asymmetrically means the shorting posts are not equispaced on the circular disc. The theory is developed for the posts, where $\phi_i \neq 0^0 or 180^0$. The given annular ring in presence of source can be considered

to be consisting of two half disks where the line of axis is through the feed point and the centre of patch.

For region I $a < c < \mathrm{b}$, the expressions for electric and magnetic fields are obtained as

$$E_z^{(1)} = -j\omega_{np}\mu\{C_1 J_n(k_{np}r) + C_2 N_n(k_{np}r)\}(\cos n\phi + C_3 \sin n\phi) \tag{3.51}$$

$$H_r^{(1)} = -(\frac{n}{r})\{C_1 J_n(k_{np}r) + C_2 N_n(k_{np}r))\}(\sin n\phi - C_3 \cos n\varphi) \tag{3.52}$$

and

$$H_\phi^{(1)} = -k_{np}\{C_1 J_n^{'}(k_{np}r) + C_2 N^{'}(k_{np}r)\}(\cos n\phi + C_3 \sin n\phi) \tag{3.53}$$

where $\mathrm{J_n}(k_{np}.r)$ is Bessel function of first kind of order n, ω_{np} and k_{np} are the angular frequency and propagation constant for $\mathrm{TM_{np}}$ mode and C_1 and C_2 are constants. Prime denotes a derivative with respect to its argument. The integer 'n' corresponds to the order of the Bessel function and p denotes the pth zero of $J_n^{'}(k_{np}r)$. The subscript 'z' is ignored for particular mode identification as the electric field is non variant along z direction. The real resonant frequency of the patch radiator has been evaluated by earlier workers by assuming that $\mathrm{Y_w} = 0$. In order to study the effect of passive post loading on the resonant frequency of the thin microstrip antenna it is, therefore, assumed that $Y_w = 0$. Similarly for region II $c < \mathrm{r} < \mathrm{b}$, the expressions for electric and magnetic fields are obtained as

$$E_r^{(2)} = -j\omega_{np}\mu\{C_4 J_n(k_{np}r) + C_5 N_n(k_{np}r)\}(\cos n\phi + C_6 \sin n\phi) \tag{3.54}$$

$$H_r^{(2)} = -(\frac{n}{r})\{C_4 J_n(k_{np}r) + C_5 N_n(k_{np}r)\}(\sin n\phi - C_6 \cos n\phi) \tag{3.55}$$

and

$$H_\phi^{(2)} = -k_{np}\{C_4 J^{'}{}_n(k_{np}r) + C_5 N_n^{'}(k_{np}r)\}(\cos n\phi + \sin n\phi) \tag{3.56}$$

Where C_4 and C_5 are constants and $N_n(k_{np}r)$ is Bessel function of second kind.

Application of vanishing tangential component of magnetic field in the two regions at the boundary edges lead to modification of field expressions. The expressions can be written as;

$$E_z^{(1)} = -j\omega_{np}\mu C_n^{(1)} F_n^{(1)}(k_{np}r)(\cos n\phi + C_3 \sin n\phi) \tag{3.57}$$

$$H_\phi^{(1)} = -k_{np} C_n^{(1)} F_n^{'(1)}(k_{np}r)(\cos n\phi + C_3 \sin n\phi) \tag{3.58}$$

$$H_r^{(1)} = -k_{np} C_n^{(1)} F_n^{(1)}(k_{np}r)(\sin n\phi - C_3 \cos n\phi) \tag{3.59}$$

and

$$E_z^{(2)} = -j\omega_{np}\mu C_n^{(2)} F_n^{(2)}(k_{np}r)(\cos n\phi + C_6 \sin n\phi) \tag{3.60}$$

$$H_\phi^{(2)} = -k_{np} C_n^{(2)} F_n^{'(2)}(k_{np}r)(\cos n\phi + C_6 \sin n\phi) \tag{3.61}$$

$$H_r^{(2)} = -k_{np} C_n^{(2)} F_n^{(2)}(k_{np}r)(\sin n\phi - C_6 \cos n\phi) \tag{3.62}$$

where

$$F_n^{(1)}(kr) = J_n(k_{np}r)N_n'(k_{np}a) - J_n'(k_{np}a)N_n(k_{np}r)$$

$$F_n^{(2)}(k_{np}r) = J_n(k_{np}r)N_n'(k_{np}b) - J_n'(k_{np}b)N_n(k_{np}r)$$

and

$$F_n^{'(1)}(k_{np}r) = J_n'(k_{np}r)N_n'(k_{np}a) - J_n'(k_{np}a)N_n'(k_{np}r)$$

$$F_n^{'(2)}(k_{np}r) = J_n'(k_{np}r)N_n'(k_{np}b) - J_n'(k_{np}b)N_n'(k_{np}r)$$

Z_0 is the impedance per unit length of the post which is same as equation (3.49). The empirical correction factor correctly predicts the effect of multiple posts on the fringe of annular ring for up to 10 posts.

The electric and magnetic fields given by equations (3.57) - (3.62) satisfy the following boundary conditions.

$$E_Z^{(2)} = E_Z^{(1)} \qquad \text{at } r = c \tag{3.63}$$

$$H_\phi^{(2)} = -Y_w E_z^{(2)} \qquad \text{at } r = a \tag{3.64}$$

$$H_\phi^{(2)} - H_\phi^{(1)} = \sum_{i=1}^{P} E_z^{(2)} / (Z_0 . 2\Delta) \qquad \text{at } r = c \quad for\ \phi_i - \alpha/2 < \phi < \phi_i + \alpha/2 \tag{3.65}$$

where α is the angle subtended by shorted post at the centre of ring cavity, Y_W is the complex wall admittance of the circular cavity. The summation over index *i* indicates that the boundary condition is applicable for all the shorting posts. Applying the boundary condition given in equation (3.63) and using the orthogonality properties of sinusoid functions, we derive the important relation that, for $n = 0$ & $\phi_i \neq 0^0 or 180^0$,

asymmetric modes are not generated. Treating the orthogonal modes of the electric fields in equation (3.65) independently, the following relation is obtained

$$\frac{C_6}{C_5} = 1$$

Applying boundary conditions given by equation (3.63 - 3.65) two homogenous equations in $C_n^{(1)}$ and $C_n^{12)}$ are obtained. For $C_n^{(1)}$ and $C_n^{(2)}$ to be non vanishing the determinant of the equations so derived should be zero, which leads to

$$\frac{\mathrm{F_n}^{(2)}{}'(\mathrm{tx})}{\mathrm{F_n}^{(2)}(\mathrm{tx})} - \frac{\mathrm{F_n}^{(1)}{}'(\mathrm{tx})}{\mathrm{F_n}^{(1)}(\mathrm{tx})} = \sum_{i=1}^{P} \frac{\varepsilon_n(1+\cos 2n\phi_i + \mathrm{C}_6 \sin 2n\phi_i)}{2\mathrm{k}_{\mathrm{np}} c X_T} \tag{3.66}$$

and

$$\frac{\mathrm{F_n}^{(2)}{}'(\mathrm{tx})}{\mathrm{F_n}^{(2)}(\mathrm{tx})} - \frac{\mathrm{F_n}^{(1)}{}'(\mathrm{tx})}{\mathrm{F_n}^{(1)}(\mathrm{tx})} = \sum_{i=1}^{P} \frac{\varepsilon_n(1-\cos 2n\phi_i + \sin 2n\phi_i / \mathrm{C}_6)}{2\mathrm{k}_{\mathrm{np}} c X_T} \tag{3.67}$$

Solving for C_5 leads to a quadratic equation whose solutions are given as

$$\mathrm{C}_5 = \frac{(\pm 1 - \cos 2n\phi_i)}{\sin 2n\phi_i} \tag{3.68}$$

Substitution of C_5 values ultimately result in two simple transcendental equations,

$$\frac{\mathrm{F_n}^{(2)}{}'(\mathrm{tx})}{\mathrm{F_n}^{(2)}(\mathrm{tx})} - \frac{\mathrm{F_n}^{(1)}{}'(\mathrm{tx})}{\mathrm{F_n}^{(1)}(\mathrm{tx})} - \sum_{i=1}^{P} \frac{\varepsilon_n}{k_{np} c X_T} = 0 \tag{3.69}$$

$$\frac{\mathrm{F_n}^{(2)}{}'(\mathrm{tx})}{\mathrm{F_n}^{(2)}(\mathrm{tx})} - \frac{\mathrm{F_n}^{(1)}{}'(\mathrm{tx})}{\mathrm{F_n}^{(1)}(\mathrm{tx})} = 0 \tag{3.70}$$

where $\mathrm{t} = \frac{\mathrm{r}_2}{\mathrm{r}_1}$, $x = k_{np} r_1$, $t_2 = \frac{r_1}{\Delta}$

$$X_T = \frac{j\omega\mu}{2\pi}\{\ln(\frac{2}{\gamma k \Delta}) + \frac{\pi}{2} J_0(kc) N_0(kc)\} CF$$

It is interesting to note that for these cases angular dependence vanishes as it is clear from equation (3.69) that the angle (ϕ) is not present in the equation, this means that the post can be located at any position. Thus for $P = 1$ and $\phi_i \neq 0^0 or 180^0$, dual resonance is produced at any angular location and for all normal modes except for $n = 0$. Since equation (3.69) is same as unperturbed value, altering the radial distance of shorting posts can vary the separation between these two frequencies.

3.3.3 Results and Discussion

The transcendental equations representing asymmetric loading have been computed for typical antenna. A theoretical model is made to analyze the annular ring resonator with shorting pins, which are located asymmetrically (means pins are not equispaced). The results of annular ring antenna are compared with simulated results obtained from method of moments (MOM) based commercial solver IE3D. For analysis of resonator, the dimensions chosen are; a = 30 mm, b = 60 mm, c = 50 mm, h = 1.59 mm, $\varepsilon_r = 2.2$ r_0 = 35 mm (feed location), Δ = 1 mm and Δ = 2 mm. Variation of resonant frequency with the radial location of posts is shown in table 3.2 for fist dominant mode. Table 3.3 represents the resonant frequency for second dominant mode. The computed and measured results are in good agreement. The maximum error in prediction is upto 2.5 %.The return loss is also calculated for the dominant mode n = 1 and n = 2 for asymmetric loading and is shown in table 3.4.

The variation of resonant frequency with radial location of posts is shown in figure 3.10 for Δ = 1mm and Δ = 2 mm. The particular case displays frequency for TM_{11} mode when P = 1 and $\phi_i \neq 0^0 or 180^0$. The numerical results show good agreement with simulated results and error for Δ = 1 mm is 2 % and that for Δ = 2 mm is 1 - 2 %. Figure 3.11 shows the variation of resonant frequency with the radius of post when the post is located at c = 50 mm. The numerical and simulated results are again in good agreement. The angular dependence vanishes for asymmetric loading of posts. This can be shown when we change the angular position of post the resonant frequency is not altered. The post is loaded at different angles *i.e.* $\phi_i = 30^0, \phi_i = 60^0$, $\phi_i = 90^0$ then the values of resonant frequency at these positions are 0.9655 GHz, 0.9653 GHz and 0.9652 GHz respectively. This change is marginal showing that the resonant frequency is independent of the angular location of the posts as shown in equation (3.70).

Using the correction factor in the impedance expression leads to a prediction in resonant frequency for the dominant mode in shorted patch within 2.5 % of the measured result whereas without the correction factor the error is large. It is to be noted for all these cases the shorting pin is close to the periphery of the patch where

Table 3.1 Correction factor values.

No. of posts	Q_i	R_i
1	0.3	$0.12\varepsilon_n$
2	0.55	$0.35\varepsilon_n$
3	0.6	$0.6\varepsilon_n$
4	0.6	$0.9\varepsilon_n$
5	1.0	2.0
6	1.05	2.5
7	1.0	3.0
8	0.95	3.5
9	0.9	4.5
10	0.85	5.0

Table 3.2 Comparison of measured and computed values of resonant frequency of asymmetrically shorted ring resonator for $n = 1$ (first dominant mode).

No. of posts	Resonant Frequency (GHz) for n = 1		% Error
	Computed	Measured	
1	0.9655	0.9653	0.021
2	1.12	1.09	2.3
4	1.6812	1.695	0.814
8	2.285	2.275	0.44
10	2.39	2.3922	0.09

Table 3.3 Comparison of measured and computed values of resonant frequency of asymmetrically shorted ring resonator for $n = 2$ (second dominant mode).

No. of posts	Resonant Frequency (GHz) for $n = 2$		% Error
	Computed	Measured	
1	1.6125	1.6347	1.35
2	1.7686	1.784	0.86
4	1.7986	1.7911	0.41
8	2.791	2.801	0.36
10	2.811	2.871	2.09

Table 3.4 Return Loss of asymmetrically loaded ring resonator for $n = 1$ and $n = 2$ (first and second dominant mode).

No. of Posts	Measured Return Loss (dB) for $n = 1$	Measured Return Loss (dB) for $n = 2$
1	-14.86	-9.848
2	-10.85	-1.512
4	-11.24	-10.21
8	-2.111	-10.87
10	-6.463	-12.55

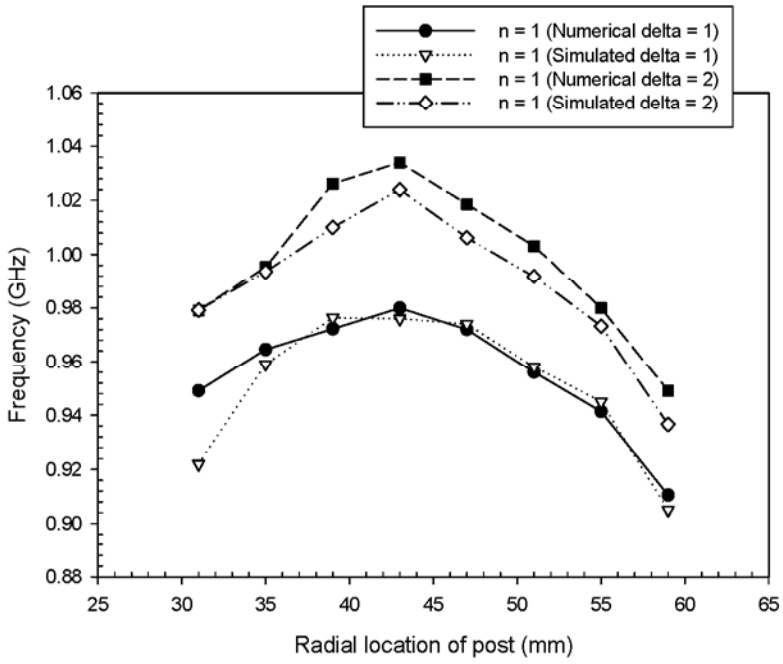

Figure 3.10 Comparison of present theory with simulated data: Resonant Frequency with Radial location of post (a = 30 mm, b = 60 mm, h = 1.59 mm, ε_r = 2.2 and P =1).

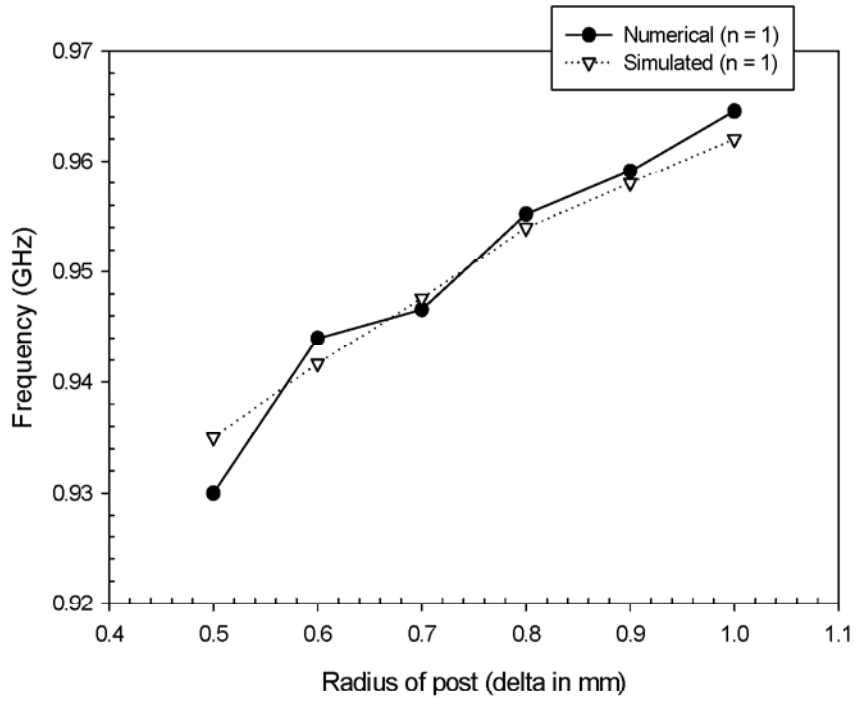

Figure 3.11 Comparison of present theory with simulated data: Resonant Frequency with Radius of post (a = 30 mm, b = 60 mm, c = 50 mm, h = 1.59 mm and P = 1).

the maximum reduction in size takes place. The same method can be extended to obtain the input impedance for a shorted annular ring. Similar is the case of radiation pattern. So intuitively, it can be suggested that cross-polarization is not degraded by the loading of pins. The resonant frequency for dominant mode and other higher order modes is predicted with accuracy. The major results are listed as follows:

(i) The resonant frequency strongly depends upon the radial location of posts. However the relative variation of these modes is different for different radial locations.

(ii) TM_{11} is the dominant mode for asymmetric loaded antenna. For the antenna under consideration, the reduction in resonant frequency is as much as 3 times as compared to the unperturbed patch.

(iii) The resonant frequency increases with increasing the radius of post.

(iv) The metallic post incurs a small amount of power loss, therefore the gain of the antenna will be reduced.

(v) In asymmetric loading the dual resonance is produced at any location for all normal modes except for $n = 0$. The resonance for each mode is independent of the angular location as long as $\phi_i \neq 0^o /180^o$.

3.4 Conclusion

In this chapter we have presented an analytical method to find the input impedance and other parameters of annular ring antenna using cavity model along with circuit theory approach. The method formulated is for the first few modes. It is observed that TM_{11} is the dominant mode for the annular ring fed by coaxial feeding. The resonant resistance is quite high and it goes on decreasing for the other higher modes such as for TM_{12} mode thus showing that the TM_{12} mode is the best for antenna application. Dominant mode resonance is used as high Q cavity. Q can be further increased by using substrate of high dielectric constant. The model developed is quite intuitive, fast to compute and does not demand high computational tools. In the later half of the chapter we have analysed loaded annular ring antenna with asymmetric posts. One interesting application of this analysis tool is to design a dual band antenna with flexible band separation. When close separation is needed, one asymmetrically loaded shorting post with suitable location will suffice. The model

developed for calculating the resonant frequency due to asymmetric loading is simple and accurate. The resonant frequency does not depend upon angle. The analysis can be further extended to find out the input impedance and radiation pattern of the asymmetric loaded annular antenna.

References

1. Chang, K. and H. L. Hseih, "Microwave ring structures and related structures," Wiley Interscience, USA, 2004
2. Bernard, A. P. and J. M. Gautary, "Measurement of Dielectric constant using microstrip ring resonator," IEEE Trans. Microwave Theory Tech. vol. 9, 1991, pp. 592 - 595
3. Troughton, P., "Measurement techniques in microstrip," Electronic Letts, vol. 5, 1969, pp. 25 - 26
4. Edwards, C., "Measurement techniques in microstrip," IEEE MTT-S Int. Microwave Sym Dig., Boston, 1982, pp. 338 - 341
5. Stephson, M. I. and B. Easter, "Resonant techniques for establishing the equivalent circuits of small discontinuities in microstrip," Electronic Letts., vol. 7, 1971, pp. 369 - 374
6. Bao, L. X. and M. J. Amman, "Dual- frequency circularly polarized patch antenna with compact size and small frequency ratio," IEEE Trans. Antennas and Propag., vol. 55, no. 7, July 2007, pp. 2104 - 2107
7. Bahl, I. J., Stuchly, S. S. and M.A. Stuchly, "A new microstrip radiator for medical applications," IEEE Trans. on Microwave Theory and Techniques, vol. MTT-28, 1980, pp. 1464 - 1468
8. Bhattacharyya, A. K. and R. Garg, "Input impedance of annular ring microstrip antenna using circuit theory approach," IEEE Trans Antennas Propag., vol. AP 33, 1985, pp. 369 - 374
9. Wang, B. F. and Y. T. Lo, "Microstrip antennas for dual-frequency operation," IEEE Trans. Antennas Propag., vol. AP-32, 1984, pp. 938 - 943
10. Chow, Y. D. S., Tuan-Yung, H. and J. S. Row, "Dual-frequency shorted triangular patch antenna," Proc. Asia-Pacific Conference APMC, 2005, vol. 4, 2005, pp. 4 - 7
11. Lu, J. H., Tang, C. L. and K. L. Wong, "Novel Dual frequency and broad band designs of slot loaded equilateral triangle microstrip antennas," IEEE Trans. Antenna Propag., vol. 48, 2000, pp. 1048 - 1054

12. Deshmukh, A. and G. Kumar, "Compact broadband gap-coupled shorted square microstrip antennas," Microwave and Optical Technology Letters, vol. 48, 2006, pp. 1261 - 1265
13. Harrington, R.F. "Time Harmonic Electromagnetic Fields," McGraw-Hill, N.Y., 1961
14. Yano, S. and A. Ishimaru, " A theoretical study of input impedance of a circular microstrip disk antenna," IEEE Trans. Antennas Propag., vol.29, no. 1, 1981, pp. 77 - 83
15. Collin, R.E. and F.J. Zucker, "Antenna Theory Part-I," Mc-Graw Hill, New York, 1969
16. Zheng, J.X. and D. C. Chang, "End-Correction Network of a coaxial probe for microstrip patch antennas," IEEE Trans. Antennas Propag., AP-39, no. 1, 1991, pp. 115 - 118
17. Garg, R., Bhartia, P., Bahl, I. and A. Ittipiboon, "Microstrip antenna design handbook," Artech House, Norwood, MA 02062, 2001
18. Bhattacharya, A. and R. Garg, "Self and mutual conductance between two concentric, coplanar, concentric circular radiating current sources," Proc Inst. Elec. Eng., vol. 131, no. 3, 1984, pp. 217 - 219
19. Shen, L.C., "Analysis of a circular printed circuit antenna," Proc Inst. Elec. Eng., vol. 126, no. 12, 1979, pp. 1220 - 1222
20. Chakravarty, T., Biswas, S., Majumdar, A. and A. De, "Computation of resonant frequency of annular ring loaded circular patch using cavity model analysis," Microwave and Optical_Technology Letters, vol.48, 2006, pp. 622 - 626
21. Liao, S., "Microwave devices and circuits," Pearson Education Limited, 2003
22. Bancroft, R., "Microstrip and printed antenna design," Prentice – Hall of India, 2006
23. De, A., "Studies on rectangular and circular patch radiators", PhD Thesis, Indian Institute of Technology, Kharagpur, 1985
24. Lan, G. L. and D. L. Sengupta, "Tunable circular patch antennas," Electron. Letts., vol. 21, 1985, pp. 1022 - 1023

25. Sengupta, D. L. and L. F. Martins-Camelo, "Theory of dielectric-filled edge-slot antennas," IEEE Trans. Antennas Propag., vol. Ap-28, no.4, 1980, pp. 481 - 490

26. Chakravarty, T. and A. De, "Design of tunable modes and dual-band circular patch antenna using shorting posts," IEE Proc-Microw. Antennas Propag., vol. 146, no. 3, 1999, pp. 224 - 228

27. Finch, K.L. and N. G. Alexopoulas, "Shunt posts in microstrip transmission lines," IEEE Trans. Microwave Theory Tech., vol. MTT-38, no.11, 1990, pp. 1585 - 1594

4.1 Introduction

Shorting posts in microstrip antennas have recently come into use in order to take the advantage of different properties such as dual frequency, tenability and compactness [1-3]. Different geometries such as triangular and square patch microstrip antennas have been studied for dual band operation and to enhance bandwidth [4-8]. A circular disk with off-centred shorting posts was first proposed by De [9]. In this, a treatment is developed for single or multiple posts when the posts are symmetrically located *i.e.* equi-spaced along the circumference of circle concentric with the patch radiator. For a single post, symmetry is maintained when $\phi = 0^0/180^0$ *i.e.* the post is located in the same line as that connecting the feed point and the centre of the patch. It was shown that the resonant frequency for each mode depends on $t = r_2/r_1$, where r_2 is the radial distance of the posts from the centre of the patch and r_1 is the radius of the patch. The resonance also depends on the ratio $t = r_1/\Delta$, where the post radius is Δ. As the posts move towards the edge of the patch, the resonance frequency of TM_{11} mode first increases and then drops down. This effect is more pronounced when number of posts P is large. The lowest resonance for post-loaded patch was shown to be (0,1) mode. The higher order modes like (0,2) and (1,2) show interesting results. For both these modes, there exists a critical value of t, where the resonant frequency is same as that for the unperturbed patch. On both sides of this radial distance, the resonant frequency increases. Design of tunable modes and dual band circular patch antenna using shorting posts have been presented by Chakravarty *et al.* [10]. The theoretical model demonstrated that, by locating shorting pins in proper positions, a circular patch can be either tuned in frequency or used as a dual frequency antenna without scattering the low profile structure. Resonant frequency, fields, radiation pattern and input impedance of a short-circuited ring working at TM_{01} mode [11] have been presented.

In chapter III, the effect of loading due to asymmetric passive conducting post is presented. The analysis shows that the resonant frequency does not depend upon the angular variation. The analysis can be extended to symmetric loading where resonant frequency depends on the angular variation. Hence, in this chapter the resonant frequency and input impedance due to symmetric loading has been analysed. For the

purpose of analysis, the structure is divided into two concentric regions and the expressions for the fields in each region are obtained from solution of Helmholtz equation in cylindrical co-ordinates. The constants appearing in the solutions are determined from the boundary conditions. The analysis leads to transcendental equation, the solution of which gives the resonant frequency of the radiator. In this case, for simplification of analysis, the posts are assumed to be located symmetrically(The posts are equidistant from one another) but at different radii concentric with the patch. The analysis is further extended to multiple posts upto 10. Finally the input impedance is also calculated for annular ring loaded with symmetrical multiple posts.

4.2 Analysis of Annular Ring Antenna Loaded with Multiple Posts Located Symmetrically

The basic ring geometry with shorting posts is shown in figure 4.1. The annular ring of inner radius a and outer radius b is loaded with P number of passive conducting posts of radius Δ at angular locations $\phi_i = (i = 1,2,....,P)$ on the circumference of a concentric circle of radius c where $a < c < b$. The given annular ring in presence of source can be considered to be consisting of two half disks where the line of axis is through the feed point and the centre of patch. The same assumption of converting the ring into two rings is assumed here, thereby converting the structure into two regions I and II. The analysis is based on cavity model where variation of electric field within the substrate has only z – component. The magnetic field has essentially x - component and y - component.

For region I $(a < r < c)$, the expressions for electric and magnetic fields are obtained as

$$E_z^{(1)} = -j\omega_{np}\mu\{C_1 J_n(k_{np}r) + C_2 N_n(k_{np}r)\}\cos n\phi \tag{4.1}$$

$$H_r^{(1)} = -(\frac{n}{r})\{C_1 J_n(k_{np}r) + C_2 N_n(k_{np}r)\}\sin n\phi \tag{4.2}$$

and

$$H_\phi^{(1)} = -k\{C_1 J_n^{'}(k_{np}r) + C_2 N^{'}(k_{np}r)\}\cos n\phi \tag{4.3}$$

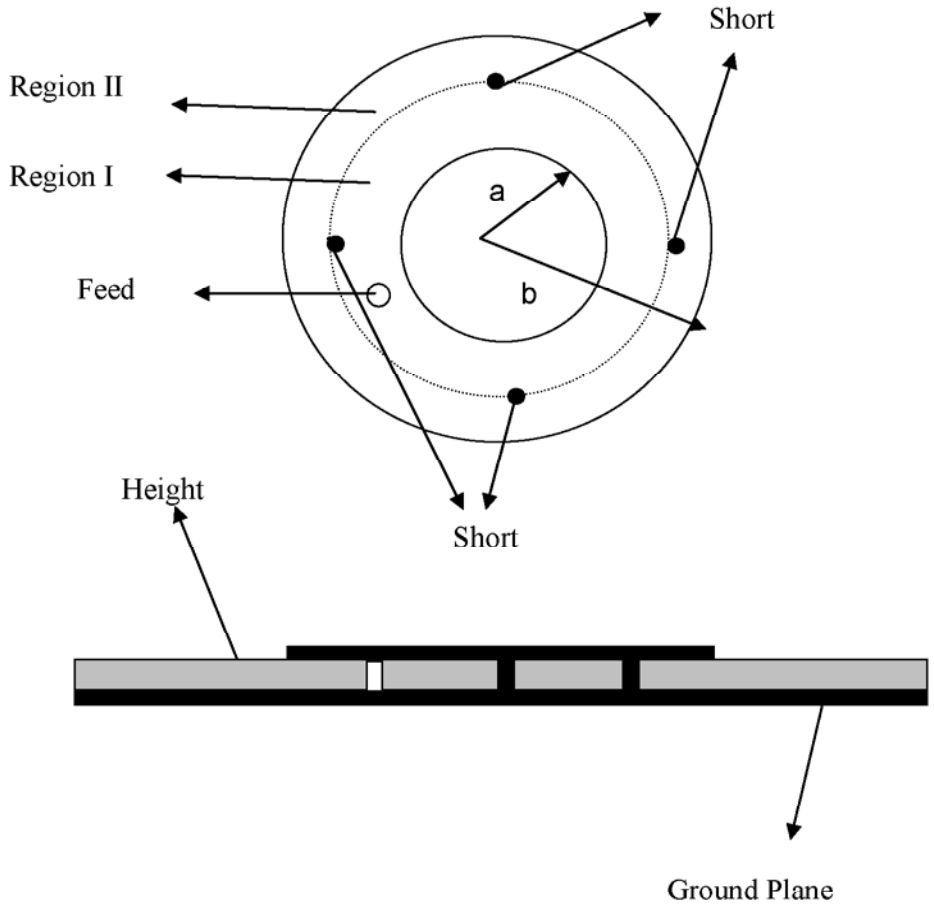

Figure 4.1 Geometry of symmetrically loaded annular ring antenna.

where $J_n(k_{np}r)$ is Bessel function of first kind of order n, ω_{np} and k_{np} are the angular frequencies and propagation constant for TM_{np} mode and C_1 and C_2 are constants. Prime denotes a derivative with respect to its argument. The integer n corresponds to the order of the Bessel function and p denotes the p^{th} zero of $J_n'(k_{np}r)$. The subscript z is ignored for particular mode identification as the electric field is non variant along z direction. Similarly for region II, $c < r < b$ the expressions for electric and magnetic fields are obtained.

$$E_r^{(2)} = -j\omega\mu\{C_3 J_n(k_{np}r) + C_4 N_n(k_{np}r)\}\cos n\phi \tag{4.4}$$

$$H_r^{(2)} = -(\frac{n}{r})\{C_3 J_n(k_{np}r) + C_4 N_n(k_{np}r)\}\sin n\phi \tag{4.5}$$

and

$$H_\phi^{(2)} = -k\{C_3 J'_n(k_{np}r) + C_4 N'_n(k_{np}r)\}\cos n\phi \tag{4.6}$$

where C_3 and C_4 are constants and $N_n(k_{np}r)$ is Bessel function of second kind.

Application of vanishing tangential component of magnetic field in the two regions at the boundary edges lead to modification of field expressions as follows;

$$E_z^{(1)} = -j\omega_{np}\mu C_n^{(1)} F_n^{(1)}(k_{np}r)\cos n\phi \tag{4.7}$$

$$H_\phi^{(1)} = -kC_n^{(1)} F_n^{'(1)}(k_{np}r)\cos n\phi \tag{4.8}$$

and

$$E_z^{(2)} = -j\omega_{np}\mu C_n^{(2)} F_n^{(2)}(k_{np}r)\cos n\phi \tag{4.9}$$

$$H_\phi^{(2)} = -kC_n^{(2)} F_n^{'(2)}(k_{np}r)\cos n\phi \tag{4.10}$$

where

$$F_n^{(1)}(kr) = J_n(k_{np}r)N'_n(k_{np}a) - J'_n(k_{np}a)N_n(k_{np}r)$$

$$F_n^{(2)}(k_{np}r) = J_n(k_{np}r)N'_n(k_{np}b) - J'_n(k_{np}b)N_n(k_{np}r)$$

and

$$F_n^{'(1)}(k_{np}r) = J'_n(k_{np}r)N'_n(k_{np}a) - J'_n(k_{np}a)N'_n(k_{np}r)$$

$$F_n^{'(2)}(k_{np}r) = J'_n(k_{np}r)N'_n(k_{np}b) - J'_n(k_{np}b)N'_n(k_{np}r)$$

It is assumed that the diameter of the circular post is small. Such a thin post can be assumed to be replaced by a conductor in the form of a circular arc strip having arc length equal to diameter of the post coincident with a circle of radius c. For arc

strip of small arc length the axial current may be assumed to be uniform along its width. This current per unit width is given as E_z/Z_0, where Z_0 is the impedance per unit length of the post. The impedance per unit length of such a post carrying uniform current and connected between two conducting disks is given as [12]

$$Z_0 = \frac{\eta k}{4}[1 - J_0^{\,2}(kc) + j\{\frac{2}{\pi}\ln(\frac{2}{\gamma k\Delta}) + J_0(kc)N_0(kc)\}] \tag{4.11}$$

where c is the radial distance of the post from the centre of the patch.

$$Z_0 = \frac{j\omega\mu}{2\pi}\{\ln(\frac{2}{\gamma k\Delta}) + \frac{\pi}{2}J_0(kc)N_0(kc)\}CF = X_T \tag{4.12}$$

In equation (4.12) CF is the correction factor and is described in chapter III. The use of correction factor is described in detail by Chakravarty *et al.* [13,14]. The empirical correction factor correctly predicts the effect of multiple posts on the fringe of annular ring for up to 10 posts.

The electric and magnetic fields given by equations (4.7) - (4.10) satisfy the following boundary conditions.

$$E_z^{(2)} = E_z^{(1)} \qquad at\ \mathrm{r} = \mathrm{c} \tag{4.13}$$

$$\mathrm{H}_\phi^{(2)} - \mathrm{H}_\phi^{(1)} = \sum_{i=1}^{P} \mathrm{E}_z^{(2)}/(\mathrm{Z}_0.2\Delta)$$

$$\text{at } \mathrm{r} = \mathrm{c} \text{ for } \phi_i - \alpha/2 < \phi < \phi_i + \alpha/2 \tag{4.14}$$

where α is the angle subtended by shorted post at the centre of ring cavity. The summation over index i indicates that the boundary condition is applicable for all the shorting posts.

From equations (4.13, 4.14) it is found that

$$\frac{C_n^{(2)}}{C_n^{(1)}} = \frac{F_n^{(1)}(k_{np}c)}{F_n^{(2)}(k_{np}c)} \tag{4.15}$$

and

$$\frac{C_n^{(2)}}{C_n^{(1)}} = \frac{F_n^{'(1)}(k_{np}c)}{F_n^{'(2)}(k_{np}c) - F_n^{(2)}(k_{np}c)\sum_{i=1}^{P} \frac{j\omega\mu}{2X_t k_{np}c\varepsilon_n\pi}[1 + \cos(2n\phi_0)]} \tag{4.16}$$

Now using equations (4.15) and (4.16)

$$\frac{F_n^{'(2)}(k_{np}c)}{F_n^{(2)}(k_{np}c)} - \frac{F_n^{'(1)}(k_{np}c)}{F_n^{(1)}(k_{np}c)} - \sum_{i=1}^{P} \frac{\varepsilon_n(1+\cos(2n\phi))}{2k_{np}cX_T} = 0 \tag{4.17}$$

The resonance frequency for a given mode *np* is obtained by solving equation (4.17) where *n* integer denotes the order of Bessel's function and *p* corresponds to the p^{th} zero of equation (4.17). The equation shows that the resonant frequency is depending on the angular location of posts (ϕ). This equation is used for the analysis of resonant frequency of symmetrically loaded annular ring antenna with multiple shorting posts.

4.2.1 Results and Discussion

For the analysis of annular ring antenna loaded with shorting pins located symmetrically the following design parameters are used; $\varepsilon_r = 2.2$, $h = 1.59$ mm , $a = 30$ mm , $b = 60$ mm , feed point location $r_0 = 35$ mm and $\Delta = 1$ mm and 2 mm where Δ is the radius of post. Equation (4.17) is used to find out resonant frequency of annular ring resonator with multiple shorting pins (posts). The structure is loaded with multiple shorting posts, which are distributed uniformly. The results of annular ring with varying number of posts are compared with simulated results obtained from commercial solver IE3D based on method of moments (MOM). But some of the results are also verified by measured results. For analysis numbers of posts have been varied from 1 to 10. For every case the angular distance of the posts on the ring is constant (*e.g.* for P = 9, the angular separation between the shorts on ring is $2\pi/9$). The comparison between simulated and numerically calculated values of resonant frequencies for first three modes with different radial location of posts (n = 0, 1 and 2) are shown in table 4.1, 4.2 and 4.3 respectively for P = 4. The maximum error is also calculated for the first three modes. The results numerically calculated by the present model are used for the practical design of ring resonator and the comparison is being done between measured and numerical results. The numbers of posts for measured results are 1, 2, 4 and 10. The measured results of return loss are given in table 4.4. The measured and numerically calculated values of resonant frequencies for first three modes (n = 0, 1 and 2) are shown in table 4.5. Both numerical and measured results are in good agreement. The error percentage is less than 3 %.Variation of resonant

Table 4.1 Comparison of numerical and simulated values of resonant frequency of shorted ring resonator for $P = 4$ and $\Delta = 1$ mm for TM_{01}mode.

Radial location of pin (mm)	**Resonant frequency for TM_{01} mode (GHz) for $\Delta = 1$ mm**		**% error**
	Numerical	**Simulated**	
31	0.83904	0.8058	3.9
35	0.88750	0.9048	1.9
39	0.925	0.9282	0.3
43	0.937	0.9498	1.34
47	0.9125	0.9335	1.9
51	0.875	0.8858	1.2
59	0.75	0.7608	1.41

Table 4.2 Comparison of numerical and simulated values of resonant frequency of shorted ring resonator for $P = 4$ and $\Delta = 1$mm for TM_{11} mode.

Radial location of pin (mm)	**Resonant frequency for TM_{11} mode (GHz) for $\Delta = 1$**		**% error**
	Numerical	**Simulated**	
31	1.0873	1.122	1.77
35	1.1216	1.156	0.03
39	1.1558	1.164	.017
43	1.1601	1.1688	0.33
47	1.1815	1.1440	1.07
51	1.164	1.117	1.71
59	1.0788	1.122	0.03

Table 4.3 Comparison of numerical and simulated values of resonant frequency of shorted ring resonator for P = 4 and Δ = 1 mm for TM_{21} mode.

Radial location of pin (mm)	**Resonant frequency for TM_{21} mode (GHz) for Δ = 1**		**% error**
	Numerical	**Simulated**	
31	1.7123	1.738	1.023
35	1.7894	1.832	1.68
39	1.8664	1.9349	2.3
43	1.9435	2.0462	2.5
47	2.0034	2.1147	2.4
51	1.9949	2.0062	1.1
59	1.8579	1.8435	0.775

Table 4.4 Measured values of return loss of antenna at different modes with different posts.

No. of posts	Measured Return loss (dB)		
	$n = 0$	$n = 1$	$n = 2$
1	-2.103	-3.762	-6.53
2	-3.07	-5.0	-8.7
4	-15.8	-5.9	-10.3
10	-3.58	-23.7	-13.27

Table 4.5 Comparison of measured and computed values of resonant frequency of shorted ring resonator.

No. of posts	Resonant Frequency (GHz)					
	$n = 0$		$n = 1$		$n = 2$	
	Computed	Measured	Computed	Measured	Computed	Measured
1	0.214	0.2198	0.6678	0.6706	1.113	1.133
2	0.376	0.37	0.787	0.79	1.19	1.22
4	0.60	0.6127	0.79	0.7884	1.36	1.388
10	1.036	1.072	1.44	1.4	1.738	1.74

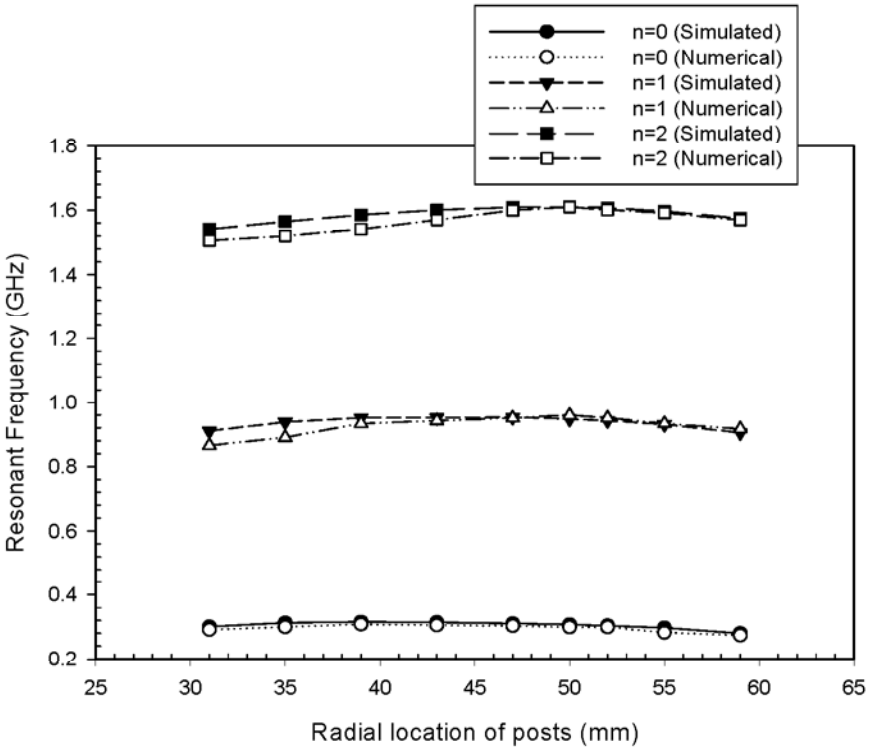

Figure 4.2 Comparison of present theory with simulated data: Resonant Frequency with Radial location of posts (a = 30 mm, b = 60 mm, h = 1.59 mm, ε_r = 2.2 and P = 1).

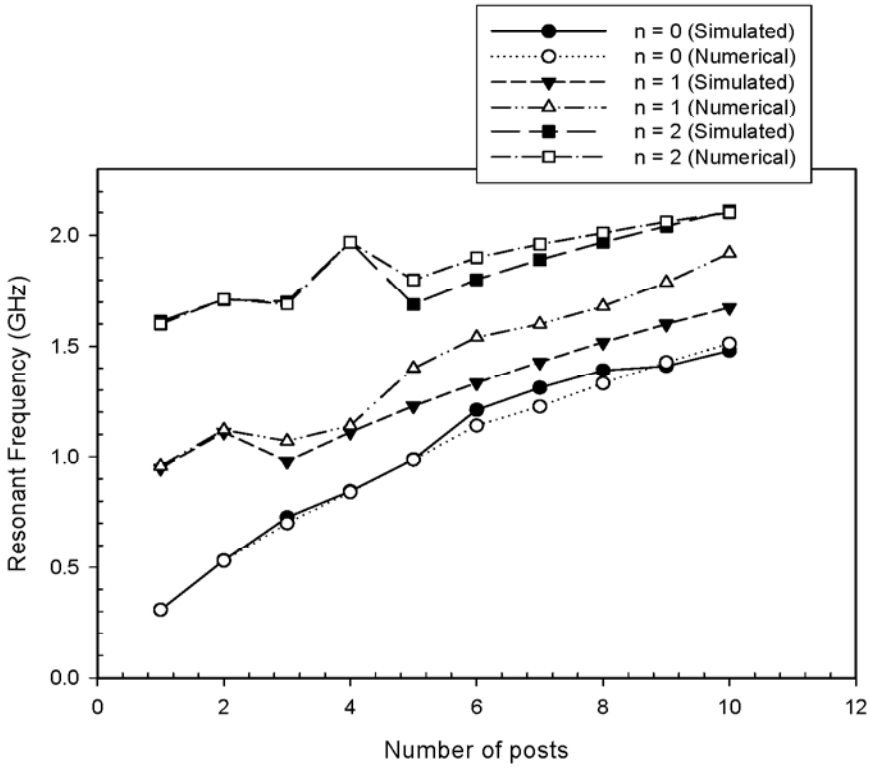

Figure 4.3 Comparison of present theory with simulated data: Resonant frequency with Number of posts (a = 30 mm, b = 60 mm, c = 50 mm, h = 1.59 mm and ε_r = 2.2).

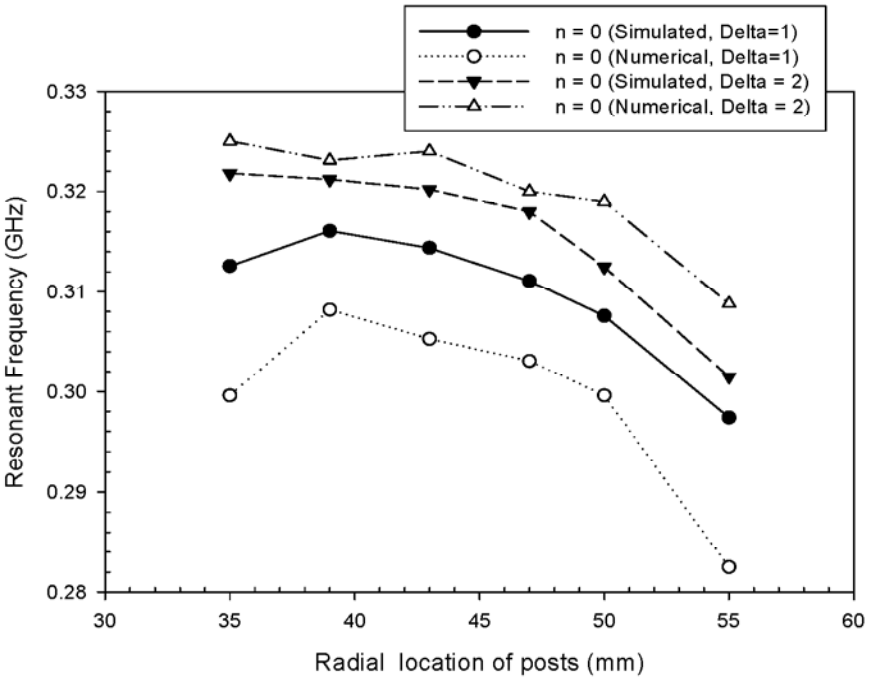

Figure 4.4 Comparison of present theory with simulated data: Resonant Frequency with Radial location of posts for dominant mode ($n = 0$) for different $\Delta = 1$mm, $\Delta = 2$mm ($a = 30$ mm, $b = 60$ mm, $h = 1.59$ mm, $\varepsilon_r = 2.2$ and $P = 1$).

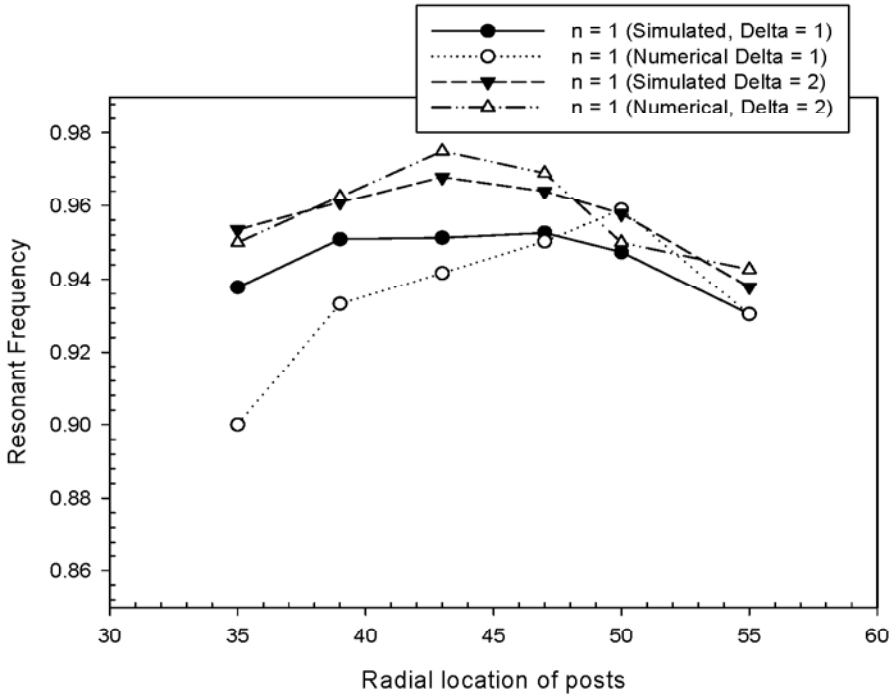

Figure 4.5 Comparison of present theory with simulated data: Resonant Frequency with Radial location of posts for higher order mode ($n = 1$) for different $\Delta = 1$ mm, $\Delta = 2$ mm ($a = 30$ mm, $b = 60$ mm, $h = 1.59$ mm, $\varepsilon_r = 2.2$ and $P = 1$).

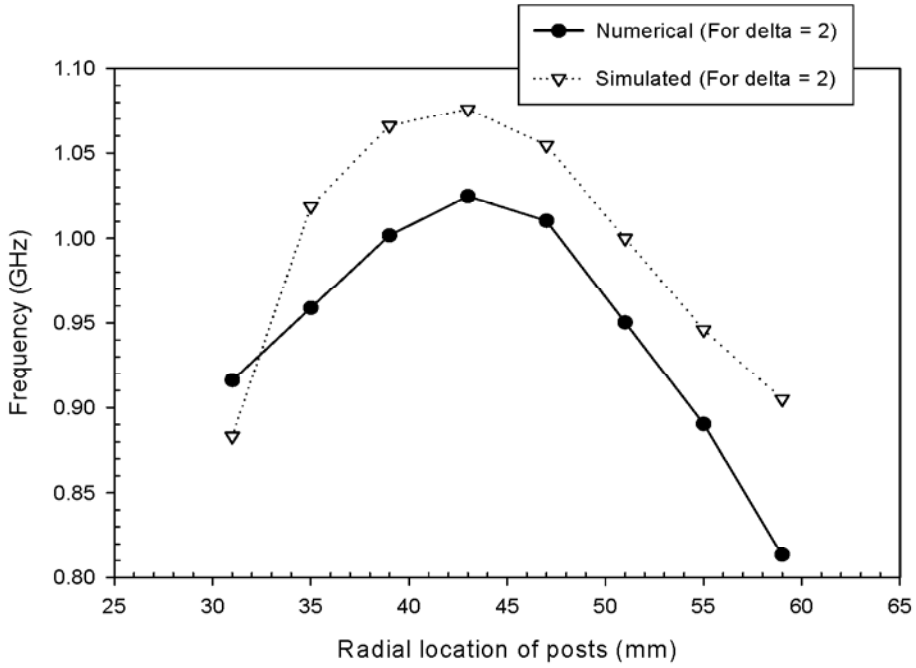

Figure 4.6 Comparison of present theory with simulated data: Resonant Frequency with Radial location of posts for dominant mode ($n = 0$) for different $\Delta = 2$ mm ($a = 30$ mm, $b = 60$ mm, $h = 1.59$ mm, $\varepsilon_r = 2.2$ and $P = 4$).

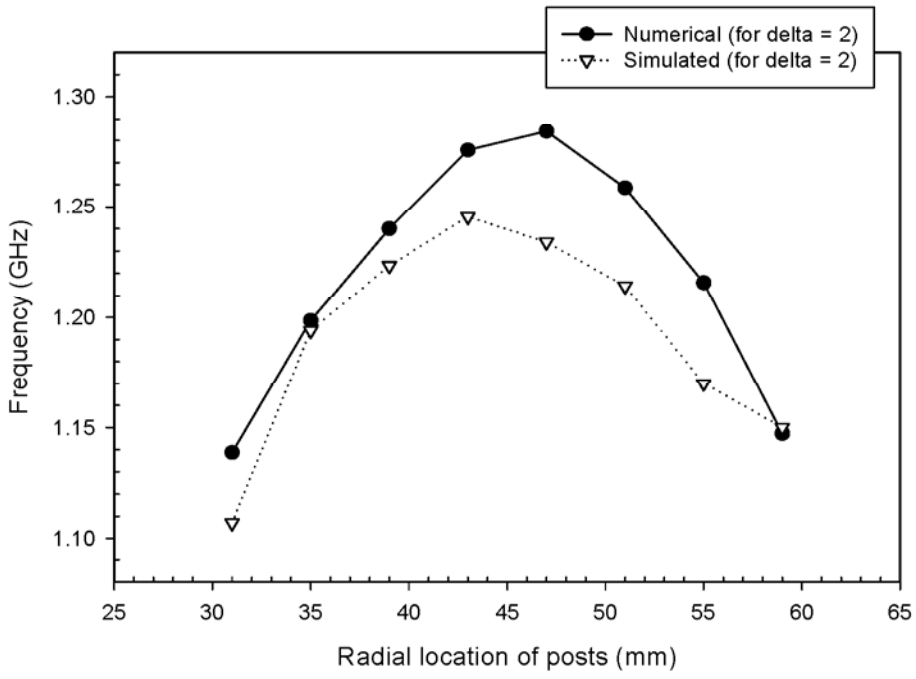

Figure 4.7 Comparison of present theory with simulated data for TM_{11} mode: Resonant Frequency with Radial location of posts ($a = 30$ mm, $b = 60$ mm, $h = 1.59$ mm, $\varepsilon_r = 2.2$ and $P = 4$).

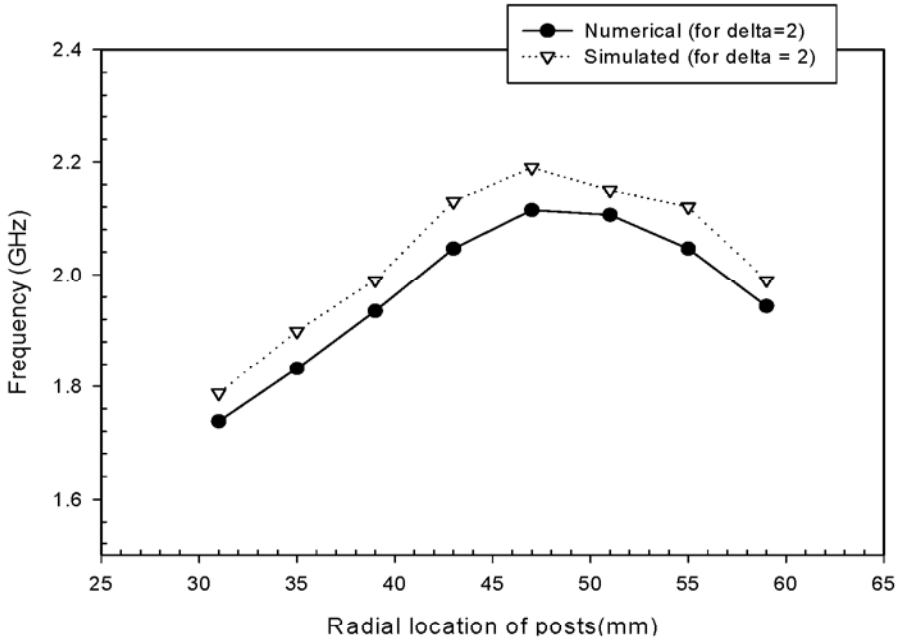

Figure 4.8 Comparison of present theory with simulated data for TM_{21} mode: Resonant Frequency with radial location of posts (a = 30 mm, b = 60 mm, h = 1.59 mm, ε_r = 2.2 and P = 4).

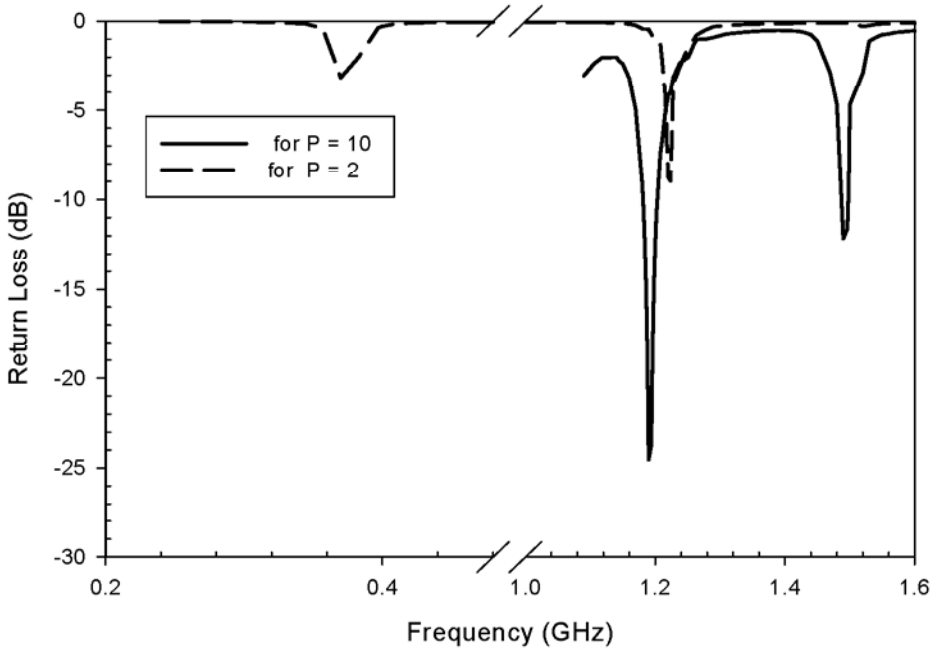

Figure 4.9 Variation of return loss with frequency for different number of posts (a = 30 mm, b = 60 mm, c = 50 mm, h = 0.159 mm and ε_r = 2.2).

frequency with the radial location of the short is also calculated for different modes (n = 0, 1, 2) and for P = 1 shown in figure 4.2. For comparison the same results are plotted with simulated data. The simulated and numerical values are in very good agreement. For dominant mode (n = 0), the maximum predicted error is less than 1 % and for higher order modes (n = 1, 2), the maximum error in prediction is 2 - 3 %. The resonant frequency changes with the number of posts. The variation of resonant frequency is also computed for dominant and higher order modes (n = 0, 1, 2) with number of posts. Figure 4.3 shows that the simulated and numerical values are in very good agreement. The maximum error in prediction is 2 - 3 %. The resonant frequency is also varied with the radial location of short by changing the radius of the pin (Δ = 1mm, Δ = 2mm). The variation of resonant frequency with radial location for different Δ with dominant mode (for n = 0) is shown in figure 4.4. The numerical results show a good agreement with the simulated results. The error for Δ = 1mm is 2 %, while the error for Δ = 2 mm is 3 – 4 %. The similar variation is also calculated for higher mode, shown in figure 4.5, (for n = 1). The numerical and simulated results are in good agreement. The maximum error for Δ = 1 mm, Δ = 2 mm is 2 – 3 %. Figures 4.6 – 4.8 show comparison for P = 4 when Δ = 2 mm. For 2 and 10 posts the plot of measured values of return loss is also shown in figure 4.9.

The model developed and presented gives reasonably accurate prediction of resonant frequencies for symmetrically loaded annular ring antenna. The measured and simulated results are in good agreement. The analysis for input impedance shows that the value of input impedance can be reduced by loading the antenna to obtain high bandwidth. The major results are summarized as;

(i) The resonant frequency strongly depends upon the radial location of posts. The resonant frequency also depends on the radius of posts.

(ii) The unperturbed ring patch has TM_{11} as dominant mode where as for the symmetrically shorted annular ring antenna is TM_{01} mode.

(iii) For symmetric loading of post the frequency depend upon the angular location of posts where as in asymmetric loading the dual resonance is produced at any location for all normal modes except for n = 0. The resonance for each mode dependent on the angular location as long as $\phi_i = 0^o / 180^o$.

4.3 Analysis of Input Impedance of Symmetrically Loaded Annular Ring Antenna

The frequency analysis is further extended to find out input impedance of the shorted annular ring antenna. The general formulation for impedance is same as described in chapter II. The analysis is based on cavity model where it is assumed that the substrate is electrically thin ($h = \lambda_0$). The analysis is done when the ring antenna is loaded symmetrically via shorting pins. The same assumption of converting the ring into two rings is assumed here, thereby converting the structure into two regions I and II. The basic ring geometry with shorting posts is same as shown in figure 4.1.The field equations for the analysis is given by equations (4.7) -(4.10) **.** The expression of input impedance is given by [15]

$$Z_{in} = -\frac{1}{I_0^{\,2}} \sum_n \sum_p \frac{(j\omega + A)p_n^2}{(j\omega - C)(j\omega + A) + \omega_{np}^2} \tag{4.18}$$

The probe can be located in any of the two regions which are formed due to the location of posts at point c and the boundary conditions at two regions are

i. Probe in region I

$$H_\phi^{(2)} - H_\phi^{(1)} = E_z^{(2)} / (Z_0 . 2\Lambda)$$

$$(\text{at } r = c \ \text{ for } \phi_i - \alpha/2 < \phi < \phi_i + \alpha/2) \tag{4.19}$$

ii. Probe in region II

$$H_\phi^{(1)} - H_\phi^{(2)} = E_z^{(1)} / (Z_0 . 2\Delta)$$

$$(\text{at } r = c \ \text{ for } \phi_i - \alpha/2 < \phi < \phi_i + \alpha/2) \tag{4.20}$$

where Z_0 is the impedance per unit length of the shorting post and is given by equation (4.11).

For computation of resonant frequency the real part of the above expression is neglected and it is rewritten as

$$Z_0 = \frac{j\omega_{np}\mu}{2\pi} X_{np} \tag{4.21}$$

The real part of the impedance expression for shorting post constitutes power loss in higher order modes and it is introduced later while computing the total power loss. For illustration of the method of formulation, we consider that the probe is located in region I. For eigen-modes denoted by $n = 0$ or when $\phi_i = 0^0/180^0$, the asymmetric modes designated by $\sin(n\phi)$ are not generated. For such cases, application of boundary condition equation (4.17) gives the following relation

$$\frac{C_n^{(2)}}{C_n^{(1)}} = \frac{F_n^{'(1)}(k_{np}c)}{\{F_n^{'(2)}(k_{np}c) - F_n^{(2)}(k_{np}c)\sum_{i=1}^{P} \frac{j\omega\mu}{2X_t k_{np} c\varepsilon_n \pi}[1+\cos(2n\phi_0)]} \tag{4.22}$$

Using above equation we can write

$$\frac{C_n^1}{C_n^2} = A_t^1$$

where A_t^1 is a constant.

In order to evaluate the constant $C_n^{(1)}$, the normalization condition[16] is used.

$$\int_V \varepsilon |E|^2 dV = 1 \tag{4.23}$$

Since the entire volume is split into two regions, the normalization condition for the problem under consideration assumes the form

$$\int_0^h \int_0^{2\pi} \{\int_0^{r_2} \varepsilon |E_z^{(1)}|^2 r dr + \int_{r_2}^{r_1} \varepsilon |E_z^{(2)}|^2 r dr\} d\phi dz = 1 \tag{4.24}$$

Substituting various values the normalisation constant is obtained.

$$C_n^{(1)} = \frac{1}{k}\sqrt{\frac{1}{h\pi\mu(I_1 + A_t^1 I_2)}}$$

In the above equation

$$I_1 = \int_a^c \left(J_n(k_{np}\cdot r)N_n'(k_{np}\cdot a) - J_n'(k_{np}\cdot a)N_n(k_{np}\cdot r)\right)^2 r dr$$

$$I_2 = \int_a^c \left(J_n(k\cdot r)N_n'(k\cdot b) - J_n'(k\cdot b)N_n(k\cdot r)\right)^2 r dr$$

The different parameters appearing in expression for input impedance (4.19) assumes the following form

$$A = Z_s \int_0^{2\pi}\int_0^{2\pi} \left\{ \left|H_\phi^{(1)}\right| + \left|H_r^{(1)}\right|^2 \right\} r dr + \int_{r_1}^{r_2} \left\{ \left|H_\phi^{(2)}\right|^2 + \left|H_r^{(2)}\right|^2 \right\}^2 r dr d\phi \tag{4.25}$$

$$C = -Y_W \int_0^{h}\int_0^{2\pi} \left|E_z^{(2)}\right| r d\phi dz \qquad (at\ r = b) \tag{4.26}$$

From this

$$A = Z_s \pi C_n^{(1)^2} [k^2 I_3 + n^2 I_4 + k^2 A_t^{(1)2} I_5 + n^2 A_t^{(1)2} I_6] \tag{4.27}$$

where surface resistance Z_s is given as

$$Z_s = \{\frac{\pi f \mu}{\sigma}\}^{\frac{1}{2}}$$

$$I_3 = \int_a^a J_n^{'}(k_{np}.r) N_n^{'}(k_{np}.a) - J_n^{'}(k_{np}.a) N_n^{'}(k_{np}.r)^2 r dr$$

$$I_4 = \int_0^{r_2} \frac{(J_n(k_{np}.r) N_n(k_{np}.a) - J_n(k_{np}.a) N_n(k_{np}.r))^2}{r^2} r dr$$

and

$$I_5 = \int_a^a J_n^{'}(k_{np}.r) N_n^{'}(k_{np}.b) - J_n^{'}(k_{.np}b) N_n^{'}(k_{np}.r)^2 r dr$$

$$I_6 = \int_0^{r_2} \frac{(J_n(k_{np}.r) N_n(k_{np}.b) - J_n(k_{np}.b) N_n(k_{np}.r))^2}{r^2} r dr$$

$$C = -Y_W h \frac{\mu}{\varepsilon} C_n^{(1)^2} A_t^1 \frac{4}{\pi\ b} \tag{4.28}$$

The expression of A corresponds to the copper loss in the microstrip. Due the presence of metallic post an additional component of power loss in the post needs to be added to the conventional copper loss component. P_{post} corresponds to the power lost in the conducting post and is given as

$$P_{post} = \mathrm{Re}(\frac{V^2}{2Z_0}) \tag{4.29}$$

In the above expression Z_0 is of the form $\alpha + j\beta$ and $V = -hE_{av}$

where

$$E_{av} = \frac{1}{2\Delta}\int_{\phi_1-\alpha/2}^{\phi_1+\alpha/2} E_z^{(i)2}(r_2,\phi)d\phi \tag{4.30}$$

4.3.1 Excitation Probe in Region I

Consider a loaded microstrip patch radiator excited by a coaxial line feeding a probe located at $(r_0,\phi_0,0)$ as shown in figure 4.1. Using the general formulation described in chapter II, the input impedance of loaded annular ring antenna can be obtained.

Using the transformation [17]

$$r = r_0 + \frac{d_f}{2}\cos\beta$$

and expanding the Bessel function in Taylor series, the function $F_n^{(1)}(k_{np}.r)$ is obtained as

$$F_n^{(1)}(k.r) = J_n(k.r_0) + \frac{k.d_f}{2}J_n'(k.r_0)\cos\beta) \tag{4.31}$$

where the higher order terms of the Taylor series expansion are neglected.

Using the transformation

$$\phi = \frac{d_f}{2r_0}\sin\beta$$

and expanding $\cos(n\phi)$ & $\sin(n\phi)$ in series of Bessel function it is found

$$\cos(n\phi) = J_0\left(\frac{nd_f}{2r_0}\right) + 2\sum_{q=1}^{\infty} J_{2q-1}\left(\frac{nd_f}{2r_0}\right)\cos(2q\beta)$$

$$\sin(n\phi) = 2\sum_{q=1}^{\infty} J_{2q-1}\left(\frac{nd_f}{2r_0}\right)\sin[(2q-1)\beta]$$

Substituting in eq.(4.39) and carrying out the integration

$$p_n = -j\omega\mu h I_0 C_n^{(1)} J_n(k.r_0) J_0\left(\frac{nd_f}{2r_0}\right)$$

Substituting eq. (3.29) in eq. (3.2), we get

$$Z_{in} = \mu^2 h^2 \sum_n \sum_p \frac{(j\omega + A)C_n^{(1)2}\omega^2\left(J_n(k.r_0)J_0\left(\frac{nd_f}{2r_0}\right)\right)^2}{(j\omega - C)(j\omega + A) + \omega_{np}^2} \tag{4.32}$$

4.3.2 Excitation Probe in Region II

Using the same transformations as mentioned earlier, the function $F_n^{(1)}(k_{np}.r)$ is obtained as

$$F_n^{(2)}(k.r) = F_n^{(2)}(k.r_0) + \frac{k.d_f}{2}\cos\beta F_n^{(2)'}(k.r_0)$$

Substituting in equation (4.39) and carrying out the integration

$$p_n = -j\omega\mu h I_0 A_X C_n^{(1)}[J_n(k.r_0)N_n'(k.r_1) - J_n'(k.r_1)N_n(k.r_0)]J_0\left(\frac{nd_f}{2r_0}\right)$$

Therefore

$$Z_{in} = \mu^2 h^2 \sum_n \sum_p \frac{(j\omega + A)A_X^2 C_n^{(1)^2}\omega^2 J_0^2\left(\frac{nd_f}{2r_0}\right)[F_n^{(2)}(k.r_0)]^2}{(j\omega - C)(j\omega + A) + \omega_{np}^2}) \qquad (4.33)$$

Equations (4.58) and (4.59) give the input impedance of loaded annular microstrip patch antenna for different probe locations.

4.3.3 Results and Discussion

The input impedance of annular ring antenna loaded with symmetric shorting posts is calculated. The posts are located symmetrically on the annular ring at a distance *c* from the centre of ring. For analysis of resonator the dimension chosen are; a = 30 mm, b = 60 mm, h = 1.59 mm, ε_r = 2.2 , c = 50 mm, P = 1, P = 4 and r_0 = 35 mm (Feed location). The radius of post taken is Δ = 1. For every case the angular distance of the posts on the ring is constant. (*e.g.* for P = 4 the angular separation between the shorts on ring is 2π/4).

Figure 4.10 shows the variation of input impedance with frequency for both real and imaginary parts when P = 1. Figure 4.11 shows the variation of input impedance with frequency for both real and imaginary parts when P = 4.The numerical and measured results are in complete agreement for P = 1 and P = 4. The variation of resonant frequency for first dominant mode for both (P = 1 and P = 4) is 1 % -1.5 % for first dominant mode. This method is quite simple. The major results can be discussed as under;

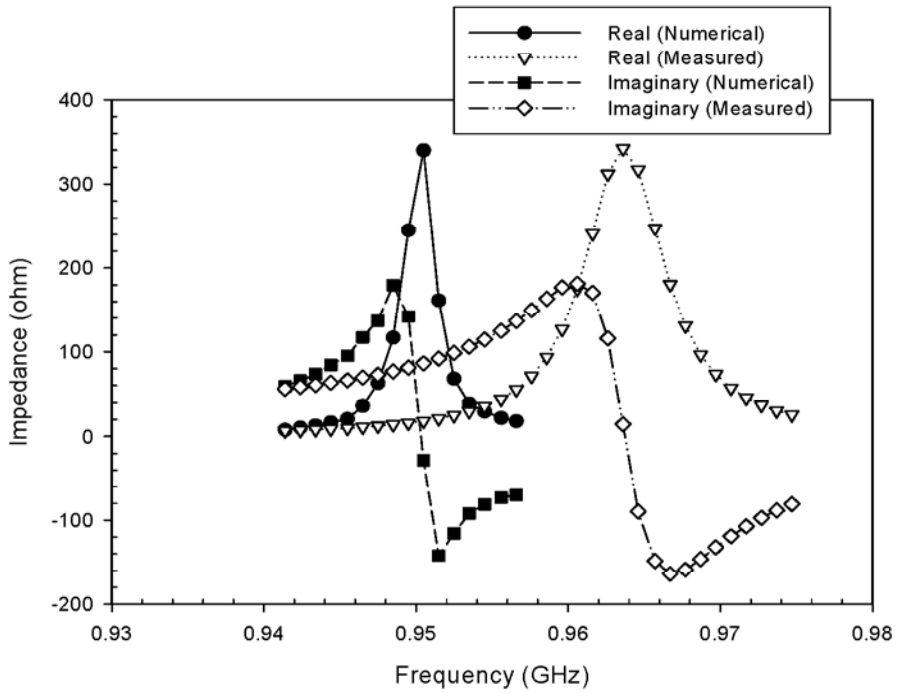

Figure 4.10 Comparison of present theory with measured data: Input impedance with Frequency (a = 30mm, b = 60 mm, c = 50 mm, h = 1.59 mm, $\varepsilon_r = 2.2$ and $P = 1$).

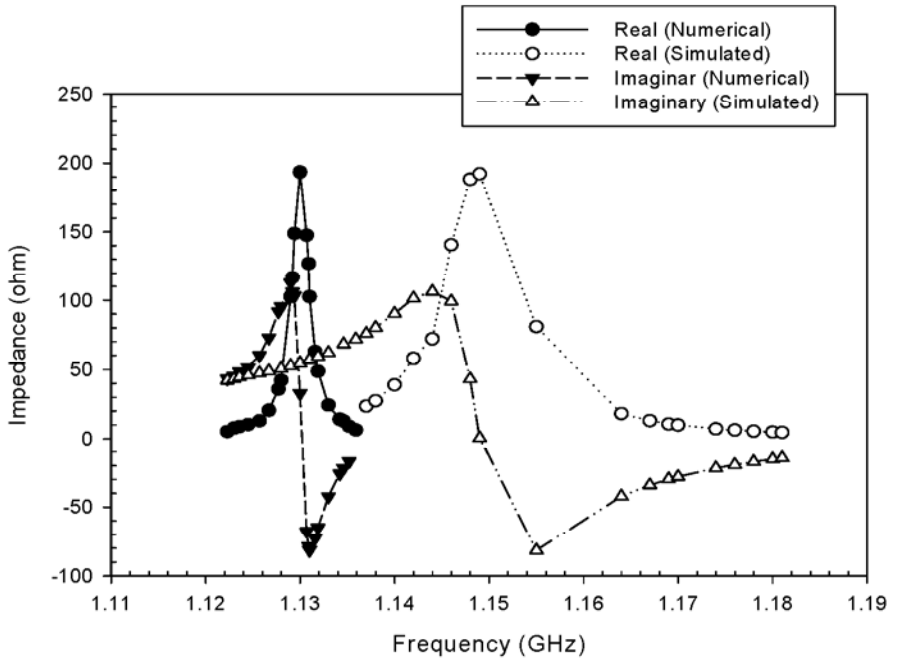

Figure 4.11 Comparison of present theory with simulated data: Input impedance with Frequency (a = 30 mm, b = 60 mm, c = 50 mm, h = 1.59 mm, $\varepsilon_r = 2.2$ and $P = 4$).

(i) The input impedance seen by the feed-probe, among other parameters, depends on the post location and the dimension.

(ii) Possibility of better impedance match increases if the probe is located in region I.

(iii) Use of wall susceptance is not required in the present method since the corrected frequency (due to fringing fields) is required to be used as an input.

(iv) Present method evaluates the total power loss while computation of input impedance.

(v) An exact evaluation of power loss in the post contributed by the real part of post impedance is required for correct estimation of impedance when the post is near the edge. The input impedance seen by the feed-probe, among other parameters, depends on the post location and the dimension.

4.4 Conclusion

The resonant frequency for symmetric loading depends upon the angular variation of posts. Thus the resonant frequency for the dominant mode and other higher order modes can be calculated with accuracy. The loading can be used to obtain compact and tunable dual frequency antennas. The analysis developed in this chapter shows that TM_{01} is the dominant mode for symmetrically loaded annular ring resonator. The analysis is further extended to find out the input impedance which shows that the bandwidth can be increased as the value of input impedance is decreased due to loading. This analysis can further extended to incorporate switching diodes or varactor diodes.

References

1. Waterhouse, R. B., "Small microstrip patch antennas," Electronic Letts., vol. 31, 1995, pp. 604 - 605
2. Waterhouse, R. B., Targonski, S. D. and D.M. Kotokoff, "Improving the mechanical tolerances and radiation performance of shorted patches," IEEE Antennas and Propag. Soc. Int. Symp., vol.3, 1997, pp. 1852 - 1855
3. Sanad, M., "Effect of the shorting posts on short circuit microstrip antennas," IEEE Antennas and Propag. Soc. Int. Symp., vol.2 , 1994 , pp. 794 - 797
4. Wang, B. F. and Y. T. Lo, "Microstrip antennas for dual-frequency operation," IEEE Trans. Antennas Propag., vol. AP-32, 1984, pp. 938 - 943
5. Chow, Y. D. S., Tuan-Yung, H. and J. S. Row, "Dual-frequency shorted triangular patch antenna," Proc. Asia-Pacific Conference APMC 2005.vol 4, 2005 pp. 4 - 7
6. Lu, J.H., Tang, C. L. and K. Wong, "Novel Dual frequency and broad band designs of slot loaded equilateral triangle microstrip antennas," IEEE Trans. Antenna Propag., vol. 48, 2000, pp. 1048 - 1054
7. Deshmukh, A. and G. Kumar, "Compact broadband gap-coupled shorted square microstrip antennas," Microwave and Optical Technology Letters, vol. 48, 2006, pp.1261 - 1265
8. Lin, Y. and L. Shafai, "Characteristics of concentrically shorted circular patch microstrip antennas," IEE Proceedings H Microwaves, Antennas & Propag., vol. 137, 1990, pp.18 – 24
9. De, A., "Studies on rectangular and circular patch radiators," Ph.D Thesis, Indian Institute of Technology, Kharagpur, 1985
10. Chakravarty, T. and A. De, "Design of tunable modes and dual-band circular patch antenna using shorting posts," IEE Proc-Microw. Antennas Propag., vol 146, no. 3, 1999, pp. 224 - 228
11. Posadas V., Vargas, D., Iglesias, E., Roy, J. and M. Pascual, " Approximate analysis of short circuited ring patch antenna working at TM_{01}mode," IEEE Trans. Antennas and Propag., vol. AP-54, no.6, 2006, pp. 1875 - 1879
12. Sengupta, D. L. and L. F. Martins-Camelo, "Theory of dielectric-filled edge-slot antennas," IEEE Trans. Antennas Propag., vol. Ap-28, no.4, 1980, pp. 481 - 490

13. Chakravarty, T. and A. De, "Resonant frequency of a shorted circular patch with the use of a modified impedance expression for a metallic Post," Microwave and Optical Technology Letters, vol. 33, no. 4, 2002, pp. 252 - 255
14. Chakravarty, T. and A. De, "Using cavity model analysis for design of dual-band dual-slant-polarized microstrip antenna," Microwave and Optical Technology Letters, 2003, vol. 35, no. 5, pp. 252 - 256
15. Collin, R. E. and F. J. Zucker, "Antenna theory Part-I", McGraw-Hill, 1969
16. Harrington, R.F., "Time Harmonic Electromagnetic Fields," McGraw-Hill, N.Y., 1961
17. Yano, S. and Ishimaru, A., " A theoretical study of input impedance of a circular microstrip disk antenna," IEEE Trans. Antennas Propag., vol.29, no. 1, 1981, pp.77 - 83

5.1 Introduction

Electromagnetically coupled microstrip dipoles have been investigated by empirical or approximate analysis techniques. Electromagnetic coupling scheme is also known as proximity coupled feed. Two dielectric substrates are used such that the feed line is in between the two substrates and the radiating patch is on the top of upper substrate. The main advantage of this feed technique is that it eliminates spurious feed radiation and provides very high bandwidth (as high as 13 %) due to overall thickness of the microstrip patch antenna. The major disadvantage of this antenna is that it is difficult to fabricate because two dielectric layers need proper alignment. During the past decades a number of different types of microstrip radiators have been described [1]. The majority of these employs resonant elements and differs primarily in their particular shapes and manner in which microstrip feed line are attached. Six different EMC microstrip dipole configurations are described [1]. These employ varying amounts of electric and magnetic coupling and have been found to radiate with varying degree of efficiency. Katehi *et al.* [2] described the modeling of electromagnetically microstrip antenna. This model is developed by obtaining the current distribution along the dipole and transmission line, including all mutual interactions. The method of moments (MOM) has been applied for the determination of current distribution in the longitudinal dimension; the current dependence in transverse direction has been chosen so as to satisfy the edge condition at the effective width location. Pozar *et. al* [3] presented a microstrip antenna using microstrip feed line proximity coupled to a patch antenna printed on a superstrate above the feedline. 13% increase in bandwidth is obtained. The copolarised and crosspolarised radiation patterns were measured over this band with good results.

In the present work a numerical model using, the cavity model along with circuit theory has been used to calculate input impedance of a ring resonator loaded by a microstrip line. A ring resonator is fed by a narrow microstrip line underneath the ring. The proposed structure is analyzed and the input impedance is computed. The computed results are then compared with simulation. This model is a simple method to predict the input impedance of a loaded ring resonator by a microstrip line. In this proposed model a ring is used for the purpose of radiation in its fundamental mode.

5.2 Impedance Expression for Annular Ring Antenna Electromagnetically Coupled to a Microstrip Line

The geometry of electromagnetically coupled ring resonator is shown in figure 5.1. The ring resonator is constructed on a substrate of thickness h and relative dielectric constant ε_r. The inside radius is a, the outside radius is b. The ring is fed by a transmission line of length l and width w underneath with an insertion of s.

The computation method has three steps; first the impedance of a probe-fed ring is computed. It is then transformed by a capacitive tap constituting the overlap area of the ring and the microstrip line. In the final step, the net impedance is transformed at the line end using classical transmission line transformation.

The equivalent circuit is shown in figure 5.2. A probe fed ring resonator for dominant TM_{11} mode is analyzed using cavity model. Initially the impedance of a probe fed ring resonator is obtained. The input impedance for a probe location at r_0 is given thereby [5]

$$Z_{in} = \mu^2 h^2 \sum_n \sum_p \frac{(j\omega + A)C_n^{(1)^2}\omega^2 \left[(J_n(k.r_0)Y_n'(k.b_e) - J_n'(k.b_e)N_n(k.r_0))J_0\left(\frac{nd_f}{2r_0}\right)\right]^2}{(j\omega - C)(j\omega + A) + \omega_{np}^2} \tag{5.1}$$

The parameters A & C are given as

$$A = Z_s \int |H_i|^2 \, dS$$

$$C = -Y_w \int |E_i|^2 \, dS$$

where ω_{np} corresponds to the resonance of eigen-mode corresponding to TM_{np} mode, b_e and a_e represent the effective radius due to fringing fields. $J_n(k.r)$ is the Bessel function of order n and $J_n'(k.r)$ is the derivative of first order Bessel function. For the computation of impedance, the expression for wall admittances and mutual admittances has been obtained using [6]. Once the input impedance of ring resonator has been obtained, the same impedance has been transformed to impedance of electromagnetically coupled transmission line of length l and width w.

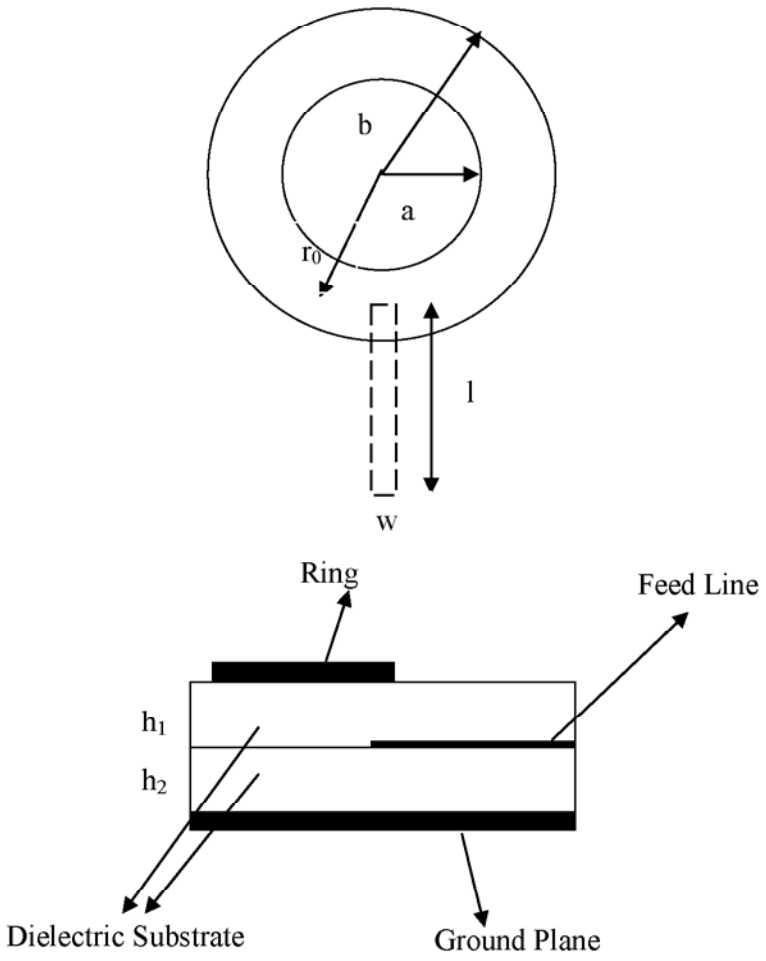

Figure 5.1 Geometry of the microstrip line fed ring resonator.

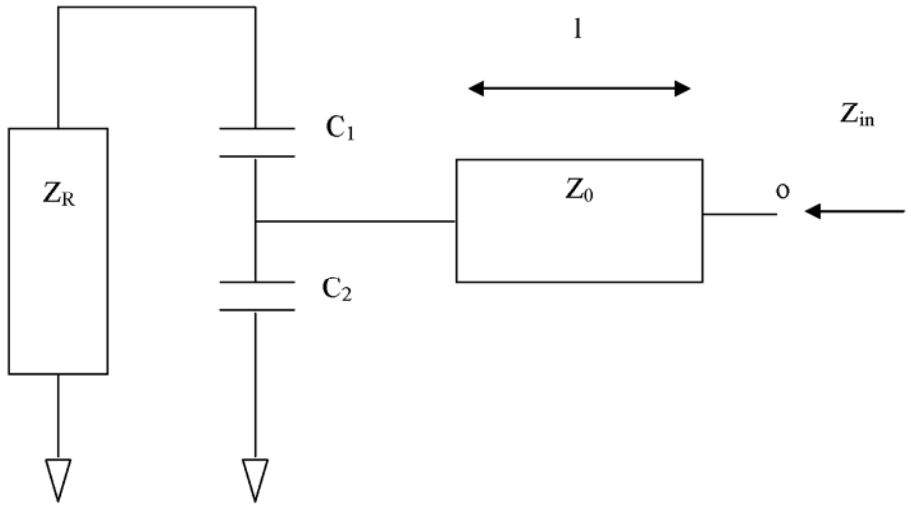

Figure 5.2 Equivalent circuit of the microstrip line fed ring resonator.

5.2.1 Computation of Capacitance

The capacitance is calculated from the capacitive tap formed. It is calculated by two different methods for comparison.

5.2.1.1 Classical Transmission Line Approach

The microstrip line is fed below the ring with an insertion of s. The line underneath the ring forms a capacitive tap with ring on the top and ground plane below. The capacitance between two conductors is defined by the relation

$$C = \frac{Q}{V}$$

where V is the voltage or potential difference between the conductors and Q is magnitude of charge. For such coupling lines the capacitive coupling can be approximated as [7], a coupling between two cylindrical lines of length s, radius $w/2$ and separation h_1 (or h_2).

$$C = \frac{\pi \varepsilon_0 \varepsilon_r s}{\ln\left(\frac{p + \sqrt{p^2 - 4a_w^2}}{2t}\right)} \tag{5.2}$$

where $p = h_1 + w$

$a_w = \frac{w}{2}$ and p is the separation between the lines from centre to centre.

5.2.1.2 Variational method

The capacitance is also calculated using variational method. Following [8], it is seen that capacitance formulation has two components namely parallel plate capacitance between two layers and fringe capacitance along the open end of line. Here, we use the variational analysis for computation of capacitance, where the addition of the two components is obtained. This technique is described in detail in literature [9]. For sake of brevity we outline only the formulation used. Figure 5.3 displays the structure under study. For this structure the admittance has been computed on the charge plane (line) as Y_+ and Y..

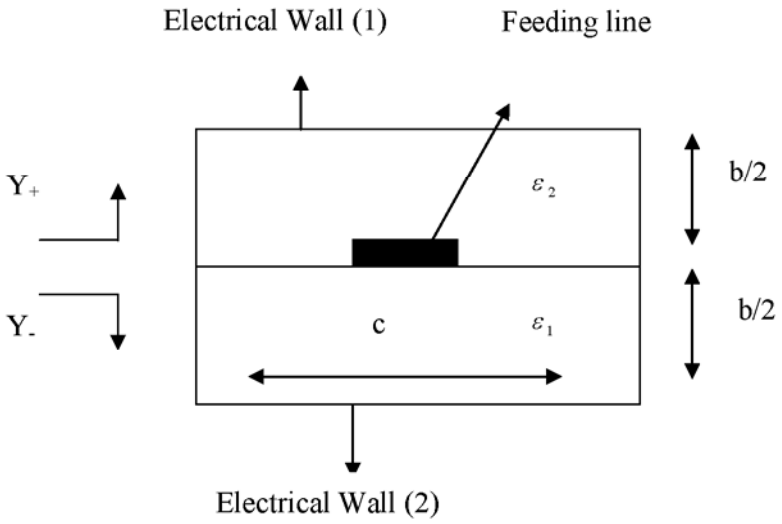

Figure 5.3 Structure of multilayered stripline.

Substituting the parameters in the following expression gives the capacitance between line and the respective walls.

$$C = \frac{(1+0.25A)^2}{\sum_{n\,odd}\left(\frac{T_n P_n}{Y}\right)} \tag{5.3}$$

$$Y_+ = \varepsilon_0 \varepsilon_1 \coth \beta b/2 \tag{5.4}$$

$$Y_- = \varepsilon_0 \varepsilon_2 \coth \beta b/2 \tag{5.5}$$

where

$$T_n = (L_n + AM_n)^2$$

$$L_n = \sin(\frac{\beta_n \omega}{2})$$

here

$$\beta_n = \frac{n\pi}{c}$$

$$M_n = (2/\beta_n w)^3[3\{(\beta_n w/2)^2 - 2\}\cos(\beta_n w/2) + (\beta_n w/2)\{(\beta_n w/2)^2 - 6\}\sin(\beta_n w/2) + 6]$$

$$P_n = (2/n\pi)(2/\beta_n w)^2$$

$$A_n = -\frac{\sum_{nodd} \frac{(L_n - 4M_n)L_n P_n}{Y_+}}{\sum_{nodd} \frac{(L_n - 4M_n)M_n P_n}{Y_-}} \tag{5.6}$$

where c represents the transverse wall spacing. For the present case c is taken to be a large value. Using the equation (5.6) capacitance in a multilayer structure can be obtained. It is also seen that the simple equation given by (5.3) also shows reasonably accurate results.

Let the transmission line of characteristic impedance Z_0 and length l be loaded by Z_R that is impedance of ring and the capacitive tap, the combined load on the transmission line may be denoted as Z_L. Therefore the input impedance seen by a source is given as

$$Z = Z\frac{Z_L + jZ_0 \tan(\beta l)}{Z_0 + jZ_L \tan(\beta l)} \tag{5.7}$$

For our analysis we have considered a loss less line. Therefore by using equations (5.1), (5.2) and (5.7) we have evaluated the input impedance of ring resonator. For accuracy, an exact estimation of capacitance in multilayer structure is necessary.

5.3 Results and Discussion

The theory formulated in the previous section is validated by comparing the results obtained through computation and simulation on IE3D software which is based on the Method of Moments. The dimension of the ring is chosen as follows; a = 30 mm, b = 60 mm, h_1 = 0.787 mm, h_2 = 0.787 mm and ε_r = 2.2. A microstrip line of given width w and length l is drawn on height h_2 = 0.787 mm with an insertion of s underneath the ring. The characteristic impedance of the line in the proposed environment is evaluated. If the proposed insertion is, for example, 10 mm underneath the ring (from the edge), then equation (5.1) is evaluated for the input impedance of the ring considering a probe location r_0 = 35 mm.

For comparison, three different widths of the line are chosen with two different insertion namely s = 10 mm and s = 20 mm. From figures (5.4), (5.5) and (5.6), it is seen that excellent agreement exists in the resonant resistance of TM_{11} mode of the loaded ring resonator between theory and simulation with transmission line loading.

Figure (5.7) and (5.8) show the resonant resistance of TM_{12} mode. The comparison is done for widths, w = 0.50 mm and w = 0.95 mm. There is an excellent agreement between the measured and numerical results. The higher order mode is more suitable for radiation purposes. The discrepancies observed for the higher width is due to the fact that in the present proposal, we are considering the capacitive coupling between two cylindrical lines. Such assumption, though reasonably accurate for thin lines, starts failing once the width of the line increases. Present theory displays a resonance at 733 MHz whereas the measurement shows 745 MHz for dominant mode. For higher mode (n = 2), the resonance is at 1440 MHz where as the measured values show resonance at 1467 MHz. The corresponding error in frequency estimation is less than 2 % for dominant mode and 1.8 % for higher mode. In figure (5.9), the computed resonant resistance of a probe fed ring resonator is presented. It is seen that the ring displays a very high resonant resistance. As proposed in the theory,

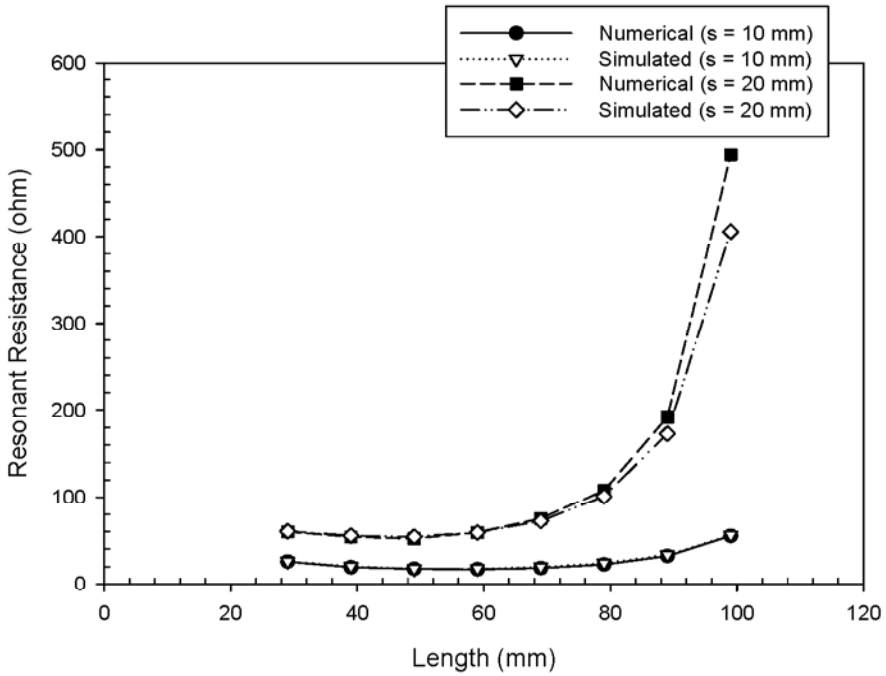

Figure 5.4 Comparison of present theory with simulated data: Resonant Resistance with Length for $w = 1.5$ mm for $n = 1$.

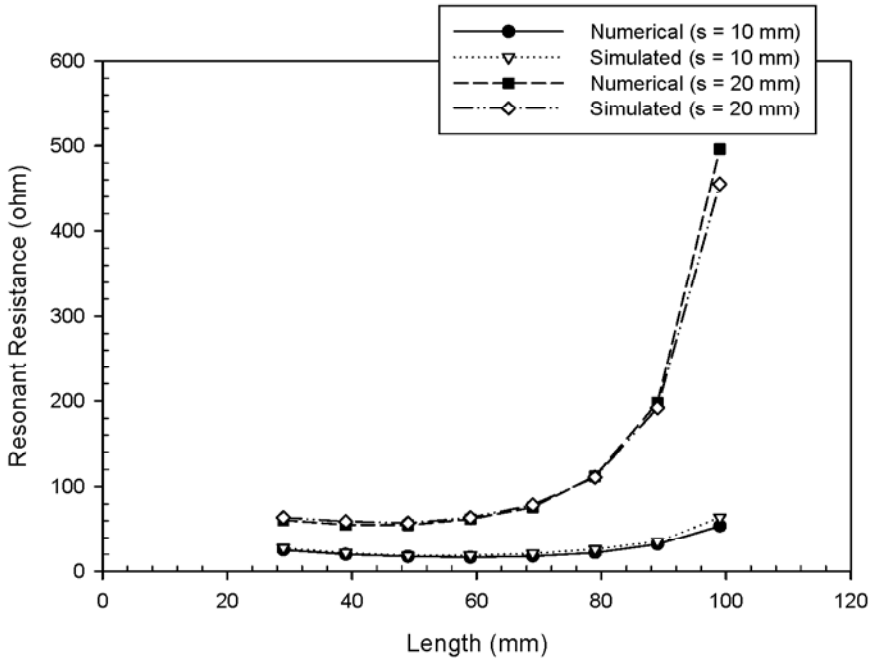

Figure 5.5 Comparison of present theory with simulated data Resonant Resistance with Length for $w = 0.95$ mm for $n = 1$.

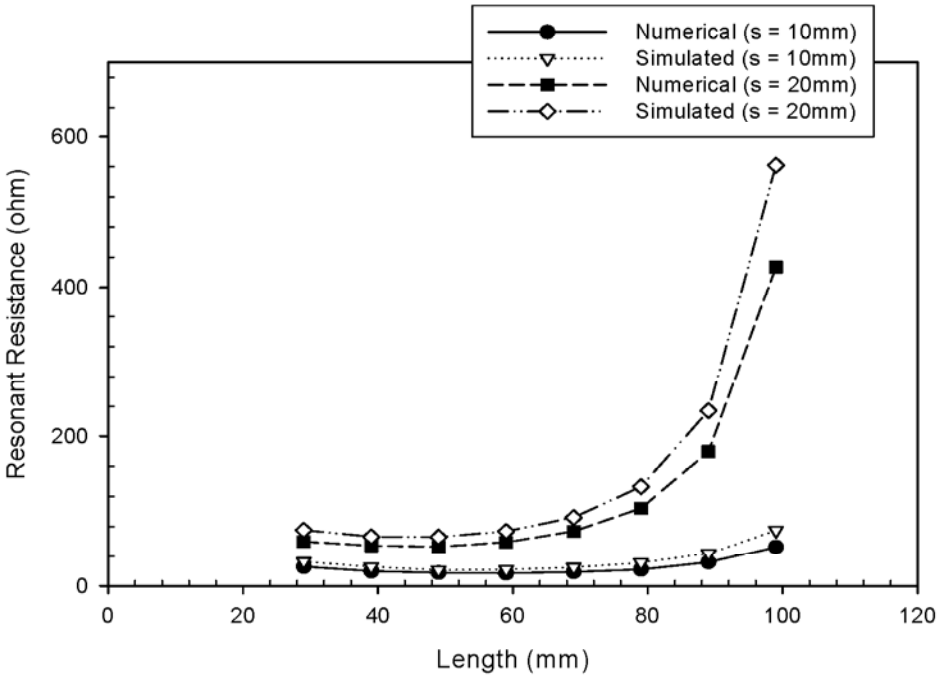

Figure 5.6 Comparison of present theory with simulated data: Resonant Resistance with Length for $w = 0.50$ mm for $n = 1$.

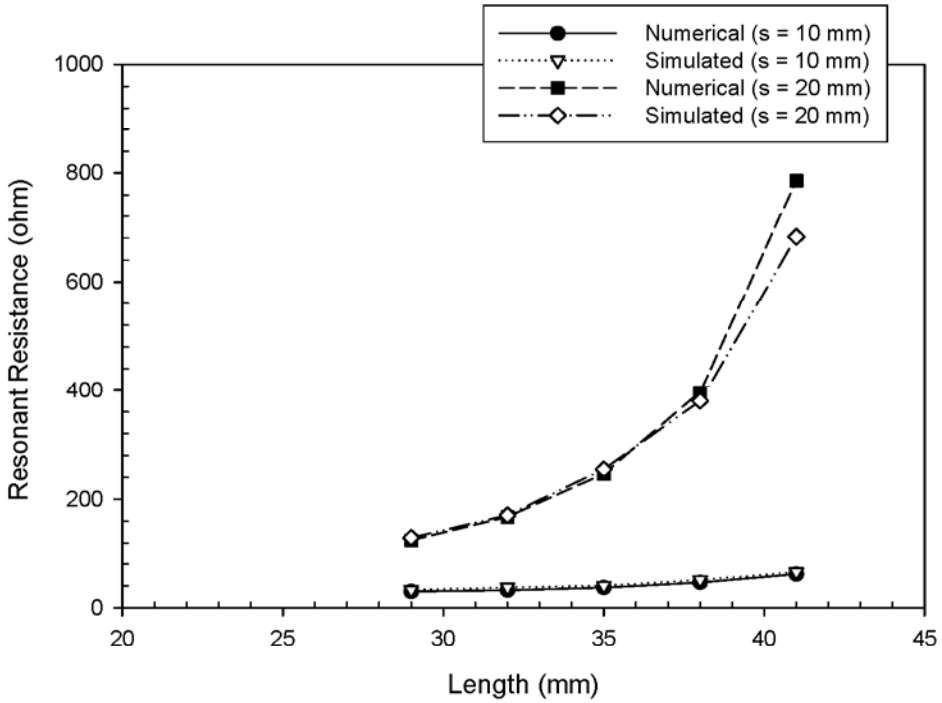

Figure 5.7 Comparison of present theory with simulated data: Resonant Resistance with Length for $w = 0.50$ mm for $n = 2$.

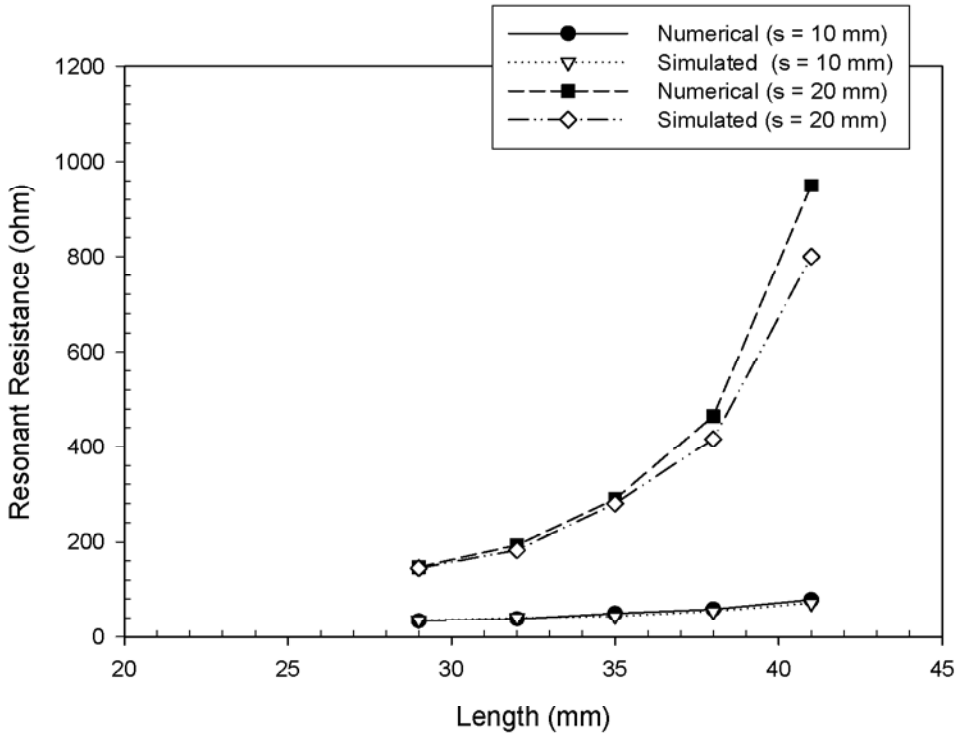

Figure 5.8 Comparison of present theory with simulated data: Resonant Resistance with Length for $w = 0.95$ mm for $n = 2$.

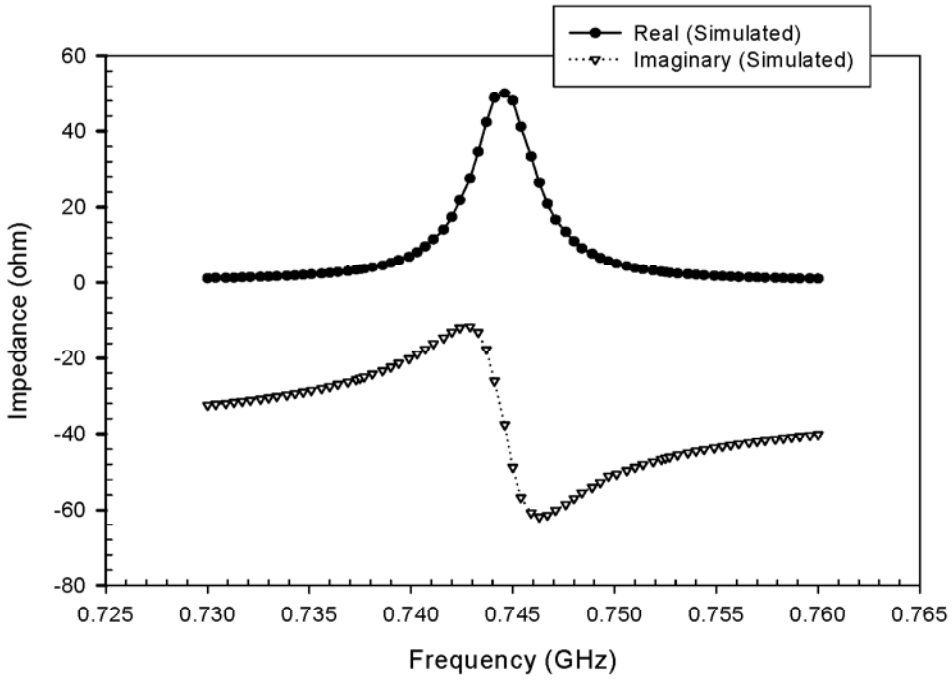

Figure 5.9 Impedance of a probe fed ring resonator with Frequency of its fundamental mode (a = 30 mm, b = 60 mm and r_0 = 35 mm).

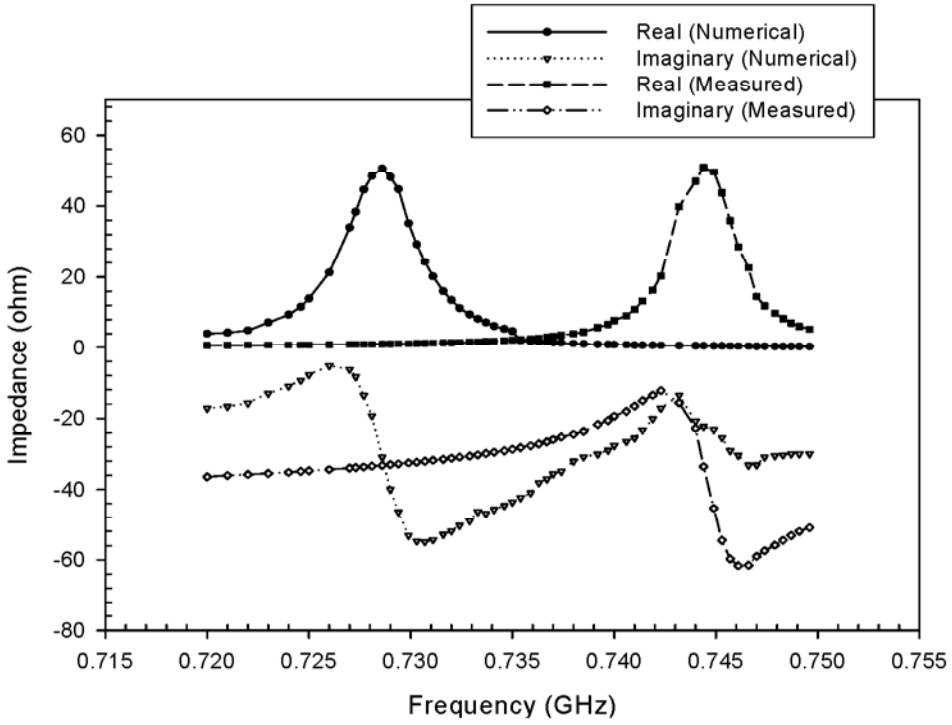

Figure 5.10 Input impedance with Frequency of fundamental mode of ring resonator loaded with transmission line (a = 30 mm, b = 60 mm, w = 0.95 mm and l = 29 mm).

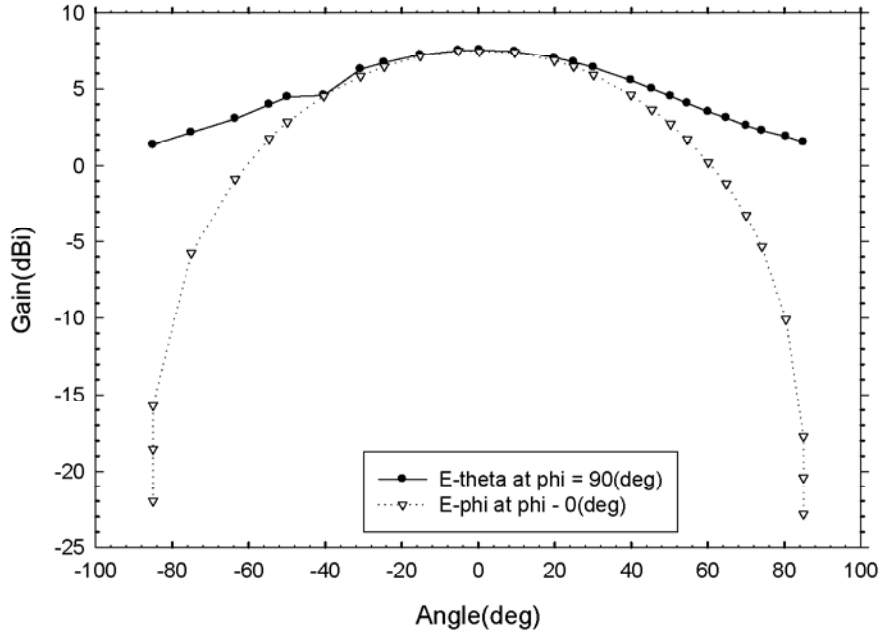

Figure 5.11 Gain of electromagnetically fed microstrip ring resonator.

this can be brought down to 50 Ω by suitable insertion of a transmission line underneath the ring. The computed and measured values of the input impedance are shown in figure 5.10. It is seen that there is a very good agreement between the computed values and the measured results, except for a 2.5 % error in the prediction of the resonant frequency. Figure 5.11 shows the gain of electromagnetically fed ring resonator. Electromagnetic feeding is the best method of feeding as it provides enhanced bandwidth. The model developed uses the concept of capacitive coupling and capacitance is calculated by two different methods for comparison. The model developed predicts the input impedance of ring resonator electromagnetically coupled to a transmission line with accuracy. Thus the developed model is simple, accurate and fast to compute the results.

5.4 Conclusion

In this chapter a method for computation of the input impedance of a ring resonator electromagnetically coupled to a microstrip line of given characteristic impedance and electrical length is presented. The computed values at fundamental mode show excellent agreement with the simulated results using IE3D. The results are also validated through measurements. Normally a ring antenna is used for radiation purposes in the TM_{21} mode, which has a higher resonance frequency. Unlike the conventional use, this proposed structure can be used in its dominant TM_{11} mode giving the advantage of a compact antenna. This simple method of computation is also very useful when an array of rings is to be designed for low side lobes since the amplitude taper can be easily achieved using varying lengths and widths of transmission line.

References

1. Oltman, H.G. and D. A. Huebner, "Electromagnetically coupled Microstrip dipoles," IEEE Trans. Antennas Propag., vol. 29, 1981, pp. 151-157
2. Katehi, P. B. and N.G. Alexopoulos, "On the modeling of electromagnetically coupled microstrip antennas- Printed strip dipole," IEEE Trans. Antennas Propog., vol. 32, 1984, pp. 1179 - 1186
3. Pozar, D.M. and B. Kaufmann, "Increasing the bandwidth of microstrip antenna by proximity coupling," Electron. Letts., vol. 23, 1987, pp. 368 - 369
4. Garg, R., Bhartia, P., Bahl, I. and A. Ittipiboon, "Microstrip Antenna Design Handbook,", Artech House, 2001
5. Mahajan, M., Khah, S. and T. Chakravarty, "An improved method of approaching impedance computation of probe fed ring resonator," Microwave and Optical Technology Letters, vol. 49, no. 7, 2007, pp. 1681 - 1684
6. Bhattcharya, A. K. and R. Garg, "Input impedance of annular ring microstrip antenna using circuit theory approach," IEEE Trans. Antennas Propag., vol. AP-33, 1985, pp. 369 - 374
7. Jordan, E. C. and Keith. G. Balmain, "Electromagnetic waves and radiating systems," second edition, Prentice hall of India, 1968
8. Arora, N. D., Raol, K.V., Schumann, R. and L. M. Richardson, "Modeling and extraction of interconnect capacitances for multilayer VLSI circuits," IEEE Trans. Computer aided design of Circuits and systems, vol. 15, no. 1, 1996, pp. 58 - 67
9. Bhat, B. and S. K. Koul, "Unified approach to solve a class of strip and microstrip like transmission lines," IEEE Trans.MTT, vol. 30, no.5, 1982, pp. 679 - 686

Cavity model is the one of the simplest model to analyze microstrip patch antennas. In this thesis, investigations are carried out to analyze the circular and annular ring microstrip geometries by cavity model. The computed results are compared to the results obtained from IE3D software based on method of moments. Firstly a model for circular antenna based on cavity model is developed and this analysis is further extended to stacked circular disc. The results are compared to simulated results. Good agreement is obtained between the two results. Gain is considerably high in case of stacked elements and radiation efficiency is more than 94% for different cases. From the results it is observed that in this method the cavity model is extended beyond $h << \lambda_0$ and it is observed that the model is successful for determining various parameters of the stacked antenna.

The ring antenna with coaxial feeding is analyzed with the help of cavity model and circuit theory. The method obtained is quite simple, accurate and can be used to predict the impedance of first few modes. TM_{11} is the dominant mode. The computed results are compared to previously published data for TM_{12} mode. The result show that there is disagreement for the real part of impedance with earlier published data and this is possibly due to the method of feeding used. A high degree of agreement is observed between the parameters calculated by this method and IE3D software. The method developed is intuitive and does not demand high computation power.

Continuing with the analysis of similar structures the effect of loading on annular ring antenna is also studied. This is the method to enhance the bandwidth of microstrip antennas. Cavity model is used to find out the resonant frequency of TM_{np} mode of loaded annular ring antenna via shorting posts. The posts are thin in diameter with respect to the diameter of ring. For accurate estimation of frequency under loaded condition, the close form expression for the impedance of shunt post as given by Sengupta has been modified to incorporate an empirically generated "Correction Factor". The analysis is extended to the case when posts are loaded randomly (asymmetrically) on an annular ring antenna at (r_2, ϕ_i) where r_2 is the radial distance of the post from the centre of the patch and ϕ_i is the angle between the line joining the centre of the patch and the feed probe, and the angular location of the post. This can be shown when we change the angular position of post the resonant frequency is not

altered. For this analysis the resonant frequency does not depend upon the angular location of post. Thus for P =1 and $\phi_i \neq 0^o/180^o$, dual resonance is produced at any angular location and for all normal modes except for n = 0. Hence TM_{11} is the dominant mode unlike symmetric loading where TM_{01} is the dominant mode. The variation of resonant frequency is also observed with the radius of posts and it increases as the radius of posts increases. The numerical and simulated results are in complete agreement.

The resonant frequency when the posts are located symmetrically (equi-spaced along the circumference of circle concentric with the patch radiator) is analysed. It is shown that the resonant frequency for each mode depends on the radial distance of the posts from the centre of the patch and radius of post. As the posts move towards the edge of the patch, the resonance frequency of TM_{11} mode first increases and then drops down. This effect is more pronounced when number of posts P is large. For the loaded patch, the lowest non-zero mode corresponds to TM_{01} mode with a resonant frequency less than the dominant TM_{11} mode of the unloaded patch. Interestingly the use of wall susceptance is not required in the present method. Then the input impedance is calculated for symmetric loading of posts. The resonant resistance decreases as the number of pins increases. Good accuracy is obtained between the measured and simulated results. It is seen that for better impedance matching at both the frequencies a thicker substrate is more useful.

The input impedance of a ring resonator electromagnetically coupled to a microstrip line is calculated by developing a simple model based on cavity model and circuit theory. The line underneath the ring forms a capacitive tap with ring on the top and ground plane below. The capacitance between two conductors is found by two methods. The input impedance is obtained in three main steps. Firstly the impedance of probe fed ring resonator is obtained, secondly the capacitance is calculated and lastly the net impedance is transformed at the line end using classical transmission line transformation. In the first method the capacitance is found by coupling between two cylindrical lines and other is the variational method. The capacitance obtained by both the methods is same. An excellent agreement exists in the resonant resistance of TM_{11} mode of the loaded ring resonator between theory and simulation with

transmission line loading. It is seen that the ring displays a very high resonant resistance. As proposed in the theory, this can be brought down to 50 Ω by suitable insertion of a transmission line underneath the ring. Normally a ring antenna is used for radiation purposes in the TM_{21} mode, which has a higher resonance frequency. Unlike the conventional use, this proposed structure can be used in its dominant TM_{11} mode giving the advantage of a compact antenna. This simple method of computation is also very useful when an array of rings is to be designed for low side lobes since the amplitude taper can be easily achieved using varying lengths and widths of transmission line.

The investigations carried out in this work have led to the design techniques and characterization of broadband antennas. Using the simple method outlined in this thesis, it is possible to design broadband and dual frequency antennas by stacking and loading of antennas. This analysis can further extended to incorporate switching diodes or varactor diodes. By changing the bias level of varactor diodes, the resonant frequency is tuned. Varactor diodes have also been used for design of polarization agile antenna. The resonant impedance of such loaded antenna is thereby increasing the utility of the design application. It is also fruitful to investigate the effect of an asymmetrically loaded off-centred shorting post in presence of a centred short of finite dimension. The said investigation should lead to computation of resonant frequency, input impedance and radiation pattern of loaded annular ring antennas.

List of Publications

Journals:

1. **M.Mahajan**, T Chakravarty, S.K.Khah, "Resonant frequency of asymmetrically loaded microstrip annular ring antenna," **Microwave and Optical Technology Letters,** vol. 50, no. 9., 2008, pp. 2351 - 2353
2. **M.Mahajan**, T Chakravarty, S.K.Khah, A.De " Computation of resonant frequency of annular ring antenna loaded with multiple posts," **IET Microwaves Antennas & Propagation ,** vol. 2, no. 1, 2008**,** pp.1 - 5
3. **M.Mahajan**, T Chakravarty, S.K.Khah, "Extended cavity model for input impedance of annular microstrip antenna loaded with multiple shorting posts," **Journal of Electromagnetic Waves and Applications (JEMWA)**, vol. 22, 2008, pp. 1333 - 1340
4. **M.Mahajan,** T Chakravarty, S.K.Khah, "An improved method of approaching impedance computation of probe fed ring resonator," **Microwave and Optical Technology Letters,** vol. 49, no. 7. (2007), pp. 1681 - 1684
5. ***M.Mahajan,** T Chakravarty, S.K.Khah, "Analysis of ferrite based planar array of rectangular patch microstrip antenna in X-band," **Indian Journal of Physics** vol. 81 (9), (2007), pp.301 - 306
6. **M.Mahajan**, T Chakravarty, S.K.Khah, "Extended cavity model analysis of stacked circular disc", **Progress in Electromagnetic Research," PIER 65**, pp. 287 - 308, (2006)

Conferences:

1. **M.Mahajan**, T Chakravarty, S.K.Khah, "Resonant frequency of annular ring antenna using shorting pins," **Proceedings of 2008 Asia-Pacific EMC Symposium and 19th EMC Zurich Symposium**, Singapore, May 2008, IEEE Catalog Number: 08EX2004C, pp.862 - 865
2. ***M.Mahajan,** S.K.Khah, "Analysis of circular patch microstrip antenna with superstrate in X-band," **Proceedings of Nat. Conf. Recent Adv. Microwave**

Techniques & Appl., Oct-2006, (University of Rajasthan Jaipur India), pp.345 - 347

3. *Himanshu, Jaideep, **M.Mahajan**, S.K.Khah, "C/C++ based software for the simulation of rectangular microstrip patch antenna," **Proceedings of Nat. Conf. Recent Adv. Microwave Techniques & Appl**., Oct-2006, (University of Rajasthan Jaipur India), pp.214 - 216
4. ***M.Mahajan,** T Chakravarty, S.K.Khah, "Analysis of superstrate covered circular microstrip antenna," **Optical and Wireless Communication, Conference** Punjab Engineering College, Chandigarh, Dec 13-15, 2007, pp.84 - 86
5. ***M.Mahajan,** T Chakravarty, S.K.Khah, "Analysis of planar array of rectangular and circular patch microstrip antenna in X-band," **Optical and Wireless Communication, Conference** Punjab Engineering College, Chandigarh, Dec 13-15, 2007, pp. 87 - 90

Papers Communicated:

1. **M.Mahajan,** T Chakravarty, S.K.Khah, "A Circuit Model of Electromagnetically Coupled Ring Antenna at higher order modes" **Eucap2009 (Berlin) (Accepted)**
2. **M.Mahajan,** T Chakravarty, S.K.Khah, "An analytical tool for computation of the input impedance of a ring resonator electromagnetically coupled to a transmission line," **IEEE Trans. Antenna & Propagation. (under review)**

*** Not Included in Thesis**